Università degli studi di Roma Tor Vergata

Doctoral Thesis

Perturbative Methods and Proper Elements for the Satellite and Space Debris Problem

---

Author:
Tudor Vartolomei

Supervisor:
Prof. Alessandra Celletti
Co-supervisor:
Prof. Giuseppe Pucacco
Ph.D. Coordinator:
Prof. Carlangelo Liverani

A thesis submitted in fulfillment of the requirements
for the degree of Doctor of Philosophy

in the

Dipartimento di Matematica

Cycle XXXV
Academic year 2021/2022

Contents

List of Figures

List of Tables

Acknowledgements

During my Ph.D. journey, there were several persons who played essential roles in teaching and supporting me to face all the challenges and accomplish this important stage in my career.

First of all, I would like to express my deepest gratitude to my supervisor, Professor Alessandra Celletti, who was always there when I needed her support, reviewing my progress constantly, and guiding me through my Ph.D. studies. Her immense knowledge and motivation helped me to make my first steps as a researcher in Mathematics and Celestial Mechanics. I would also like to extend my sincere thanks to my co-supervisor, Professor Giuseppe Pucacco, for his valuable advice which was a source of inspiration in my research.

I would like to acknowledge the support of the Stardust-R project (EU H2020 MSCA ETN Stardust-Reloaded Grant Agreement 813644) for financing and training of my early-stage research career. I want to thank my colleagues from the Stardust-R project for the stimulating discussions and exchanging of knowledge. Special thanks to Professor Christos Efthymiopoulos and Dr. Victor Rodriguez-Fernandez for their practical and helpful suggestions.

I also wish to thank Professor Cătălin Galeș for useful discussions and all the guidance, support, and outstanding feedback. I would like to acknowledge the assistance of Professor Marius Apetrii, Professor Domenico Marinucci and Dr. Christoph Lothka for several interesting discussions on the related topics. Many thanks to all the members of Department of Mathematics, from both Tor Vergata University and "Al. I. Cuza" University, for their professionalism and friendly support.

I want to give my deepest appreciation to my wife, Andrada, for her emotional support and patience, who was constantly encouraging me over the years. Last but not the least, I would like to thank my whole family and God for always being there for me.

Chapter 1

Introduction

The main objective of the present thesis is the study of classical and powerful methods of perturbation theory for Hamiltonian systems in the context of an important and applied topic, which is the space debris and Earth's artificial satellites dynamics problem. Using a Galilean approach, one can start from the two-body problem and then consider a much more complex problem, adding gradually the forces that act on the debris or the satellite, like the ones due to the non-sphericity of the Earth, third body perturbations by Sun and Moon, the pressure of Solar radiation, etc.

The methods of perturbation theory are developed with the aim of reducing very complex dynamical systems to simpler systems, which are easier to analyze, though retaining the main physical features of the original ones. For the Hamiltonian systems, the complexity reduction is achieved using a suitable canonical change of coordinates. The classical variables used in Celestial Mechanics problems are the *Keplerian orbital elements*: a - semi-major axis, e - eccentricity, i - inclination, Ω - longitude of the ascending node, ω - argument of periapsis, M - mean anomaly (or, equivalently, f - true anomaly). This set of coordinates describes the shape and size of the orbit and, as well, the orbital position of the object along its osculating trajectory. The above set of orbital elements is equivalent to the Cartesian coordinates that give the position and the velocity of an object in a coordinates system.

In this thesis, we are interested in the analysis of the secular evolution of the orbital elements, by defining a model, in the Hamiltonian formalism, that describes the dynamics of the Earth's satellite objects, and by developing and applying effective techniques based on perturbation theory. The secular evolution of the orbital elements means the changing in the eccentricity and inclination of the orbit over a long period of time, and also the evolution of the argument of perigee and the longitude of the ascending nodes. The exact position of an object is given by the *osculating orbital elements* (hereafter osculating elements), which are the orbital elements that depend on time, while the *mean orbital elements* (hereafter mean elements) are the orbital elements obtained after the averaging of the system w.r.t. the short-periodic variables.

The work presented in this thesis aims at computing a new set of variables, the so-called *proper orbital elements* (hereafter proper elements) for a space object, which are quasi-integrals of motion, namely quantities that are stable for long periods of time. Our model problem will depend on coordinates that vary on different time scales; hence, we will implement a hierarchical perturbation theory to get rid of the different evolution associated to such variables. The proper elements are obtained from the mean elements after a canonical change of coordinates that averages the Hamiltonian function w.r.t. the semi-short and long-periodic variables. The main advantage of the proper elements is indeed their stability over long periods of time. This property will be used for the classification of the space debris. Our method will prove to be very effective in practical applications, even allowing to reconnect the space debris to their parent body.

1.1 Space debris

Space debris, or orbital debris, or space junk, are artificial or non-operational objects in orbit around the Earth. According to (Klinkrad, 2006), the definition of space debris, adopted by the Inter-Agency Space Debris Coordination Committee (IADC) in 2002, is the following:

"*Space debris are all man-made objects including fragments and elements thereof, in Earth orbit or re-entering the atmosphere, that are non-functional.*"

The examples of space debris are diversified: remnants of space mission like rocket stages, old satellites, fragments from disintegration, lost equipments like bolts, paint flakes, batteries, etc.
A first classification of space debris is based on their visibility in the sky; there exist catalogues of space debris, which are trackable from the Earth and covers objects larger than 5 cm in LEO and larger than 30 cm in GEO, together with estimates of small space debris. For the small objects, their number and sizes are predicted by statistical methods.
The most recent update by the European Space Agency (ESA)[1] says that the number of the space debris tracked by the Space Surveillance Networks is equal to 31740. On the other hand the numbers of estimated space debris are the following:

1. **36500** space debris objects greater than **10 cm**;
2. **1 million** space debris objects from **1 cm to 10 cm**;
3. **130 million** space debris objects from **1 mm to 1 cm**.

The total mass of the all man-made objects in space is greater than 10000 tons.
The largest amount of space debris at this moment is represented by fragments generated by break-up events, such as collisions or explosions. The report by ESA (ESA Space Debris Office, 2022) estimates more than 600 fragmentation events since 1961. Due to their high impact velocity, a collision with a

1. **10 cm** projectile would produce a catastrophic fragmentation of a satellite;
2. **1 cm** object would most likely disable a spacecraft and penetrate the International Space Station shields;
3. **1 mm** object could destroy sub-systems on board a spacecraft.

These aspects, together with the large number of space debris in space, induce the possibility of a fast growth of the number of space debris in the future. The worst scenario, described in (Kessler and Cour-Palais, 1978), and called the *Kessler syndrome* (after one of the authors), predicts a chain reaction of break-up events such that the prevention of future collisions becomes impossible and the space missions' design becomes highly affected.

1.1.1 Literature of space debris and Earth's artificial satellites dynamics

From the perspective of the dynamical system theory, the problems of Earth's artificial satellites dynamics and of space debris dynamics represent the same problem, which is basically the perturbed two-body problem. These problems have been studied from different points of view in the literature. From the development of purely analytical theories that describe the dynamical problem to the improved numerical methods for the computation of the approximate solution, a lot of works have been done in the last years. In the present thesis, we

[1] https://www.esa.int/

FIGURE 1.1: Space debris around the Earth. Credits: ESA

focus on the analytical (and semi-analytical) study of the dynamical system that describes the space debris problem, namely the development and study of the Hamiltonian formalism of the problem. Several works like (Celletti and Galeş, 2014), (Celletti and Galeş, 2015), (Celletti, Galeş, and Pucacco, 2016), (Celletti and Galeş, 2017) were devoted to the construction of an accurate Hamiltonian model in different regimes and the analysis of the resonances by using chaos indicators and mathematical tools from dynamical system theory as in (Rossi, 2008), (Gkolias et al., 2016), (Gkolias et al., 2019), (Celletti, Galeş, and Lhotka, 2020). A detailed overview of the different approaches to the study of the dynamical system of space debris motion can be found in (Celletti et al., 2017).
Since the dynamics is affected by several forces, we need to study the problem using different models, each one depending on the studied region. The most common classification is done w.r.t. the altitude (or the value of the semi-major axis) and it gives the following subdivision of the sky around the Earth:

1. The *Low-Earth-Orbits* (LEO) region is located between 90 km and 2000 km above the Earth's surface. Since it is a region at low altitudes, apart from the monopole attraction of the Earth, the objects are mainly affected by the air drag and the oblateness of the Earth.

2. The *Medium-Earth-Orbits* (MEO) region is between 2000 km and 35000 km in altitude, and the motion of the objects is perturbed in this region by the Earth's quadrupole (J_2 and J_{22}) and by the third body perturbations (Moon and Sun). The effect of the Solar radiation pressure (SRP) is also visible in this region for objects with considerable area-to-mass ratio.

3. The *Geosynchronous-Earth-Orbits* (GEO) region is located at altitudes around 35000 km. The same forces as in the MEO region are applied to the objects in GEO, with the peculiarity that the magnitude of the third body perturbations increases with the altitude.

As we mentioned before, to describe the dynamics of a space object around the Earth we need to find the evolution of its orbital elements. In a problem that contains the perturbation due to the Moon (or the Sun), the dynamics include also the orbital elements of the third body, and the angles that describe the rotation of the Earth as well. Since there are several variables involved, we need also to make a classification w.r.t. the period of the angles as follows:

1. The *fast angles* are the short-periodic variables, which in this case are the angle of Earth's rotation θ (1 rotation per day) and the mean anomaly M (from 1 to 15 revolution per day, depending on the altitude of the satellite),

2. The *semi-fast angles* are the variables with a longer period (semi-secular), from 1 rotation per month to 1 rotation per year (the mean anomalies of the third body perturbations),

3. The *slow angles* are the long-periodic variables (secular), which include the argument of perigee ω and the longitude of the ascending node Ω of the space object, and also the argument of periapsis and the longitude of the ascending node of the third body perturbations (usually, 1 rotation takes from 1 to several years).

An important phenomenon in the space debris dynamics is the occurrence of the resonant motion between the revolution of the space object and different rotations of the other bodies. For example, we talk about a *mean-motion resonance* whenever there is a commensurability between the angle of the Earth's rotation θ and the mean anomaly of the particle M (the most important cases are related to the 2:1 resonance in MEO and the 1:1 resonance in GEO). On the other hand, when the commensurability is between the slow angles, we say that there is a *secular resonance* between the object and the third body perturbation.
All the above mentioned phenomena have been studied in detail in the literature from the very beginning of the launch of the Earth's satellites (1957) to the present time. Among classical papers about Earth's satellites dynamics, we quote (Kozai, 1959), (Brouwer, 1959), (Brouwer and Hori, 1961), (Lyddane, 1963), (Cook, 1966), (Deprit and Rom, 1970), (Hughes, 1980), (Coffey, Deprit, and Miller, 1986), (Ely and Howell, 1997), (Breiter, 2001), etc. Recent works focus on particular cases of the dynamics, for example (Lemaître, Delsate, and Valk, 2009), (Colombo, Lücking, and McInnes, 2012), (Celletti and Galeş, 2016), (Lhotka, Celletti, and Galeş, 2016), (Colombo, 2019), (Daquin et al., 2021), (Daquin et al., 2022); these articles describe very important aspects of the dynamics both for the theoretical purposes and for applications to real space objects..

1.1.2 Dynamical model - Hamiltonian formalism

In the present work, we model the dynamics of the space debris following an approach similar to that described in (Celletti et al., 2017), in which we include the perturbations due to the Earth (with a non-spherical shape), Moon and Sun, Solar radiation pressure, and the effect of the atmospheric drag.
After giving in Chapter 3 the definition of the Hamiltonian functions of each perturbation in terms of the mean elements, we make a classification of the Hamiltonian functions as follows. We describe the secular dynamics of a space object which is outside the LEO region and far from all tesseral resonances, by using the Hamiltonian function

$$\begin{aligned}\mathcal{H}_{full}(e,i,i_M,a_S,\omega,\Omega,\Omega_M,M_S;a) &= \overline{H_{J_2}}(e,i;a)+\overline{H_{J_3}}(e,i,\omega;a)\\ &+ \overline{H_M}(e,i,i_M,\omega,\Omega,\Omega_M;a)+\overline{H_S}(e,i,\omega,\Omega;a)\\ &+ \overline{H_{SRP}}(e,i,a_S,\omega,\Omega,M_S;a),\end{aligned} \tag{1.1}$$

where the indexes M and S pertain to the elements of the Moon and Sun, respectively.
The secular dynamics of a space object close to a tesseral resonance is modeled by the Hamiltonian function

$$\begin{aligned}\mathcal{H}^{res}_{full}(a,e,i,i_M,a_S,M,\omega,\Omega,\Omega_M,M_S,\theta) &= \mathcal{H}_{full}(e,i,i_M,a_S,\omega,\Omega,\Omega_M,M_S;a)\\ &+ \mathcal{H}_{res}(a,e,i,M,\omega,\Omega,\theta)+\mathcal{H}_{Kep}(a),\end{aligned} \tag{1.2}$$

where $\mathcal{H}_{res}$ is the Hamiltonian function representing the perturbations due to a tesseral resonance and $\mathcal{H}_{Kep}$ is the Hamiltonian of the pure Keplerian model. For the dissipative case which includes the air drag, we cannot define the Hamiltonian function, but we define the dynamical model for a space debris in LEO through Hamilton's equation for which we add the averaged dissipative effects due to the air drag $F_a(a,e,i), F_e(a,e,i)$, that affect only the eccentricity and the inclination.
To make use of the methods from perturbation theory, we transform the Hamiltonian function, by using the Delaunay's variables (described in Chapter 4) instead of the mean orbital elements.

1.2 Normal forms

The computation of the normal form of a dynamical system consists in a series of changes of coordinates such that the transformed dynamical system has the same behavior as the initial one, with a much simpler form. In the case of Hamiltonian systems, all the transformations of coordinates must be canonical, which means, for example, that Hamilton's equations in the new variables describe the same system as the initial Hamilton's equations in the old variables. To obtain a canonical transformation, one can use the preservation property of the Poisson brackets. In the present work, we give an appropriate statement of the theorem that describes the construction of the normal form, as follows.

Theorem 1 *Let $(\boldsymbol{I},\boldsymbol{\varphi}) \in B \times \mathbb{T}^n$ be the action-angles variables, where $B \subset \mathbb{R}^n$ is an open set and n denotes the number of degrees of freedom, for a Hamiltonian function $\mathcal{H} = \mathcal{H}(\boldsymbol{I},\boldsymbol{\varphi})$ defined by*

$$\mathcal{H}(\boldsymbol{I},\boldsymbol{\varphi}) = \mathcal{H}_0(\boldsymbol{I}) + \varepsilon\mathcal{H}_1(\boldsymbol{I},\boldsymbol{\varphi}) \,,$$

where $\mathcal{H}_0(\boldsymbol{I})$ represents the integrable part, ε is a small parameter and $\mathcal{H}_1(\boldsymbol{I},\boldsymbol{\varphi})$ is a trigonometric perturbation. We assume that $\mathcal{H}_1$ is an analytic function on $B \times \mathbb{T}^n$ that can be written as a Fourier expansion over a set of indexes $\mathcal{K}$:

$$\mathcal{H}_1(\boldsymbol{I},\boldsymbol{\varphi}) = \sum_{\boldsymbol{k}\in\mathcal{K}} b_{\boldsymbol{k}}(\boldsymbol{I}) \exp(i\boldsymbol{k}\cdot\boldsymbol{\varphi}).$$

If the frequency vector $\boldsymbol{\nu} = \frac{\partial\mathcal{H}}{\partial\boldsymbol{I}}$ satisfies the following non-resonance condition

$$|\boldsymbol{\nu}(\boldsymbol{I}_0)\cdot\boldsymbol{k}| > 0, \forall \boldsymbol{k} \in \mathcal{K}, \text{ and } \forall \boldsymbol{I}_0 \in B,$$

then there exists a canonical transformation $(\boldsymbol{I},\boldsymbol{\varphi}) \to (\boldsymbol{I}',\boldsymbol{\varphi}')$ such that the Hamiltonian in the new variables becomes

$$\mathcal{H}'(\boldsymbol{I}',\boldsymbol{\varphi}') = \mathcal{H}'_0(\boldsymbol{I}') + \varepsilon^2\mathcal{H}'_1(\boldsymbol{I}',\boldsymbol{\varphi}').$$

The proof of Theorem 1 is constructive and gives an explicit procedure to compute the transformation from the old variables to the new variables of the proof of Theorem 1 and the normal form of a Hamiltonian system that satisfies the assumptions. All the details are given in Section 2.3.

1.2.1 Literature on perturbation theory for the space debris problem

The analytical investigation of the Earth satellites motions has begun with the papers by (Brouwer, 1959) and (Kozai, 1959), which were published almost at the same time. In both

papers, the authors aim to derive the time evolution of the six orbital elements, by developing the perturbation due to the Earth in terms of the mean elements of the space object and then by applying techniques of perturbation theory to obtain a closed-form solution for the elements. The method presented in (Kozai, 1959) gives the solution for the orbits far from singularities due to the small eccentricity and inclination, while in (Brouwer, 1959) the solution is obtained for any kind of eccentricity and inclination, but far from the critical value corresponding to an inclination equal to 63.4°.
In the subsequent paper (Brouwer and Hori, 1961), the authors continue the study of the analytical development of the orbital elements, by including the forces due to the atmospheric drag. A similar result is obtained in (Brouwer, 1959), but including the contribution of the air drag for the evolution of the semi-major axis and the eccentricity.
The theory of Brouwer is re-considered by (Lyddane, 1963) which analyzed in details the cases of small eccentricity and small inclination. The method presented in this paper uses a set of variables (Poincaré coordinates) that avoids the singularities.
The theory of canonical perturbation with Lie series applied to the problem of the Earth's satellites dynamics is firstly introduced in (Hori, 1966), where the theoretical procedure is presented and applied to the same case as in (Kozai, 1959) and (Brouwer, 1959). Three years later, (Deprit, 1969) published an article that describes perturbation theory, but for a Hamiltonian function that depends on small parameters. The article presents in detail the procedure of Lie series transformation, a method that is used also in the present paper.
In the same period, several works have been done in the direction of improving the existing theory, as in (Kamel, 1969), (Kamel, 1970), (Henrard, 1970), but also in the direction of extending the theory to non-Hamiltonian systems as in (Kamel, 1971) and (Hori, 1971).
In recent works that make use of the normalization procedure, the Hamiltonian function is split in different parts and a "book-keeping" parameter is introduced as described in (Efthymiopoulos, 2011). This procedure creates a hierarchy of the perturbations and reduces the computational time for large Hamiltonian functions. This normalization method has been used in different contexts, for example to describe the dynamics of space debris around the resonances in (Gkolias et al., 2019), (Daquin et al., 2022), or the dynamics of objects with high area-over-mass ratio in (Gachet et al., 2017), and even for the estimate of the stability of the system as in (De Blasi, Celletti, and Efthymiopoulos, 2021). In the present thesis, we will adopt a similar technique to compute the proper elements both for the synthetic space debris obtained after a simulated break-up event as in (Celletti, Pucacco, and Vartolomei, 2022) and for some real cases as shown in (Celletti, Pucacco, and Vartolomei, 2021).

1.2.2 Normal form of the space debris Hamiltonian function

The most complicated part presented in this work consists in a preliminary preparation of the Hamiltonian function (1.1). Since the motion is affected by several forces, we have a hierarchy of perturbations. At the same time, we want the integrable part to be linear in the action variables.
After we use the transformation of the Hamiltonian function (1.1) from orbital elements to the Delaunay's variables, we obtain a new Hamiltonian function

$$\mathcal{H}(G, H, H_M, L_S, g, h, h_M, l_S; L), \tag{1.3}$$

which describes a 4 DoF system. The procedure for the preliminary transformation of the Hamiltonian function (1.3) is the following:

1. Make a linear (canonical) change of coordinates, by shifting the variables G and H w.r.t. the initial conditions of the orbit G_0 and H_0. Substitute also L with L_0.

2. Define the new set of variables $P = G - G_0$, $Q = H - H_0$, and, to keep a consistent notation, also use $(Q_M, R_S, p, q, q_M, r_S) = (H_M, L_S, g, h, h_M, l_S)$.

3. Since the new variables P and Q are close to the origin, expand the Hamiltonian around $P = 0$ and $Q = 0$ up to a high enough order[2] and, after ordering the terms, one obtains:

$$\begin{aligned} \mathcal{H}_{exp}(P, Q, Q_M, R_S, p, q, q_M, r_S) &= Z_0(P, Q, Q_M, R_S) \\ &+ R_0(P, Q, Q_M, R_S, p, q, q_M, r_S), \end{aligned} \tag{1.4}$$

where

$$Z_0(P, Q, Q_M, R_S) = \nu_P P + \nu_Q Q + \nu_{Q_M} Q_M + \nu_{R_S} R_S.$$

Denote by $\nu = (\nu_P, \nu_Q, \nu_{Q_M}, \nu_{R_S})$ the frequency vector. The function R_0 contains the perturbation from all the considered forces.

4. Adding the book-keeping parameter λ, split the Hamiltonian function into two parts:

$$\begin{aligned} \mathcal{H}^{(0)}(P, Q, Q_M, R_S, p, q, q_M, r_S) &= Z_0(P, Q, Q_M, R_S) \\ &+ \lambda R_0(P, Q, Q_M, R_S, p, q, q_M, r_S), \end{aligned} \tag{1.5}$$

Once we get the Hamiltonian function in the form of (1.5), we start the normalization procedure by splitting the perturbation R_0 into two parts:

$$\begin{aligned} R_0(P, Q, Q_M, R_S, p, q, q_M, r_S) &= F(P, Q, Q_M, R_S) \\ &+ \sum_{\mathbf{k} \in \mathbf{I}} G_{\mathbf{k}}(P, Q, Q_M, R_S) \cdot \begin{matrix}\sin \\ \cos\end{matrix}(k_1 p + k_2 q + k_3 q_M + k_4 r_S), \end{aligned} \tag{1.6}$$

where F and $G_{\mathbf{k}}$ are polynomial functions depending only on the actions variables and $\mathbf{k} = (k_1, k_2, k_3, k_4)$ is the coefficient vector of the angles involved in the expansion.
To compute the normal form of (1.5) at the first order, we look for a generating function $\chi^{(1)}$ such that $(P, Q, Q_M, R_S, p, q, q_M, r_S) = S^{\lambda}_{\chi^{(1)}}(P^1, Q^1, Q^1_M, R^1_S, p^1, q^1, q^1_M, r^1_S)$ and

$$\begin{aligned} \mathcal{H}^{(1)}(P^1, Q^1, Q^1_M, R^1_S, p^1, q^1, q^1_M, r^1_S) &= Z_0(P^1, Q^1, Q^1_M, R^1_S) + \lambda Z_1(P^1, Q^1, Q^1_M, R^1_S) \\ &+ \lambda^2 R_1(P^1, Q^1, Q^1_M, R^1_S, p^1, q^1, q^1_M, r^1_S). \end{aligned} \tag{1.7}$$

The generating function $\chi^{(1)}$ is obtained by solving the homological equation:

$$\begin{aligned} &\sum_{\mathbf{k} \in \mathbf{I}} G(P^1, Q^1, Q^1_M, R^1_S) \cdot \begin{matrix}\sin \\ \cos\end{matrix}(k_1 p^1 + k_2 q^1 + k_3 q^1_M + k_4 r^1_S) \\ &+ \left\{ Z_0(P^1, Q^1, Q^1_M, R^1_S), \chi^{(1)}(P^1, Q^1, Q^1_M, R^1_S, p^1, q^1, q^1_M, r^1_S) \right\} = 0, \end{aligned} \tag{1.8}$$

where the symbol $\begin{matrix}\sin \\ \cos\end{matrix}$ represents either a sine or a cosine function.
The algebraic computations are given in detail in Chapter 2, Sections 2.3.1, 2.3.3 and Chapter 5. As well, the implementation of the methods is presented in Appendix A.
Once obtained the generating function $\chi^{(1)}$, we can compute the normal form of the Hamiltonian function by applying the Lie series operator to the initial Hamiltonian

$$\mathcal{H}^{(1)}(P^1, Q^1, Q^1_M, R^1_S, p^1, q^1, q^1_M, r^1_S) = S^{\lambda}_{\chi^{(1)}} \mathcal{H}^{(0)}(P, Q, Q_M, R_S, p, q, q_M, r_S)$$

[2] Depending on the initial conditions, one might need a lower or higher expansion to get a good approximation of the initial (non-expanded) Hamiltonian.

and disregarding the terms depending on λ^2. Substituting $\lambda = 1$, we obtain the normal form

$$\mathcal{H}^{(1)}_{NF}(P^1, Q^1, Q^1_M, R^1_S, p^1, q^1, q^1_M, r^1_S) = Z_0(P^1, Q^1, Q^1_M, R^1_S) + Z_1(P^1, Q^1, Q^1_M, R^1_S). \quad (1.9)$$

The computation can continue as described in Section 2.3.3, or rather one can stop at the first order and use the generating function to compute the proper elements.

1.3 Proper elements

The proper elements are usually identified with the orbital elements (semi-major axis, eccentricity, inclination) obtained after the elimination of the short-periodic angles and the long-periodic angles. In essence, the proper elements are quasi-integrals of motion for a dynamical system, or, alternatively, we can define them as integrals of motion for a simplified dynamical system. Intuitively, the proper elements are quantities that are nearly constant in time.
In view of studying the dynamics of space debris, the main applications of the proper elements are:

1. A classification of the space objects into families (due to their small variability),
2. A determination of the ancestor of a space object and an evolution of the physical characteristics of the break-up event.

The advantage of using the proper elements, instead of mean or osculating elements, is that they have almost the same value for a long period of time, while the other elements might vary a lot over time. The property of almost constancy induces that the proper elements are almost the same at the time of the break-up event and after a long interval of time. If two, or more objects, have similar proper elements, we can deduce that they are part of the same family.

1.3.1 Literature on proper elements

The computation of proper elements is not a recent subject, since it has been studied for a long time in the literature in the framework of the Main Belt asteroids dynamics. The concept of the proper elements appeared more than one century ago, when the article "Groups of asteroids probably of common origin" was published by (Hirayama, 1918). In this paper, Hirayama tries to group the asteroids by checking the similarities in the elements obtained after using a linear theory of secular perturbations. The idea is that the asteroids with similar inclination and eccentricity are likely to be of the same origin. The term *proper elements* explicitly appeared for the first time in (Hirayama, 1922) together with a detailed description of the theory used. In (Brouwer, 1951), the author computed a comprehensive list of asteroids proper values and compared them with the results obtained by Hirayama. As well, Brouwer used a linear theory of secular perturbations for a more realistic model of planetary motion.

The analysis of the asteroids with high inclination and eccentricity was firstly approached in (Kozai, 1962) where the proper parameters used for the family identifications were different from the classical ones. In his Ph.D. thesis, in (Williams, 1969), and in the succesive papers (see (Williams, 1971), (Williams and Hierath, 1987)), Williams described a new method of computing the proper elements even for objects with high eccentricity and high inclination. This new method does not need an expansion in eccentricity or inclination of the perturbing functions.

New advances were made with the work of (Schubart, 1982), (Schubart, 1982) and (Bien and Schubart, 1983), where the authors approached the problem of the computation of proper

elements for the resonant case, namely the Hildas and Trojans groups. A second breakthrough was performed by Bien and Schubart that developed a synthetic theory of proper elements. The synthetic computation of the proper elements consists in a purely numerical method, which is described in detailed in (Carpino, Milani, and Nobili, 1987) and later in (Knežević and Milani, 2001).

Since the '90s, a lot of major improvements in both analytic and synthetic methods were done by different authors. We mention here only some works, mentioning the the detailed historical overview of the computational methods of proper elements can be found in (Knežević, 2015), (Knežević, Lemaître, and Milani, 2002), (Lemaître, 1993). In the direction of analytic and semi-analytic methods we quote the works in (Milani and Knežević, 1990) and (Knežević and Milani, 1994), for an efficient method of the computation of proper elements for asteroids with low and medium eccentricity and inclination, the semi-analytic theory for high eccentricities and high inclinations being improved by (Lemaître and Morbidelli, 1994) and (Lemaître, 1993). The synthetic theory presented in (Knežević and Milani, 2001) significantly increased the accuracy of the computation of proper elements for any kind of orbits, with the drawback of a quite long computational time. Moreover, proper elements for non (mean motion) resonant NEAs have been computed in (Gronchi and Milani, 2001), using a technique of singularity extraction to deal with planet crossing orbits. The main goal of the computation of the proper elements is to determine the families of asteroids; however, for the analysis of tens of thousands objects, it is needed to use some classification algorithm as described in (Carruba, Aljbaae, and Lucchini, 2019) and the references therein. Recently, the topic of the analytical computation of proper elements has been reconsidered in (Fenucci, Gronchi, and Saillenfest, 2022) in the case of planet crossing asteroids with mean motion resonances.

Regarding the computation of the proper elements for the space debris or Earth's artificial satellites' problem, we quote the results in (Gachet, 2016) and (Gachet et al., 2017), where the computation was done by using the Hamiltonian function in cylindrical coordinates, mainly for the space debris in the geosynchronous region. A synthetic theory was approached in (Rosengren et al., 2019), (Rosengren, Bombardelli, and Amato, 2019) and (Wu and Rosengren, 2021), where the computation of the proper elements was done purely numerically by starting from the evolution of the osculating elements.

1.3.2 Computation and results

In the problem of the secular dynamics of space debris, the evolution of the semi-major axis is almost always constant. Apart from the cases of tesseral resonances, the proper semi-major axis for a Hamiltonian function like (1.1) is defined as the initial value of the mean semi-major axis. The computation of the proper eccentricity and the proper inclination is done by using the normal form (1.9) and the generating function $\chi^{(1)}$ as follows. Since the normal form is a Hamiltonian function that depends only on the action variables, the closed

form solution of the system is given by Hamilton's equation:

$$\begin{aligned}
P^1(t) &= P^1_0, \\
Q^1(t) &= Q^1_0, \\
Q^1_M(t) &= Q^1_{M,0}, \\
R^1_S(t) &= R^1_{S,0}, \\
p^1(t) &= p^1_0 + \frac{\partial H_{NF}}{\partial P^1}(P^1_0, Q^1_0, Q^1_{M,0}, R^1_{S,0})t, \\
q^1(t) &= q^1_0 + \frac{\partial H_{NF}}{\partial Q^1}(P^1_0, Q^1_0, Q^1_{M,0}, R^1_{S,0})t, \\
q^1_M(t) &= q^1_{M,0} + \frac{\partial H_{NF}}{\partial Q^1_M}(P^1_0, Q^1_0, Q^1_{M,0}, R^1_{S,0})t, \\
r^1_S(t) &= r^1_{S,0} + \frac{\partial H_{NF}}{\partial R^1_S}(P^1_0, Q^1_0, Q^1_{M,0}, R^1_{S,0})t,
\end{aligned} \tag{1.10}$$

where P^1_0, Q^1_0, $Q^1_{M,0}$, $R^1_{S,0}$, p^1_0, q^1_0, $q^1_{M,0}$ and $r^1_{S,0}$ are the initial conditions for the normalized system. These values are unknown, since we only know the initial conditions for the original Hamiltonian system. The relation between the old initial conditions and the new initial conditions is given through the transformation obtained with the generating function $\chi^{(1)}$. We firstly compute the expression of the new variables as a function of the old variables as follows:

$$\begin{aligned}
P^1(P, Q, Q_M, R_S, p, q, q_M, r_s) &= (S^{\lambda}_{\chi^{(1)}})^{-1} P, \\
Q^1(P, Q, Q_M, R_S, p, q, q_M, r_s) &= (S^{\lambda}_{\chi^{(1)}})^{-1} Q, \\
Q^1_M(P, Q, Q_M, R_S, p, q, q_M, r_s) &= (S^{\lambda}_{\chi^{(1)}})^{-1} Q_M, \\
R^1_S(P, Q, Q_M, R_S, p, q, q_M, r_s) &= (S^{\lambda}_{\chi^{(1)}})^{-1} R_S, \\
p^1(P, Q, Q_M, R_S, p, q, q_M, r_s) &= (S^{\lambda}_{\chi^{(1)}})^{-1} p, \\
q^1(P, Q, Q_M, R_S, p, q, q_M, r_s) &= (S^{\lambda}_{\chi^{(1)}})^{-1} q, \\
q^1_M(P, Q, Q_M, R_S, p, q, q_M, r_s) &= (S^{\lambda}_{\chi^{(1)}})^{-1} q_M, \\
r^1_S(P, Q, Q_M, R_S, p, q, q_M, r_s) &= (S^{\lambda}_{\chi^{(1)}})^{-1} r_S.
\end{aligned} \tag{1.11}$$

The new initial conditions P^1_0, Q^1_0, $Q^1_{M,0}$, $R^1_{S,0}$, p^1_0, q^1_0, $q^1_{M,0}$ and $r^1_{S,0}$ are obtained now by computing the following quantities:

$$\begin{aligned}
P^1_0 &= P^1(P_0, Q_0, Q_{M,0}, R_{S,0}, p_0, q_0, q_{M,0}, r_{S,0}), \\
Q^1_0 &= Q^1(P_0, Q_0, Q_{M,0}, R_{S,0}, p_0, q_0, q_{M,0}, r_{S,0}), \\
Q^1_{M,0} &= Q^1_M(P_0, Q_0, Q_{M,0}, R_{S,0}, p_0, q_0, q_{M,0}, r_{S,0}), \\
R^1_{S,0} &= R^1_S(P_0, Q_0, Q_{M,0}, R_{S,0}, p_0, q_0, q_{M,0}, r_{S,0}), \\
p^1_0 &= p^1(P_0, Q_0, Q_{M,0}, R_{S,0}, p_0, q_0, q_{M,0}, r_{S,0}), \\
q^1_0 &= q^1(P_0, Q_0, Q_{M,0}, R_{S,0}, p_0, q_0, q_{M,0}, r_{S,0}), \\
q^1_{M,0} &= q^1_M(P_0, Q_0, Q_{M,0}, R_{S,0}, p_0, q_0, q_{M,0}, r_{S,0}), \\
r^1_{S,0} &= R^1_S(P_0, Q_0, Q_{M,0}, R_{S,0}, p_0, q_0, q_{M,0}, r_{S,0}).
\end{aligned} \tag{1.12}$$

Furthermore, we can compute the proper values P_t^1, Q_t^1 at any time t by substituting the mean elements $P_t, Q_t, Q_{M,t}, R_{S,t}, p_t, q_t, q_{M,t}, r_{S,t}$ in the transformation (1.11) in the following way:

$$\begin{aligned} P_t^1 &= P^1(P_t, Q_t, Q_{M,t}, R_{S,t}, p_t, q_t, q_{M,t}, r_{S,t}), \\ Q_t^1 &= Q^1(P_t, Q_t, Q_{M,t}, R_{S,t}, p_t, q_t, q_{M,t}, r_{S,t}). \end{aligned} \tag{1.13}$$

The variables P_t^1, Q_t^1 are then used to compute the proper eccentricity and inclination of the orbit, by taking the inverse transformation from the variables $(P, Q, Q_M, R_S, p, q, q_M, r_S)$ to the orbital elements $(e, i, i_M, a_S, \omega, \Omega, \Omega_M, M_S)$. We first shift back the actions to obtain the proper Delaunay's actions, $G_t = P_t + G_0$ and $H_t = Q_t + H_0$. Then, we compute the proper eccentricity (e_t) and proper inclination (i_t) by using the formulas in (4.1). The implementation of the method is described in detail, for different models, in Chapter 5. Once the

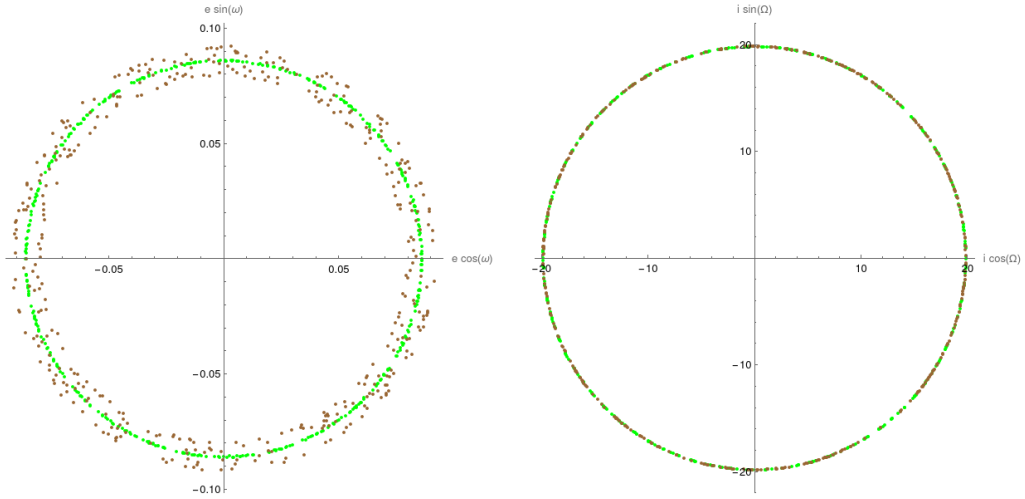

FIGURE 1.2: Mean elements (brown dots) and Proper elements (green dots) for $(e\cos(\omega), e\sin(\omega))$ (left plot) and $(i\cos(\Omega), i\sin(\Omega))$ (right plot).

computation of the proper elements is done and the accuracy of the normalization procedure is analyzed for different regions and horizons of time, we make some comparisons between the evolution of the mean elements and the evolution of the proper elements in Chapter 6. We show the stability and the small variability of the proper elements compared with the mean elements for orbits in different regimes (Figure 1.2). As well, we describe the procedure to

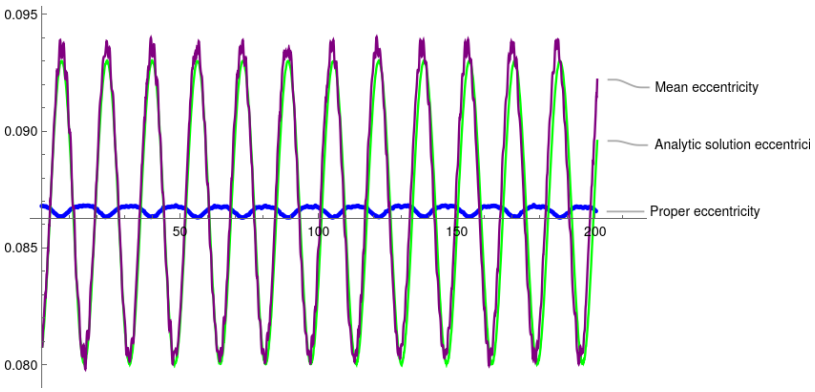

FIGURE 1.3: Mean elements (purple line), proper elements (blue line) and the analytic solution (green line) of the eccentricity.

compute the analytic solution (closed-form solution) of the mean elements, which is obtained

by the inverse transformation of $\chi^{(1)}$. This solution depends only on time and on the initial conditions. We compare the analytic solution with the numerical results for a long period of time, as it can be seen in Figure 1.3.
While in the first part of the thesis we describe the theoretical aspects of the computation of the proper elements for the space debris problem, we dedicate the last part (Chapter 6) to an important application of the theory in the case of groups of space debris. We show some experiments (using both simulated and real data) in which the proper elements are used to classify the space debris. For example, in Figure 1.4 (which is described in detail in Chapter 6), we present how the constancy of the proper elements can be used to classify the space debris from two different groups. If one instead tries to use the mean elements, the classification will return several miss-classified objects.

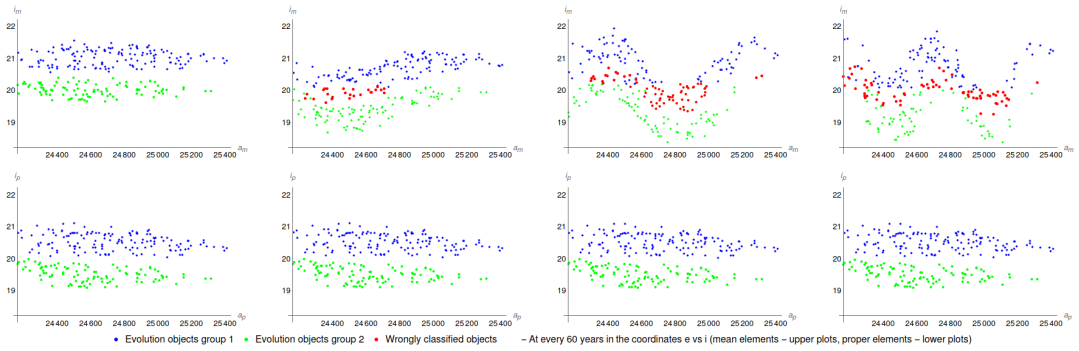

FIGURE 1.4: The evolution of the fragments generated by two nearby explosions in the mean elements (upper plots) and proper elements (lower plots) at every 60 years. We show two groups (group 1 - blue dots, group 2 - green dots) and the wrongly classified fragments (red dots) at each time following the procedure explained in Chapter 6.

1.3.3 Perspectives

The problem of the proper elements' computation is directly related to the dynamics of the space debris in a given region. Although the method presented in this thesis and the results obtained are satisfactory, there are several problems that need to be addressed in this direction. From the theoretical aspects of perturbative methods, to the practical implementation of different techniques, the problem of the Hamiltonian normalization with Lie series and the computation of proper elements is still a fervid subject, since it seems that it still has hidden layers to be explored. Further ideas are given in Chapter 7.

1.4 Thesis outline

The thesis is divided into seven chapters, including the introduction and conclusions, and it ends with three appendixes that explain in detail the computational implementation of the different methods.

The second chapter, "Canonical perturbation theory", is an overview of the most important aspects of dynamical systems, Hamiltonian systems and perturbation theory. It is structured such that one can connect the notions and concepts of perturbation theory with the problem of space debris dynamics. We start with the description of the basic notions of ordinary differential equations and dynamical systems and then we describe the canonical formalism. This chapter ends with the description of the normalization procedure with Lie series, which is the mathematical tool used to compute the proper elements.

In Chapter 3, we focus on the development of the dynamical model that describes the evolution of a space object around the Earth. We firstly define the reference frame and the proper units used in the computations. Then, we describe the Cartesian equations of motions for a space object affected by several forces. After that, the Hamiltonian formulation of the dynamical model is given in two different ways (by direct transformations from the Cartesian expressions and by using the expansions found in (Kaula, 2000) and (Lane, 1989),(Hughes, 1980)). The resulting Hamiltonian functions are checked by comparing the coefficients of both expressions. As well, the accuracy of the Hamiltonian model is verified by the comparison between the numerical integration of the Cartesian equations of motion and the numerical integration of Hamilton's equation.

The analysis of the structure of the Hamiltonian system is given in Chapter 4. We define here the concept of resonances and which are the most common effects due to these phenomena. We explain how the evolution of the orbital elements is affected by the different forces involved or by the region of the initial orbit. At the end of this chapter, we present some examples with the numerical integration of Hamilton's equations to highlight the behavior of the objects in different regimes. The goal of this chapter is to understand the structure of the Hamiltonian system and the relevant effects that must be included in the Hamiltonian function to be normalized.

The theoretical part, where we explain in detail the mathematical procedure to compute the normal form for a Hamiltonian system is described in Chapter 5. This chapter is divided in three different parts: the non-resonant normalization, the resonant normalization and the normalization for dissipative systems. For every section we describe how to compute the normal form and the generating function used for the canonical changes of coordinates and, hence, for the computation of proper elements. As well, a method to compute the analytic solution of the mean elements is given in every section.

In Chapter 6, we show the applications of the implementation of the mathematical procedure that computes the proper elements. We start by analyzing the difference between the mean and proper elements for single objects in different regimes. Afterwards, we show the accuracy of the computation and the main advantages of the proper elements; we also present some applications both for the simulated break-up events and for the real space debris. The examples given highlight the property of the proper elements to be nearly constant over a long period of time and, hence, to be useful in regrouping space objects that have the same ancestor.

We conclude the thesis with Chapter 7, where we make a brief overview of the methods and results. Also we give some suggestions for future developments and some perspectives within the problem of proper elements computation.

Appendix A contains the implementation of the normalization procedure for a Hamiltonian system in the programming language `Mathematica`©, and the auxiliary function needed to compute the proper elements and the analytic solution of the mean elements. Appendix B shows the `Mathematica`© code used for the development of the Hamiltonian functions that defines the dynamical system describing the dynamics of the space debris. It also contains the code for the Cartesian equations of motion, written in `JAVA`©. In Appendix C we give a brief description of the application `SIMPRO` used for the simulation of break-up events.

Chapter 2

Canonical Perturbation Theory

This chapter is devoted to a brief introduction of the main notions of dynamical systems, canonical formalism and perturbation theory. We aim to recall here those definitions, concepts, results that are relevant for the study of the space debris dynamics and for the computation of the proper elements. We start this chapter with a short description of continuous dynamical systems. The second section covers the most important aspects of the Hamiltonian systems and its main advantage in the study of the dynamical systems. The last section is devoted to the presentation of the normalization algorithm used in the study of the space debris problem and for the computation of the proper elements.

2.1 Dynamical systems

When we talk about dynamics, we refer to the evolution of a particle or a system of particles. The evolution can be either **discrete**, when the particles evolve in time steps, or **continuous**, when the system evolves as a continuous function of time. In our work, we are interested in the continuous evolution of dynamical systems, namely those systems that are described by a system of differential equations. Nevertheless, we start by defining the general notion of a dynamical system as a **flow** of a vector field, and then we give the most important aspects and definitions that are used in the thesis.

2.1.1 Preliminaries: classes of functions, differentiable manifolds

Let $U \subseteq \mathbb{R}^n$, $V \subseteq \mathbb{R}^m$ be two subsets and let $f : U \to V$ be a vector function, $f(x_1, x_2, \ldots, x_n) := (f_1(x_1, x_2, \ldots, x_n), f_2(x_1, x_2, \ldots, x_n), \ldots, f_m(x_1, x_2, \ldots, x_n))$.

Definition 1 *We say that f is a **function of class** C^k (or C^k-function) if the components $f_1, \ldots, f_m$ are k-times differentiable and the partial derivatives $\frac{\partial f_i}{\partial x_j}$ are continuous.*

If $k = \infty$, we say that f is a **smooth** function.

Definition 2 *A smooth function f is called **analytic** if for any point $x^0 \in U$, there exists a convergent power series that converges to f in some neighborhood of x^0.*

We define now two important classes of functions (operators).

Definition 3 *An application $\varphi : X \to Y$, where X and Y are two topological spaces, is a **homeomorphism** if:*

1. *φ is a bijection,*
2. *φ and φ^{-1} are continuous functions.*

Definition 4 *A function $f : U \to W$, $W \subseteq \mathbb{R}^n$ is a **diffeomorphism** if:*

1. *f is a bijection (a one-to-one function),*
2. *f and f^{-1} are C^k-functions, $k \geq 1$.*

Let us now introduce the notion used to define the differentiable manifolds. Let M be a topological space.

Definition 5 *M is called a **topological manifold** of dimension n if:*

1. *$\forall p \in M$, $\exists U \subset M$ open, with $p \in U$ and there exists a homeomorphism $\varphi : U \to \varphi(U) \subset \mathbb{R}^n$ (M is locally euclidean),*
2. *M is Hausdorff separable,*
3. *M is countable.*

A pair (U, φ) is called a **local chart**.

Definition 6 *We say that two local charts (U, φ) and (V, ψ) are **compatible of class** C^k if either $U \cap V = \emptyset$ or $U \cap V \neq \emptyset$ and $\psi \circ \varphi^{-1}$ is a diffeomorphism.*

Definition 7 *A family $\mathcal{A} = \{(U_\alpha, \varphi_\alpha) | \alpha \in I\}$ of local charts satisfying $\bigcup_{\alpha \in I} U_\alpha = M$ is called an **atlas** for M.*

Definition 8 *A **differentiable structure of class** C^k is given by an atlas $\mathcal{A} = \{(U_\alpha, \varphi_\alpha) | \alpha \in I\}$ that satisfies*

1. *Any two charts of $\mathcal{A}$ are compatible of class C^k,*
2. *For any (V, ψ) local chart of M that is compatible of class C^k with any $(U_\alpha, \varphi_\alpha) \in \mathcal{A}$, implies that $(V, \psi) \in \mathcal{A}$.*

Definition 9 *A **differentiable manifold** of class C^k (or C^k-manifold) of dimension n is a topological manifold of dimension n together with a differentiable structure of class C^k.*

2.1.2 Flow, phase portrait and types of orbits

A dynamical system is usually defined by three components: the space of phases, the time space and the law of time-evolution. Although the general definition can be given for any topological spaces and any topological semigroups, let us take as the phase space, a differentiable manifold of class C^k, say M, and as the time space, the group $(\mathbb{R}, +)$.

Definition 10 *A **dynamical system** is defined by a continuous map $\varphi : M \times \mathbb{R} \to M$ that satisfies*

1. $\varphi(\boldsymbol{x}, 0) = \boldsymbol{x}$
2. $\varphi(\varphi(\boldsymbol{x}, t), s) = \varphi(\boldsymbol{x}, t + s)$.

Remark 1 *The application $t \mapsto \varphi_t := \varphi(\cdot, t)$ is a morphism from the group $(\mathbb{R}, +)$ to the group of continuous maps on M. In this case, the dynamical system is called **flow**.*

Now, we introduce the concepts of orbit, trajectory and phase portrait of a dynamical system.

Definition 11 *The set $\gamma_{\boldsymbol{x}^0} := \{\varphi(\boldsymbol{x}^0, t) | t \in \mathbb{R}\}$ is the **orbit** of $\boldsymbol{x}^0 \in M$. The function $\varphi(\boldsymbol{x}^0, t)$ is called the **trajectory** that passes through $\boldsymbol{x}^0$.*

Definition 12 *The **phase portrait** of a dynamical system is the set of all trajectories.*

Different types of orbits are described by the following definitions:

Definition 13 *Let $\boldsymbol{x} \in M$ be an arbitrary point in M. We have the following definitions:*

1. *We say that $\boldsymbol{x}$ is a **stationary point** (or **equilibrium point**) if $\varphi(\boldsymbol{x}, t) = \boldsymbol{x}$, $\forall t \in \mathbb{R}$.*
2. *If there is $T \in \mathbb{R}$ such that $\gamma_{\boldsymbol{x}}(t+T) = \gamma_{\boldsymbol{x}}(t)$, $\forall t \in \mathbb{R}$, then $\gamma_{\boldsymbol{x}}$ is a **periodic orbit** of period T.*
3. *For an equilibrium point $\boldsymbol{x} \in M$, we say that γ is a **homoclinic orbit** if $\lim_{t\to\infty} \gamma(t) = \boldsymbol{x}$.*
4. *If there is another equilibrium point $\boldsymbol{y} \in M$ such that $\lim_{t\to\infty} \gamma(t) = \boldsymbol{x}$ and $\lim_{t\to-\infty} \gamma(t) = \boldsymbol{y}$, then γ is a **heteroclinic orbit**.*

Let us introduce now some concepts about the subsets of the phase portrait of a dynamical system, the definitions of invariant, stable, unstable manifold.

Definition 14 *We say that $\Omega \subset M$ is an **invariant set** if $\varphi(\Omega, t) \subset \Omega$, $\forall t \in \mathbb{R}$. We say that Ω is **stable** if $\forall U$ neighborhood of Ω, there is another neighborhood V such that $\boldsymbol{x} \in V$ implies $\gamma_{\boldsymbol{x}} \in U$, $\forall t \in \mathbb{R}$.*

Remark 2 *If Ω has a structure of C^k-manifold, then the set Ω is called an **invariant manifold**.*

Definition 15 *Let be $\boldsymbol{x}^0$ a stationary point. We define the **stable manifold** of $\boldsymbol{x}^0$ by*

$$\mathcal{W}_s(\boldsymbol{x}^0) = \{\boldsymbol{x} \in M, \lim_{t\to\infty} \varphi_t(\boldsymbol{x}) = \boldsymbol{x}^0\}.$$

*The **unstable manifold** of $\boldsymbol{x}^0$ is defined as*

$$\mathcal{W}_u(\boldsymbol{x}^0) = \{\boldsymbol{x} \in M, \lim_{t\to-\infty} \varphi_t(\boldsymbol{x}) = \boldsymbol{x}^0\}.$$

Definition 16 *A **first integral** of a dynamical system is a function $J : M \to \mathbb{R}$ that is constant on all the trajectories of the system ($J(\varphi_t(\boldsymbol{x})) = const$).*

2.1.3 Dynamical systems from ordinary differential equations

In the present thesis, we are interested in those dynamical systems for which the time-evolution law is given by the solution of a Cauchy problem (initial value problem) for a system of ordinary differential equations (ODE). More precisely, let us consider $\mathbf{I}_{open} \subset \mathbb{R}$ and $\Omega_{open} \subset \mathbb{R}^n$.

Definition 17 *A function $f : \mathbf{I} \times \Omega \to \mathbb{R}^n$ is **locally Lipschitz** in Ω if for every compact set $\mathbf{K} \subset \mathbf{I} \times \Omega$ there exists a constant $L = L(\mathbf{K}) > 0$ such that $\|f(t, \boldsymbol{y}) - f(t, \boldsymbol{x})\| \leq L\|\boldsymbol{y} - \boldsymbol{x}\|$, $\forall (t, \boldsymbol{x}), (t, \boldsymbol{y}) \in \mathbf{K}$.*

Now, we introduce the initial value problem (or the Cauchy problem) for a system of ODEs.

Definition 18 *The Cauchy problem (IVP) consists in finding a function $x : \mathbf{J} \subseteq \mathbf{I} \to \Omega$ such that it satisfies*

$$\begin{cases} \boldsymbol{x}'(t) = f(t, \boldsymbol{x}(t)) \\ \boldsymbol{x}(t_0) = \boldsymbol{x}^0 \end{cases}$$

for all $t \in \mathbf{J}$, where $t_0 \in \mathbf{J}$ and $\boldsymbol{x}^0 \in \Omega$.

The most important result from the theory of ordinary differential equations is the following.

Theorem 2 *For a locally Lipschitz function $f : \mathbf{I} \times \Omega \to \Omega$, there exists a unique solution $\boldsymbol{x}'(t) : \mathbf{J} \subset \mathbf{I} \to \Omega$ for the Cauchy problem, where $t_0 \in \mathbf{J}$.*

In the following we describe the connection between a dynamical system and the Cauchy problem.

Proposition 1 *A function $f : \mathbb{R}^n \to \mathbb{R}^n$ of class C^1 on $\mathbb{R}^n$ is locally Lipschitz on $\mathbb{R}^n$.*

Let be $\boldsymbol{X}(t; t_0, \boldsymbol{x}^0)$ a solution for a Cauchy problem.

Definition 19 *We define a dynamical system on Ω that is described by a system of differential equations of the Cauchy problem, through the flow function*

$$\varphi(\boldsymbol{y}, t) = \boldsymbol{x}(t; 0, \boldsymbol{y}).$$

Remark 3 *Since the solution $\boldsymbol{x}$ is unique and continuous (as a solution of the Cauchy problem), the flow φ is well-defined.*

The concepts of autonomous systems and dissipative systems are introduced in the following definitions.

Definition 20 *We say that a dynamical system is **autonomous**, if the function f does not depend explicitly on the time. Otherwise, we call the system **non-autonomous**.*

Definition 21 *We say that an autonomous system is (contractive) **dissipative**, if f has the property that $\det(\mathbf{J}_{\boldsymbol{x_0}}(f)) < 0$, where $\mathbf{J}$ is the Jacobian matrix and $x_0 \in \Omega$.*

Once we have defined the dynamical systems that come from an IVP of an ODE system, we can make use of the theorems and results of stability for the ordinary differential equations (see for example (Perko, 2001)).

2.2 Hamiltonian formalism

An important class of dynamical systems is represented by the Hamiltonian systems. The Hamiltonian formalism is usually introduced starting from the equations of Euler-Lagrange[1]

$$\frac{d}{dt}\left(\frac{\partial L}{\partial \dot{\boldsymbol{q}}}\right) - \frac{\partial L}{\partial \boldsymbol{q}} = 0, \tag{2.1}$$

where $\boldsymbol{q}, \dot{\boldsymbol{q}} \in \mathbb{R}^n$ and $L : \mathbb{R} \times \mathbb{R}^n \times \mathbb{R}^n \to \mathbb{R}$ is the Lagrangian function, usually defined as $L(t, \boldsymbol{q}, \dot{\boldsymbol{q}}) = T(\dot{\boldsymbol{q}}(t)) - V(\boldsymbol{q}(t))$, namely the difference between the kinetic energy and the potential energy. The equations (2.1) describe a system of n second order differential equations.
We introduce the generalized momenta $\boldsymbol{p}$ conjugated to the generalized coordinates $\boldsymbol{q}$ as

$$\boldsymbol{p}(t) = \frac{\partial L}{\partial \dot{\boldsymbol{q}}}(t, \boldsymbol{q}(t), \dot{\boldsymbol{q}}(t));$$

from the Euler-Lagrange equations we have

$$\dot{\boldsymbol{p}}(t) = \frac{\partial L}{\partial \boldsymbol{q}}(t, \boldsymbol{q}(t), \dot{\boldsymbol{q}}(t)).$$

[1]The Euler-Lagrange equations are defined by solving a variational problem (the least action principle or Maurpetuis principle,see, for example, (Arnold, 1978), (Junkins and Schaub, 2009)).

Using the Legendre transformation, we define the Hamiltonian function as

$$H(t,\boldsymbol{q},\boldsymbol{p}) = \boldsymbol{p}\cdot\dot{\boldsymbol{q}} - L(t,\boldsymbol{q},\dot{\boldsymbol{q}}), \tag{2.2}$$

for which the corresponding differential is given by

$$\begin{aligned} dH(t,\boldsymbol{q},\boldsymbol{p}) &= \dot{\boldsymbol{q}}d\boldsymbol{p} + \boldsymbol{p}d\dot{\boldsymbol{q}} - \frac{\partial L}{\partial \dot{\boldsymbol{q}}}(t,\boldsymbol{q}(t),\dot{\boldsymbol{q}}(t))d\dot{\boldsymbol{q}} - \frac{\partial L}{\partial \boldsymbol{q}}(t,\boldsymbol{q}(t),\dot{\boldsymbol{q}}(t))d\boldsymbol{q} - \frac{\partial L}{\partial t}(t,\boldsymbol{q}(t),\dot{\boldsymbol{q}}(t))dt \\ &= \dot{\boldsymbol{q}}d\boldsymbol{p} - \frac{\partial L}{\partial \boldsymbol{q}}(t,\boldsymbol{q}(t),\dot{\boldsymbol{q}}(t))d\boldsymbol{q} - \frac{\partial L}{\partial t}(t,\boldsymbol{q}(t),\dot{\boldsymbol{q}}(t))dt \end{aligned} \tag{2.3}$$

From the definition of differential of $H(t,\boldsymbol{q},\boldsymbol{p})$

$$dH(t,\boldsymbol{q},\boldsymbol{p}) = \frac{\partial H}{\partial \boldsymbol{p}}d\boldsymbol{p} + \frac{\partial H}{\partial \boldsymbol{q}}d\boldsymbol{q} + \frac{\partial H}{\partial t}dt,$$

and taking into account that $\frac{\partial L}{\partial \boldsymbol{q}}(t,\boldsymbol{q}(t),\dot{\boldsymbol{q}}(t)) = \dot{\boldsymbol{p}}(t)$, by comparison of the coefficients, we obtain

$$\begin{aligned} \dot{\boldsymbol{q}} &= \frac{\partial H}{\partial \boldsymbol{p}}(t,\boldsymbol{q},\boldsymbol{p}) \\ \dot{\boldsymbol{p}} &= -\frac{\partial H}{\partial \boldsymbol{q}}(t,\boldsymbol{q},\boldsymbol{p}), \end{aligned} \tag{2.4}$$

which are called **Hamilton's equations**. These equations define the dynamical system described by the Hamiltonian function H.

Definition 22 *If the Hamiltonian function depends explicitly on time $t \in \mathbb{R}$, then we say that the Hamiltonian system is **non-autonomous**. Otherwise, the system is **autonomous**.*

Remark 4 *An important point here is the fact that we can transform a non-autonomous Hamiltonian $H(t,\boldsymbol{q},\boldsymbol{p})$ into an autonomous one $\tilde{H}(\tilde{\boldsymbol{q}},\tilde{\boldsymbol{p}})$, by extending the phase space, namely taking $q_0 = t$ ($\dot{q}_0 = 1$) and its conjugated coordinate p_0 such that $\tilde{\boldsymbol{q}} = (\boldsymbol{q}, q_0)$, $\tilde{\boldsymbol{p}} = (\boldsymbol{p}, p_0)$, and $\tilde{H}(\tilde{\boldsymbol{q}},\tilde{\boldsymbol{p}}) := H(q_0,\boldsymbol{q},\boldsymbol{p}) + p_0$.*

In the following, we focus on the autonomous Hamiltonian system which can be shortly written as

$$\dot{\boldsymbol{x}} = \begin{bmatrix}\dot{\boldsymbol{q}}\\ \dot{\boldsymbol{p}}\end{bmatrix} = \mathbf{J}\nabla H(\boldsymbol{x}) = \begin{cases}\frac{\partial H}{\partial \boldsymbol{p}}(\boldsymbol{q},\boldsymbol{p})\\ -\frac{\partial H}{\partial \boldsymbol{q}}(\boldsymbol{q},\boldsymbol{p})\end{cases}, \tag{2.5}$$

where $\boldsymbol{x} = (\boldsymbol{q},\boldsymbol{p})^T$ and

$$\mathbf{J} = \begin{bmatrix}\mathbf{0} & \mathbf{I}_n\\ -\mathbf{I}_n & \mathbf{0}\end{bmatrix}$$

We use the notation $\mathbf{X}_H := \mathbf{J}\nabla H(\boldsymbol{x})$ for the vector field generated by H. Let us take now two Hamiltonian functions $F(\boldsymbol{q},\boldsymbol{p})$ and $G(\boldsymbol{q},\boldsymbol{p})$.

Definition 23 *We define the **Poisson bracket** of F and G, denoted as $\{\cdot,\cdot\}$, the function defined by*

$$\{F(\boldsymbol{q},\boldsymbol{p}), G(\boldsymbol{q},\boldsymbol{p})\} = \frac{\partial F}{\partial \boldsymbol{q}}\cdot\frac{\partial G}{\partial \boldsymbol{p}} - \frac{\partial F}{\partial \boldsymbol{p}}\cdot\frac{\partial G}{\partial \boldsymbol{q}}.$$

It can be easily proven that the **Jacobi identity**

$$\{\{F,G\},H\} + \{\{G,H\},F\} + \{\{H,F\},G\} = 0,$$

holds for any Hamiltonians F, G and H.
Let $f : \mathcal{M} \to \mathbb{R}$ be a real-valued differentiable function. If the flow $(\boldsymbol{q}(t), \boldsymbol{p}(t))$ is determined by the system (2.5), then the derivative of $f(\boldsymbol{q}(t), \boldsymbol{p}(t))$ is given by

$$\frac{d}{dt} f(\boldsymbol{q}(t), \boldsymbol{p}(t)) = \frac{\partial f}{\partial \boldsymbol{q}} \cdot \dot{\boldsymbol{q}} + \frac{\partial f}{\partial \boldsymbol{p}} \cdot \dot{\boldsymbol{p}} = \Big\{ f, H \Big\}. \tag{2.6}$$

Definition 24 *We introduce the **Lie derivative** as a function $L_H : \mathcal{F} \to \mathcal{F}$, where $\mathcal{F}$ is the set of differentiable functions on the manifold $\mathcal{M}$[2], defined by the following formula*

$$L_H := \frac{\partial H}{\partial \boldsymbol{p}} \cdot \frac{\partial}{\partial \boldsymbol{q}} - \frac{\partial H}{\partial \boldsymbol{q}} \cdot \frac{\partial}{\partial \boldsymbol{p}}. \tag{2.7}$$

From (2.6) and applying (2.7) to a differentiable function F, we obtain that

$$L_H F = \Big\{ F, H \Big\}. \tag{2.8}$$

We denote by L_H^k the kth composition of the Lie derivative which is given recurrently by

$$L_H^k = L_H(L_H^{k-1}).$$

We use the notation $L_H^0(F) = F$. The operator L_H^k has the following properties:

$$\begin{aligned} L_H^k(aF + bG) &= aL_H^k F + bL_H^k G, \\ L_H^k(F \cdot G) &= \sum_{0 \le p \le k} \binom{p}{k} L_H^p F \cdot L_H^{k-p} G, \\ L_H^k(\{F, G\}) &= \sum_{0 \le p \le k} \binom{p}{k} \{L_H^p F, L_H^{k-p} G\}. \end{aligned}$$

Definition 25 *The **Lie series operator** S_H^ε is defined through the expression*

$$S_H^\varepsilon := \sum_{k=0}^{\infty} \frac{\varepsilon^k}{k!} L_H^k \,, \tag{2.9}$$

when H satisfies the conditions that the series expansion in (2.9) is convergent.

In Hamiltonian systems theory, an important role is played by the change of coordinates which simplifies the form of the Hamiltonian function and preserves the canonical structure of the equations (see (Giorgilli, 2022)). Let $(\boldsymbol{q}, \boldsymbol{p})$ be the old coordinates for a Hamiltonian function H and let $(\boldsymbol{Q}, \boldsymbol{P})$ be such that $(\boldsymbol{q}, \boldsymbol{p}) = \mathcal{T}(\boldsymbol{Q}, \boldsymbol{P})$.

Definition 26 *We say that a transformation $\mathcal{T}$ is canonical if for any Hamiltonian $H(\boldsymbol{q}, \boldsymbol{p})$ we can find a Hamiltonian $K(\boldsymbol{Q}, \boldsymbol{P})$ such that one of the following conditions are satisfied*

1. *The system (2.5) is analogous to the system (the transformation preserves the canonical form of the Hamilton's equations)*

$$\begin{cases} \dot{\boldsymbol{Q}} = \frac{\partial K}{\partial \boldsymbol{P}}(\boldsymbol{Q}, \boldsymbol{P}) \\ \dot{\boldsymbol{P}} = -\frac{\partial K}{\partial \boldsymbol{Q}}(\boldsymbol{Q}, \boldsymbol{P}) \end{cases}, \tag{2.10}$$

[2] In a general case, if $\mathbf{X}$ is a vector field on $\mathbb{R}^n$, $\mathcal{D}$ the set of differentiable function on $\mathbb{R}^n$, and $\psi_t^{\mathbf{X}}$ the flow generated by $\mathbf{X}$, then the Lie derivative is a function $L_{\mathbf{X}} : \mathcal{D} \to \mathcal{D}$ defined by $L_{\mathbf{X}} F(\boldsymbol{x}) := \frac{d}{dt} F(\psi_t^{\mathbf{X}}(\boldsymbol{x}))$, for $F \in \mathcal{D}$.

2. *The new Hamiltonian K is equal to the old Hamiltonian H expressed in the new variables: $K(\boldsymbol{Q},\boldsymbol{P}) = H(\boldsymbol{q},\boldsymbol{p})|_{\boldsymbol{q}=\boldsymbol{q}(\boldsymbol{Q},\boldsymbol{P}),\boldsymbol{p}=\boldsymbol{p}(\boldsymbol{Q},\boldsymbol{P})}$.*

Proposition 2 *A transformation $\mathcal{T}$ is canonical iff it preserves the Poisson brackets, i.e.*

$$\{q_j, q_k\}_{\boldsymbol{Q},\boldsymbol{P}} = \{p_j, p_k\}_{\boldsymbol{Q},\boldsymbol{P}} = 0, \qquad \{q_j, p_k\}_{\boldsymbol{Q},\boldsymbol{P}} = \delta_{jk}, \forall j,k. \tag{2.11}$$

Remark 5 *Since the composition of two canonical transformations is a canonical transformation, a useful application of the Poisson brackets (and Lie series operator) is in finding infinitesimal canonical transformations.*

The integrability of a Hamiltonian system (2.5) is usually analyzed by the computation of the first integrals.

Definition 27 *We say that two functions F and G are in **involution**, if their Poisson bracket is zero, $\{F,G\} = 0$. Moreover, a system of functions $\{F_1(\boldsymbol{q},\boldsymbol{p}),\ldots,F_n(\boldsymbol{q},\boldsymbol{p})\}$ is said to be an involution system, if it is a functional independent system and every pair of the system is in involution.*

Definition 28 *We say that a function F is a first integral for a Hamiltonian system (2.5) iff the functions F and H are in involution.*

Theorem 3 ***(Liouville - Arnold)** We assume that an autonomous Hamiltonian system as defined in (2.5) admits an involution system $\{F_1(\boldsymbol{q},\boldsymbol{p}),\ldots,F_n(\boldsymbol{q},\boldsymbol{p})\}$ and that the manifold defined by $M_0 = \{\boldsymbol{x} \mid F_i(\boldsymbol{x}) = 0, i = \overline{1,n}\}$ is connected and compact. Then*

1. *The system (2.5) can be integrated by quadratures.*
2. *M_0 is diffeomorphic to a n-dimensional torus $T^N = \{\varphi_1,\ldots,\varphi_n \bmod 2\pi\}$. Thus, in a neighborhood $V(M_0)$ of M_0, there exists a transformation of coordinates from $(\boldsymbol{q},\boldsymbol{p})$ to the **action-angle** variables $\boldsymbol{I} \in B_{open} \subset \mathbb{R}^n$ and $\boldsymbol{\varphi} \in T^n$, such that the system (2.5) takes the form*

$$\begin{cases} \dot{\boldsymbol{\varphi}} = \frac{\partial H}{\partial \boldsymbol{I}}(\boldsymbol{I}) \\ \dot{\boldsymbol{I}} = 0 \end{cases} . \tag{2.12}$$

2.3 Perturbation theory with Lie series

Let $\mathcal{H} = \mathcal{H}(\boldsymbol{I},\boldsymbol{\varphi})$ be a Hamiltonian function defined in terms of action-angle variables $(\boldsymbol{I},\boldsymbol{\varphi}) \in B \times \mathbb{T}^n$, where $B \subset \mathbb{R}^n$ is an open set and n denotes the number of degrees of freedom. We write the Hamiltonian as

$$\mathcal{H}(\boldsymbol{I},\boldsymbol{\varphi}) = \mathcal{H}_0(\boldsymbol{I}) + \varepsilon\mathcal{H}_1(\boldsymbol{I},\boldsymbol{\varphi}) , \tag{2.13}$$

where $\mathcal{H}_0(\boldsymbol{I})$ represents the integrable part, $\mathcal{H}_1(\boldsymbol{I},\boldsymbol{\varphi})$ is the perturbing term and ε represents a small parameter. We assume that $\mathcal{H}_1$ is the sum of products between functions depending on actions, and sines or cosines of different combinations of angles; hence, $\mathcal{H}_1$ can be expanded in Fourier series as

$$\mathcal{H}_1(\boldsymbol{I},\boldsymbol{\varphi}) = \sum_{\boldsymbol{k}\in\mathcal{K}} b_{\boldsymbol{k}}(\boldsymbol{I}) \exp(i\boldsymbol{k}\cdot\boldsymbol{\varphi}) , \tag{2.14}$$

where $\mathcal{K} \subseteq \mathbb{Z}^n$ and $b_{\boldsymbol{k}}$ denote complex conjugates pairs.

2.3.1 Computation of the non-resonant normal form

In this section we describe the computation of the normal form in the case of non-resonant dynamics, namely when the scalar product between the frequency vector $\omega_0 = \frac{\partial \mathcal{H}_0}{\partial I}$ and the vector of coefficients of the angles involved in $\mathcal{H}_1$ is not equal to 0.
We look for a canonical transformation with a generating function χ that allows us to perform the change of variables from $(\boldsymbol{I}, \boldsymbol{\varphi})$ to $(\boldsymbol{I}', \boldsymbol{\varphi}')$ defined through the expressions

$$\boldsymbol{I} = S^{\varepsilon}_{\chi} \boldsymbol{I}' , \qquad \boldsymbol{\varphi} = S^{\varepsilon}_{\chi} \boldsymbol{\varphi}' , \tag{2.15}$$

where the operator S^{ε}_{χ} is the Lie derivative (2.9).
The function χ must be chosen so that the transformed Hamiltonian $\mathcal{H}^{(1)} = S^{\varepsilon}_{\chi} \mathcal{H}$ takes the following expression:

$$\mathcal{H}^{(1)}(\boldsymbol{I}', \boldsymbol{\varphi}') = \mathcal{H}^{(1)}_0(\boldsymbol{I}') + \varepsilon \mathcal{H}^{(1)}_1(\boldsymbol{I}') + \varepsilon^2 \mathcal{H}^{(1)}_2(\boldsymbol{I}', \boldsymbol{\varphi}') , \tag{2.16}$$

where $\mathcal{H}^{(1)}_0 + \varepsilon \mathcal{H}^{(1)}_1$ is the new integrable Hamiltonian (depending just on the new actions) and $\mathcal{H}^{(1)}_2$ is the remainder term.
Inserting the transformation (2.15) into (2.13), and expanding in Taylor series in the parameter ε, one obtains that the transformed Hamiltonian is given by

$$\begin{aligned} \mathcal{H}^{(1)}(\boldsymbol{I}', \boldsymbol{\varphi}') &= \mathcal{H}_0(\boldsymbol{I}(\boldsymbol{I}', \boldsymbol{\varphi}')) \\ &+ \varepsilon \mathcal{H}_1(\boldsymbol{I}(\boldsymbol{I}', \boldsymbol{\varphi}'), \boldsymbol{\varphi}(\boldsymbol{I}', \boldsymbol{\varphi}')) + \varepsilon \Big\{ \mathcal{H}_0(\boldsymbol{I}(\boldsymbol{I}', \boldsymbol{\varphi}')), \chi(\boldsymbol{I}(\boldsymbol{I}', \boldsymbol{\varphi}'), \boldsymbol{\varphi}(\boldsymbol{I}', \boldsymbol{\varphi}')) \Big\} \\ &+ \varepsilon^2 \Big\{ \mathcal{H}_1(\boldsymbol{I}(\boldsymbol{I}', \boldsymbol{\varphi}'), \boldsymbol{\varphi}(\boldsymbol{I}', \boldsymbol{\varphi}')), \chi(\boldsymbol{I}(\boldsymbol{I}', \boldsymbol{\varphi}'), \boldsymbol{\varphi}(\boldsymbol{I}', \boldsymbol{\varphi}')) \Big\} \\ &+ \frac{\varepsilon^2}{2} \Big\{ \Big\{ \mathcal{H}_0(\boldsymbol{I}(\boldsymbol{I}', \boldsymbol{\varphi}')), \chi(\boldsymbol{I}(\boldsymbol{I}', \boldsymbol{\varphi}'), \boldsymbol{\varphi}(\boldsymbol{I}', \boldsymbol{\varphi}')) \Big\}, \chi(\boldsymbol{I}(\boldsymbol{I}', \boldsymbol{\varphi}'), \boldsymbol{\varphi}(\boldsymbol{I}', \boldsymbol{\varphi}')) \Big\} + \dots \end{aligned} \tag{2.17}$$

To obtain a Hamiltonian function of the form (2.16), we must impose that the function in (2.17), that contains only terms of first order in ε, does not depend on the angles. This allows us to determine the generating function χ as the solution of the following homological equation:

$$\mathcal{H}_1(\boldsymbol{I}(\boldsymbol{I}', \boldsymbol{\varphi}'), \boldsymbol{\varphi}(\boldsymbol{I}', \boldsymbol{\varphi}')) + \Big\{ \mathcal{H}_0(\boldsymbol{I}(\boldsymbol{I}', \boldsymbol{\varphi}')), \chi(\boldsymbol{I}(\boldsymbol{I}', \boldsymbol{\varphi}'), \boldsymbol{\varphi}(\boldsymbol{I}', \boldsymbol{\varphi}')) \Big\} = \mathcal{H}^{(1)}_1(\boldsymbol{I}') . \tag{2.18}$$

Taking into account the expression (2.14) for $\mathcal{H}_1$, we look for a generating function of the form

$$\chi(\boldsymbol{I}(\boldsymbol{I}', \boldsymbol{\varphi}'), \boldsymbol{\varphi}(\boldsymbol{I}', \boldsymbol{\varphi}')) = \sum_{\boldsymbol{k} \in \mathbb{Z}^n \setminus \boldsymbol{0}} c_{\boldsymbol{k}}(\boldsymbol{I}(\boldsymbol{I}', \boldsymbol{\varphi}')) \exp(i \boldsymbol{k} \cdot \boldsymbol{\varphi}(\boldsymbol{I}', \boldsymbol{\varphi}')) , \tag{2.19}$$

where the coefficients $c_{\boldsymbol{k}}$ will be determined through (2.18). In fact, denoting by $\omega_0 = \frac{\partial \mathcal{H}_0}{\partial \boldsymbol{I}}$, we obtain

$$\Big\{ \mathcal{H}_0(\boldsymbol{I}(\boldsymbol{I}', \boldsymbol{\varphi}')), \chi(\boldsymbol{I}(\boldsymbol{I}', \boldsymbol{\varphi}'), \boldsymbol{\varphi}(\boldsymbol{I}', \boldsymbol{\varphi}')) \Big\} = -i \sum_{\boldsymbol{k} \in \mathbb{Z}^n \setminus \{\boldsymbol{0}\}} c_{\boldsymbol{k}}(\boldsymbol{I}(\boldsymbol{I}', \boldsymbol{\varphi}'))\ \boldsymbol{k} \cdot \omega_0\ \exp(i \boldsymbol{k} \cdot \boldsymbol{\varphi}(\boldsymbol{I}', \boldsymbol{\varphi}')) . \tag{2.20}$$

Then, equation (2.18) is satisfied provided the coefficients $c_{\boldsymbol{k}}$ are defined as

$$c_{\boldsymbol{k}}(\boldsymbol{I}(\boldsymbol{I}', \boldsymbol{\varphi}')) = -i \frac{b_{\boldsymbol{k}}(\boldsymbol{I}(\boldsymbol{I}', \boldsymbol{\varphi}'))}{\boldsymbol{k} \cdot \omega_0} , \qquad \boldsymbol{k} \neq \boldsymbol{0} . \tag{2.21}$$

Since $\boldsymbol{k}\cdot\boldsymbol{\omega}_0 \neq \mathbf{0}$, the condition of small divisors is satisfied. Hence, the generating function takes the form

$$\chi(\boldsymbol{I}(\boldsymbol{I}',\boldsymbol{\varphi}'),\boldsymbol{\varphi}(\boldsymbol{I}',\boldsymbol{\varphi}')) = -\sum_{\boldsymbol{k}\in\mathbb{Z}^n\setminus\mathbf{0}} i\frac{b_{\boldsymbol{k}}(\boldsymbol{I}(\boldsymbol{I}',\boldsymbol{\varphi}'))}{\boldsymbol{k}\cdot\boldsymbol{\omega}_0}\,\exp(i\boldsymbol{k}\cdot\boldsymbol{\varphi}(\boldsymbol{I}',\boldsymbol{\varphi}'))\,. \tag{2.22}$$

As a consequence, the new Hamiltonian takes the form (2.16). If one discards the terms of order ε^2, the normal form is integrable up to orders of ε^2.

Remark 6 *If, instead, we keep the terms of order ε^2, we can iterate the procedure to higher orders to improve the accuracy of the Hamiltonian normal form. In this case, the new integrable part is given by $\mathcal{H}_0^{(1)}(\boldsymbol{I}') + \varepsilon\mathcal{H}_1^{(1)}(\boldsymbol{I}')$ and the perturbation is the remainder $\varepsilon^2\mathcal{H}_2^{(1)}(\boldsymbol{I}',\boldsymbol{\varphi}')$. The algorithm will provide a new generating function that can be constructed explicitly, using a procedure similar to that leading to (2.22).*

The transformation (2.15) provides explicitly the function $\mathcal{T}$ that transforms the initial to the new variables $(\boldsymbol{I},\boldsymbol{\varphi}) = \mathcal{T}(\boldsymbol{I}',\boldsymbol{\varphi}')$. This transformation is canonical, and even more, the inverse of this transformation $\mathcal{T}^{-1}$ is given by

$$\boldsymbol{I}' = S^{\varepsilon}_{-\chi}\boldsymbol{I}\,, \qquad \boldsymbol{\varphi}' = S^{\varepsilon}_{-\chi}\boldsymbol{\varphi}\,. \tag{2.23}$$

The transformation (2.23) might be used to obtain the initial conditions for the new Hamiltonian system[3], in order to find the solution of Hamilton's equation

$$\begin{cases}\dot{\boldsymbol{\varphi}}' = \frac{\partial\mathcal{H}^{(1)}}{\partial\boldsymbol{I}'}(\boldsymbol{I}')\\ \dot{\boldsymbol{I}}' = 0\end{cases} \tag{2.24}$$

for some initial conditions $\boldsymbol{\varphi}(t_0) = \boldsymbol{\varphi}^0$ and $\boldsymbol{I}(t_0) = \boldsymbol{I}^0$.

2.3.2 Resonant normal form - small divisors

A key-point in the algorithm presented in Section 2.3 is the solution of the homological equation (2.20) in order to obtain the generating function χ. As it can be seen in (2.21), the function χ (2.22) is well-defined when $\boldsymbol{k}\cdot\boldsymbol{\omega}_0$ is non-zero.
The problem appears when the scalar product $\boldsymbol{k}\cdot\boldsymbol{\omega}_0 < \epsilon$, for a small ϵ. In this case, we need to prevent the occurrence of those terms at the denominator. This can be easily dealt by defining a set of coefficients $\mathcal{R}_\epsilon \subset \mathbf{Z}\setminus\mathbf{0}$ such that

$$\mathcal{R}_\epsilon = \{\boldsymbol{k}\in\mathbf{Z}\,|\,\boldsymbol{k}\cdot\boldsymbol{\omega}_0 > \epsilon\},$$

which will be used in the computation of the function χ (2.22) as follows

$$\chi(\boldsymbol{I}',\boldsymbol{\varphi}') = -\sum_{\boldsymbol{k}\in\mathcal{R}_\epsilon} i\frac{b_{\boldsymbol{k}}(\boldsymbol{I}')}{\boldsymbol{k}\cdot\boldsymbol{\omega}_0}\,\exp(i\boldsymbol{k}\cdot\boldsymbol{\varphi}')\,. \tag{2.25}$$

By removing the resonant terms from the generating functions, one obtains that such terms will not be removed from the Hamiltonian after the transformation $\mathcal{H}^{(1)} = S^{\varepsilon}_{\chi}\mathcal{H}$. Hence, the transformed Hamiltonian will have the following form

$$\mathcal{H}^{(1)}(\boldsymbol{I}',\boldsymbol{\varphi}') = \mathcal{H}_0^{(1)}(\boldsymbol{I}') + \varepsilon\mathcal{H}_1^{(1)}(\boldsymbol{I}',\boldsymbol{\varphi}') + \varepsilon^2\mathcal{H}_2^{(1)}(\boldsymbol{I}',\boldsymbol{\varphi}')\,. \tag{2.26}$$

[3]This transformation will be also used to compute the proper elements in the Chapter 5.

Nevertheless, the resulting normal form $\mathcal{H}_0^{(1)}(\boldsymbol{I}') + \varepsilon\mathcal{H}_1^{(1)}(\boldsymbol{I}', \boldsymbol{\varphi}')$ has still a simpler form than the initial Hamiltonian (2.13).
The number of degrees of freedom of the normal form is equal to the number of the elements of $\mathcal{R}$. Thus, if $|\mathcal{R}| = 1$, we still end up with an integrable normal form, after the first order normalization. Nevertheless, in this case it is very hard to find the solution of Hamilton's equations of $\mathcal{H}^{(1)}$, but we can still analyze the stability aspects, since we have to deal with a less complicated dynamical system.

2.3.3 Iterative algorithm to compute the normal form

As it is mentioned in Remark 6, the algorithm presented in Section 2.3, even in the resonant case can be iterated to higher orders. Let us denote by N the order of normalization. We will adopt the following notation:

1. $\mathcal{H}^{(N)}$ - the Hamiltonian function obtained after N steps of normalization.
2. $\mathcal{H}_0^{(N)}(\boldsymbol{I}^N) + \varepsilon\mathcal{H}_1^{(N)}(\boldsymbol{I}^N) + \cdots + \varepsilon^N\mathcal{H}_N^{(N)}(\boldsymbol{I}^N)$ - the normal form of the Hamiltonian after N steps of normalization.
3. $\varepsilon^{N+1}\mathcal{H}_{N+1}^{(N)}(\boldsymbol{I}^N, \boldsymbol{\varphi}^N)$ - the remainder obtained after N normalization steps.
4. χ^N - the generating function obtained at order N.
5. $(\boldsymbol{I}^N, \boldsymbol{\varphi}^N)$ - the action-angle variables at order N.

At step N, we want to find a generating function χ^{N+1} as the solution of the following equation

$$\begin{aligned}\Big\{\mathcal{H}_0^N(\boldsymbol{I}^N(\boldsymbol{I}^{N+1}, \boldsymbol{\varphi}^{N+1})), \chi^{N+1}(\boldsymbol{I}^N(\boldsymbol{I}^{N+1}, \boldsymbol{\varphi}^{N+1}), \boldsymbol{\varphi}^N(\boldsymbol{I}^{N+1}, \boldsymbol{\varphi}^{N+1}))\Big\} + \\ \mathcal{H}_{N+1}^N(\boldsymbol{I}^N(\boldsymbol{I}^{N+1}, \boldsymbol{\varphi}^{N+1}), \boldsymbol{\varphi}^N(\boldsymbol{I}^{N+1}, \boldsymbol{\varphi}^{N+1})) = \mathcal{H}_{N+1}^{(N+1)}(\boldsymbol{I}^{N+1}) \,,\end{aligned} \tag{2.27}$$

whose solution can be obtained similarly as in (2.19)-(2.22).
Once obtained the generating function χ^{N+1}, we apply the Lie derivative to the Hamiltonian function $H^{(N)}$, say $\mathcal{H}^{(N+1)} = S^{\varepsilon}_{\chi^{N+1}}\mathcal{H}^{(N)}$, and obtain the transformed Hamiltonian

$$\begin{aligned}\mathcal{H}^{(N+1)}(\boldsymbol{I}^{N+1}, \boldsymbol{\varphi}^{N+1}) &= \mathcal{H}_0^{(N+1)}(\boldsymbol{I}^{N+1}) + \cdots + \varepsilon^{N+1}\mathcal{H}_{N+1}^{(N+1)}(\boldsymbol{I}^{N+1}) \\ &+ \varepsilon^{N+2}\mathcal{H}_{N+2}^{(N+1)}(\boldsymbol{I}^{N+1}, \boldsymbol{\varphi}^{N+1}) \,.\end{aligned} \tag{2.28}$$

The canonical transformation of variables from $(\boldsymbol{I}, \boldsymbol{\varphi})$ to $(\boldsymbol{I}^{N+1}, \boldsymbol{\varphi}^{N+1})$ can be obtained recursively from $\boldsymbol{I}^N = S^{\varepsilon}_{\chi^{N+1}}\boldsymbol{I}^{N+1}, \boldsymbol{\varphi}^N = S^{\varepsilon}_{\chi^{N+1}}\boldsymbol{\varphi}^{N+1}$ as follows

$$\boldsymbol{I} = S^{\varepsilon}_{\chi^1}S^{\varepsilon}_{\chi^2}\ldots S^{\varepsilon}_{\chi^{N+1}}\boldsymbol{I}^{N+1} \,, \qquad \boldsymbol{\varphi} = S^{\varepsilon}_{\chi^1}S^{\varepsilon}_{\chi^2}\ldots S^{\varepsilon}_{\chi^{N+1}}\boldsymbol{\varphi}^{N+1} \,. \tag{2.29}$$

Remark 7 *In the computational process of higher order normal form, it usually happens that the coefficients of the angles in the new Hamiltonian will be modified at each step. This is called the "variable frequency problem" and it was described in detail in (Milani and Knežević, 1990).*

Chapter 3

A Dynamical Model of Space Debris Motion around the Earth

3.1 Introduction

The motion of an object orbiting around the Earth is affected by several forces that might be taken into account depending on the altitude of the object. The orbital position of the object at any time (past and future) can be approximated by solving a system of differential equations starting from some initial conditions given at a certain time. The accuracy of the position is directly connected with the complexity of the system of equations, and thus it becomes more precise when a very realistic model is used.

In a basic model, the main force that influences the motion of an object is the attraction of the Earth seen as a spherical body. This is usually called the "unperturbed model" or the "Keplerian problem". In order to have a more realistic behavior of the object's evolution, one has to take into account some important aspects such as: the Earth is not a perfect sphere; the object is attracted also by the Moon and the Sun; the radiation pressure of the Sun might affect some objects with large area and small mass.

The drawback of a complex dynamical system consists in its heavy integration process to find solutions. Depending on the studied problem, one has to make a trade-off between the accuracy of the solution and the computational time required to find it. Also, another important aspect is the aimed horizon of time. The accuracy of the solution is directly related to the horizon of time. If the horizon of time is small, we obtain very little, but accurate, information about an orbit. On the other hand, if the horizon of time is large, we obtain more information, but not very accurate.

In Section 3.2, we will describe the common reference frames used in the problem of space debris motion. In order to have a clear description of the forces involved, it is important to decide the initial time T_0 and which is the position of the objects involved at that time. Then, we can define our proper units in order to simplify the computations. Section 3.3 is devoted to the Newtonian approach of the problem. In Section 3.4, we will describe the Hamiltonian formulation of the problem in two different ways.

3.2 Reference frame

There are two main sets of elements that describe the position of an object in the Earth's orbit: the state vector and the Keplerian orbital elements. The state vector is a vector of six components that describes the position and the velocity of an object in the Earth's orbit. The position and the velocity have to be expressed w.r.t. a well-defined reference system and time (a detailed description can be found, for example, in (Vallado and McClain, 2001)). There are several reference frames that can be used in different situations (Montenbruck, Gill, and Lutze, 2002), but we will describe in this section the most important one for our purpose.

3.2.1 Reference system

In astrodynamics, the motion of an object is seen as the motion of a particle in a Euclidean space; hence the reference system could be a simple non-rotating Cartesian coordinate system.

Let O be the origin of an arbitrary reference system, and let $\{\hat{i}, \hat{j}, \hat{k}\}$ be three orthogonal unit vectors. We have the following definitions:

Definition 29 *An **Earth Centered Inertial Frame** (ECIF) is a reference system in which the origin of the reference system is the center of mass of the Earth, and the unit vectors are defined such that $\hat{i}$ is the unit vector pointing towards the First Point of Aries*[1]*, $\hat{k}$ is the unit vector in the direction of the North Pole of the Earth's rotation axis, and $\hat{j}$ is the unit vector chosen to be orthogonal to $\hat{i}$ and $\hat{k}$ with the right-hand rule.*

Definition 30 *We define a **J2000 system** as an ECIF, where $\{\hat{i}, \hat{j}, \hat{k}\}$ are the orthogonal coordinates such that $\hat{i}$-$\hat{j}$ is the plane coinciding with the equatorial plane of the Earth, with $\hat{i}$ pointing the Vernal Equinox of the epoch 2000 January 1, noon (corresponds to 2451545.0 Julian day), and $\hat{k}$ pointing towards to the North Pole of the Earth's rotation axis for the same epoch.*

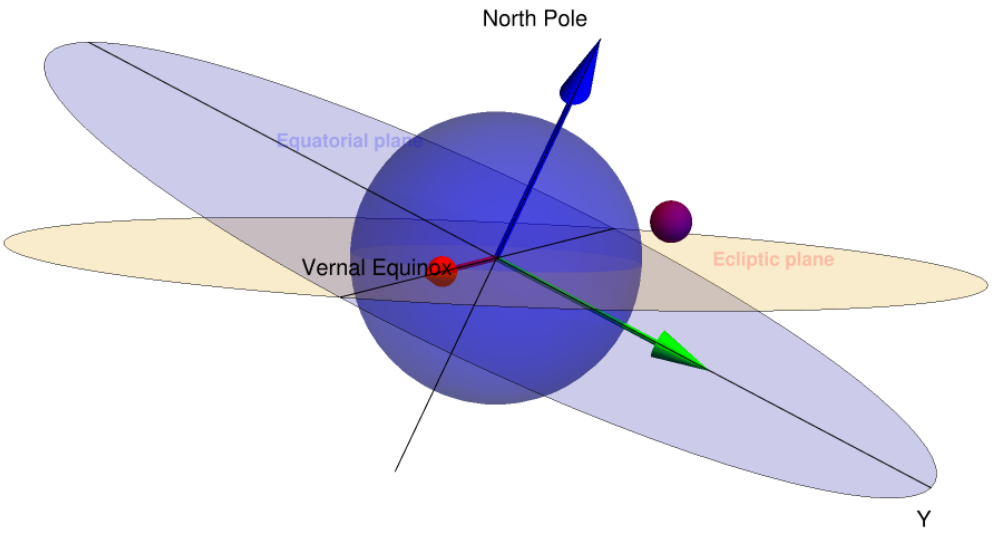

FIGURE 3.1: The ECIF and the J2000 systems.

Definition 31 *A **solar day** is the time it takes for the Earth to complete one rotation around its axis such that the Sun is at the same position at the beginning and the end of the day. The **sidereal day** is the time of the Earth's rotation around its axis with respect to a very distant star. The sidereal day is about 4 minutes shorter than the solar day.*

Denoting by θ the sidereal time, let us define the unit vectors $\{\hat{i}', \hat{j}', \hat{k}'\}$ such that $\hat{k} = \hat{k}'$ and the plane $\hat{i}'$-$\hat{j}'$ is rotated by the angle θ around the axis of the Earth's rotation.

Definition 32 *A **synodic frame** is a rotating reference system with the origin coinciding with the center of mass of the Earth, and the unit vectors $\{\hat{i}', \hat{j}', \hat{k}'\}$ defined as before.*

[1] The vector obtained at the intersection between equatorial and ecliptic planes, pointing to the Vernal Equinox.

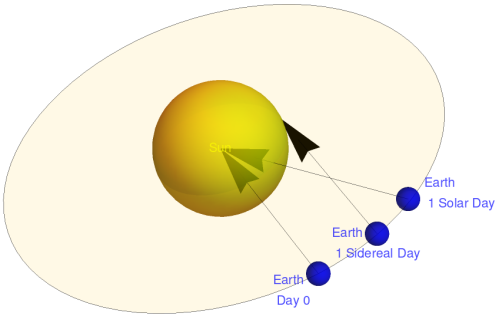

FIGURE 3.2: Solar vs sidereal day.

Remark 8 *The synodic reference frame will be used to describe the potential of the Earth in spherical harmonics. Then, we will use the following relation to define the equations of motion in the J2000 system:*

$$\begin{bmatrix} \hat{i} \\ \hat{j} \\ \hat{k} \end{bmatrix} = \begin{bmatrix} \cos(\theta) & \sin(\theta) & 0 \\ -\sin(\theta) & \cos(\theta) & 0 \\ 0 & 0 & 1 \end{bmatrix} \begin{bmatrix} \hat{i'} \\ \hat{j'} \\ \hat{k'} \end{bmatrix} \tag{3.1}$$

Any point-mass object in space has three degrees of freedom, that means one needs six parameters to describe its motion. In the above reference frame, these parameters are called the state vector of the object, which is composed by the position x, y, z and the velocity v_x, v_y, v_z. However, these elements do not provide a full overview of an object in its orbit for long periods of time. For this purpose, it is convenient to introduce the orbital elements of a space object, a set of elements that describe the size, the shape and the orientation of the orbit, and also the location of the object in the orbit.

3.2.2 From state vector to Keplerian orbital elements

Definition 33 *The Keplerian (classical) orbital elements are the parameters that describe the orbit of an object. They are composed by the following elements:*

- *a is the semi-major axis of the orbit, that gives the size of the orbit*
- *e is the eccentricity of the orbit, that gives the shape of the orbit*
- *i is the inclination of the orbit, that gives the location of the orbit*
- *Ω is the longitude of the ascending node of the orbit, that gives the orientation of the orbit*
- *ω is the argument of periapsis of the orbit, that gives the orientation of the orbit*
- *M is the mean anomaly of the orbit, that gives the location of the object in its orbit*

Proposition 3 *Starting from the state vector $\mathbf{r} = (x, y, z)$ and $\mathbf{v} = (v_x, v_y, v_z)$ of an object in the ECIF reference system, there is a function $\mathcal{X}$ that relates $\mathbf{r}, \mathbf{v}, \mu$ to the orbital elements a, e, i, Ω, ω, M, where μ is the standard gravitational parameter of the Earth.*

Proof 1 Let us denote by $r = \sqrt{x^2+y^2+z^2}$ and $v = \sqrt{v_x^2+v_y^2+v_z^2}$ the distance and speed of the object. The angular momentum per unit mass of the object is $\mathbf{h} = \mathbf{r}\times\mathbf{v}$. The magnitude of the angular momentum is $h = \sqrt{h_x^2+h_y^2+h_z^2}$. From Kepler's third law[2] and the general formula of circular velocity, one can write the energy of the system in two different ways: $\mathcal{E} = \frac{v^2}{2} - \frac{\mu}{r}$ and $\mathcal{E} = -\frac{\mu}{2a}$. Equating the two equations, we obtain that the semi-major axis can be expressed as

$$a = \frac{1}{\frac{2}{r} - \frac{v^2}{\mu}}.$$

The eccentricity vector is pointing from the center of the Earth to the perigee of the orbit and has the following form:

$$\mathbf{e} = \frac{\mathbf{v}\times\mathbf{h}}{\mu} - \frac{\mathbf{r}}{r}.$$

The eccentricity of the orbit is the magnitude of the eccentricity vector $e = \|\mathbf{e}\|$. From the definition of $\mathbf{h}$, we have that $\cos(i) = \frac{h_z}{h}$ and so

$$i = \arccos(\frac{h_z}{h}).$$

The ascending line vector is defined as the intersection of the equatorial plane and the orbital plane, and it is defined as the vector $\mathbf{n} = \hat{k}\times\mathbf{h}$. The longitude of the ascending node is the angle between the ascending node vector and the x axis:

$$\Omega = \begin{cases} \arccos(\frac{n_x}{n}), \text{if } n_y \geq 0 \\ 2\pi - \arccos(\frac{n_x}{n}), \text{if } n_y < 0 \end{cases}.$$

The argument of perigee is the angle between $\mathbf{n}$ and the eccentricity vector:

$$\omega = \begin{cases} \arccos(\frac{\mathbf{n}\cdot\mathbf{e}}{\|\mathbf{n}\|\cdot\|\mathbf{e}\|}), \text{if } e_z \geq 0 \\ 2\pi - \arccos(\frac{\mathbf{n}\cdot\mathbf{e}}{\|\mathbf{n}\|\cdot\|\mathbf{e}\|}), \text{if } e_z < 0 \end{cases}.$$

To compute the mean anomaly, we need to compute the eccentric anomaly, and then the true anomaly which is the angle between the eccentricity vector and the position vector of the object:

$$\nu = \begin{cases} \arccos(\frac{\mathbf{r}\cdot\mathbf{e}}{\|\mathbf{r}\|\cdot\|\mathbf{e}\|}), \text{if } \mathbf{r}\cdot\mathbf{v} \geq 0 \\ 2\pi - \arccos(\frac{\mathbf{r}\cdot\mathbf{e}}{\|\mathbf{r}\|\cdot\|\mathbf{e}\|}), \text{otherwise.} \end{cases}$$

Therefore the eccentric anomaly is computed as:

$$E = 2\arctan(\frac{\tan\frac{\nu}{2}}{\sqrt{\frac{1+e}{1-e}}}).$$

Using Kepler's equation (see, for example, (Celletti, 2010)), we define

$$M = E - e\sin(E)$$

[2] Kepler's laws are the following:

1. The planetary orbits are elliptical with the Sun at a focus,
2. The radius vector from the Sun to a planet sweeps equal areas in equal times,
3. The ratio of the square of the period of revolution and the cube of the ellipse semi-major axis is the same for all planets.

as the mean anomaly.

3.2.3 Proper units

The natural units for distance, time and mass in the space debris problem are kilometers, seconds and kilograms, respectively. However, in order to simplify the computation and to keep a good precision of the numerical results, one might use different units. For example, in this work the unit distance is defined as the distance from the center of the Earth to GEO, and the mass and the time are chosen such that the standard gravitational parameter is equal to 1.

Let us denote by $a_{GEO} = 42164.1715[km]$ our unit distance, $T_{SD} = 86164.0905[s] =$ 1 sidereal day and $\mu_E = 3.986 \cdot 10^5[\frac{km^3}{s^2}]$ the standard gravitational parameter of the Earth.

Name	Value	Unit	Notation
Mean radius of the Earth	≈ 6371	km	R_E
Earth-Sun distance (1 AU)	≈ 149597870.691	km	a_S
Earth-Moon distance	≈ 384400	km	a_M
LEO (Low Earth Orbit)	$[0, 2000]$	km	-
MEO (Medium Earth Orbit)	$(2000, 35000]$	km	-
GEO (Geosynchronous Orbit)	≈ 35786	km	-
High Earth Orbit	> 36000	km	-
Earth standard gravitational parameter	398600.442	$\frac{km^3}{s^2}$	μ_E
Sun standard gravitational parameter	132712440018	$\frac{km^3}{s^2}$	μ_S
Moon standard gravitational parameter	4904.8695	$\frac{km^3}{s^2}$	μ_M
Sidereal day	86164.0905	s	T_{SD}
Solar day	86400	s	T_{Solar}

TABLE 3.1: Parameters in standard units.

Now, we need to transform every value in Table 3.1 to the new proper units. We have the following

Proposition 4 *The unit time in proper units is defined as the time taken by the Earth to make a full rotation (2π radians).*

Proof 2 From Kepler's third law, we have that

$$T^2[s^2] = \frac{4\pi^2 a^3[km^3]}{\mu[\frac{km^3}{s^2}]},$$

which leads to

$$1[s] = \sqrt{\frac{4\pi^2 a^3[km^3]}{T^2 \mu_E[\frac{km^3}{s^2}]}}.$$

If we apply the formula above for an object in GEO where the distance in proper units is equal to 1, and take into account that in proper units $\mu_E = 1$, we obtain:

$$1[s] = \sqrt{\frac{4\pi^2 \cdot 1}{T_{SD}^2 \cdot 1}}[pt],$$

namely

$$1[s] = \frac{2\pi}{1\text{sidereal day}}[pt],$$

which means that

$$1[pt] = \frac{1\text{sidereal day}}{2\pi}[s].$$

Using Proposition 4, and the fact that every distance is normalized with a_{GEO}, and that the standard gravitational parameter of the Earth is equal to 1 in proper units, we obtain the values listed in Table 3.2.

Name	Value	Unit	Notation
Mean radius of the Earth	≈ 0.1511	pd	R_E
Earth-Sun distance (1 AU)	≈ 3547.99	pd	a_S
Earth-Moon distance	≈ 9.1167	pd	a_M
Earth standard gravitational parameter	1	pu	μ_E
Sun standard gravitational parameter	333060.4016	pu	μ_S
Moon standard gravitational parameter	0.0123	pu	μ_M
Sidereal day	2π	pt	T_{SD}
1 second	$\frac{2\pi}{86164.0905}$	pt	-

TABLE 3.2: Parameters in the new proper units (pd = proper distance, pu = proper units, pt = proper time).

3.3 Newtonian model

The Newtonian approach will give a closed form solution for the two-body problem (Kepler problem). Therefore, it can be used to compute the exact position and velocity of a small object orbiting around a massive body (Murray and Dermott, 2000). However, if the motion is perturbed by external forces (such as the non-spherical shape of Earth, or the attraction of Sun or Moon), we cannot use this approach to find an analytic solution of the problem. Nevertheless, the Newtonian framework can be used to find with high accuracy the numerical solution of the dynamical system. In the present work, we will use this approach only to validate the Hamiltonian model and to validate the numerical solution of the problem.

3.3.1 Spherical Earth's potential

The equations of motion for the simple Keplerian problem can be derived from the Newton's universal gravitational law. The potential function is defined as follows:

$$V = -\frac{\mu_E}{r},$$

and then the acceleration is given by

$$\ddot{\mathbf{r}} = -\frac{\mu_E}{r^3}\mathbf{r}. \tag{3.2}$$

3.3.2 Geopotential of non-spherical Earth

Let us denote by

$$V(\mathbf{r}) = -\mathcal{G}\int_{V_E}\frac{\rho(\mathbf{r}_p)}{|\mathbf{r}-\mathbf{r}_p|}d\mathbf{r}_p \tag{3.3}$$

the gravitational potential of the Earth seen as an extended body and with $\nabla_{\mathbf{f}}$ the gradient with respect to the synodic frame.

Spherical harmonics

The Earth gravitational potential can be written as a series of spherical harmonics. Let us introduce spherical coordinates in the synodic frame:

$$\begin{cases} X = r\cos\phi\cos\lambda, \\ Y = r\cos\phi\sin\lambda, \\ Z = r\sin\phi, \end{cases} \tag{3.4}$$

where

$$0 \le \lambda < 2\pi, \quad \frac{-\pi}{2} \le \phi < \frac{\pi}{2}.$$

The series expansion of V in spherical harmonics is given by

$$V(r,\phi,\lambda) = -\frac{\mathcal{G}m_E}{r}\sum_{n=0}^{\infty}\left(\frac{R_E}{r}\right)^n \sum_{m=0}^{n} P_{nm}(\sin\phi)\Big[C_{nm}\cos(m\lambda) + S_{nm}\sin(m\lambda)\Big]. \tag{3.5}$$

Here P_{nm} is defined in terms of the Legendre polynomials $P_n(x)$ as

$$P_{nm}(x) = (1-x^2)^{m/2}\frac{d^m}{dx^m}P_n(x), \tag{3.6}$$

and C_{nm}, S_{nm} are the harmonic coefficients obtained by the following formulas

$$C_{nm} = \frac{2-\delta_{0m}}{M_E}\frac{(n-m)!}{(n+m)!}\int_{V_E}(\frac{r_p}{R_e})^n P_{nm}(sin\phi_p\cos(m\lambda_p)\rho(\mathbf{r}_p)dV_e$$

$$S_{nm} = \frac{2-\delta_{0m}}{M_E}\frac{(n-m)!}{(n+m)!}\int_{V_E}(\frac{r_p}{R_e})^n P_{nm}(sin\phi_p)\cos(m\lambda_p)\rho(\mathbf{r}_p)dV_e,$$

where M_E is the mass of the Earth, (r_p, ϕ_p, λ_p) denote the spherical coordinates associated to a point P inside the Earth and, again, r_p is its radius vector (δ_{jm} is the Kronecker symbol).

The Cartesian equations of motion in the ECIF reference frame are given by the rotation (3.1) and computing the partial derivatives of the potential with respect to spherical coordinates up to $n = m = 2$:

$$R_3(-\theta)\nabla_{\mathbf{f}}V(\mathbf{r}) = \Big(\frac{\partial V}{\partial X}\cos\theta - \frac{\partial V}{\partial Y}\sin\theta\Big)\hat{i} + \Big(\frac{\partial V}{\partial X}\sin\theta + \frac{\partial V}{\partial Y}\cos\theta\Big)\hat{j} + \frac{\partial V}{\partial Z}\hat{k}, \tag{3.7}$$

where the potential up to order $n = m = 2$ in the synodic frame is given by

$$V(X,Y,Z) = -\frac{\mathcal{G}M_E}{r} - \frac{\mathcal{G}M_E}{r}(\frac{R_E}{r})^2\Big[C_{20}\Big(\frac{3Z^2}{2r^2} - \frac{1}{2}\Big) + 3C_{22}\frac{X^2-Y^2}{r^2} + 6S_{22}\frac{XY}{r^2}\Big]. \tag{3.8}$$

By deriving the V function with respect to X, Y, Z and substituting the results in (3.7), one obtains:

$$\ddot{x} = -\frac{3\mu_E R_E^2}{2r^7}\left(C_{20}x\left(r^2-5z^2\right)-2\left(C_{22}\left(x\cos(2\theta)\left(2r^2-5x^2+5y^2\right)+2y\sin(2\theta)\left(r^2-5x^2\right)\right)\right.\right.$$
$$\left.\left.+S_{22}\left(x\sin(2\theta)\left(-2r^2+5x^2-5y^2\right)+2y\cos(2\theta)\left(r^2-5x^2\right)\right)\right)\right)$$
$$\ddot{y} = -\frac{3\mu_E R_E^2}{2r^7}\left(C_{20}y\left(r^2-5z^2\right)+2C_{22}\left(y\cos(2\theta)\left(2r^2+5x^2-5y^2\right)-2x\sin(2\theta)\left(r^2-5y^2\right)\right)\right.$$
$$\left.+2S_{22}\left(y\sin(2\theta)\left(-2r^2-5x^2+5y^2\right)-2x\cos(2\theta)\left(r^2-5y^2\right)\right)\right)$$
$$\ddot{z} = -\frac{3z\mu_E R_E^2}{2r^7}\left(C_{20}\left(3r^2-5z^2\right)+10\left(C_{22}\left(\cos(2\theta)\left(x^2-y^2\right)+2xy\sin(2\theta)\right)\right.\right.$$
$$\left.\left.+S_{22}\left(\sin(2\theta)\left(y^2-x^2\right)+2xy\cos(2\theta)\right)\right)\right).$$

3.3.3 The third body perturbation

Let us denote by $\mathbf{r}_{3rd}$ the position vector of the third body in the J2000 system. According to Figure 3.3, detailed in (Murray and Dermott, 2000), the potential of the third body perturbation is given by the following formula

$$V_{3rd} = \frac{\mu_{3rd}}{|\mathbf{r}-\mathbf{r}_{3rd}|} - \mu_{3rd}\frac{\mathbf{r}\cdot\mathbf{r}_{3rd}}{r_{3rd}^3},$$

and thus the acceleration due to the third body is

$$\ddot{\mathbf{r}} = -\mu_{3rd}\left(\frac{\mathbf{r}-\mathbf{r}_{3rd}}{|\mathbf{r}-\mathbf{r}_{3rd}|} - \frac{\mathbf{r}_{3rd}}{r_{3rd}^3}\right). \tag{3.9}$$

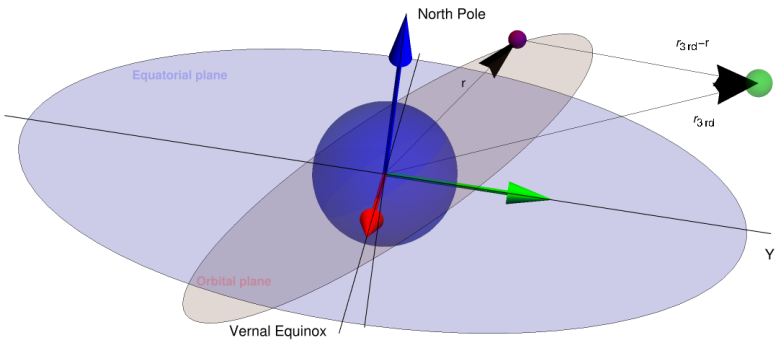

FIGURE 3.3: Third body perturbation.

We will denote by $\mathbf{r}_{\leftmoon}$ and $\mathbf{r}_{\odot}$ the position vectors of the Moon and the Sun, respectively. An approximation of the Lunar and Solar position can be obtained by assuming that they have elliptic orbits in the J2000 system. The exact formulas can be found in (Montenbruck, Gill, and Lutze, 2002) and their implementation in JAVA© are provided in Appendix B.2.

3.3.4 Solar radiation pressure

The force induced by the Solar radiation pressure is expressed in terms of the distance from the Sun and the cross-section of the satellite (see (Montenbruck, Gill, and Lutze, 2002), (Celletti et al., 2017)). Then, the acceleration due to this force can be written as:

$$\ddot{\mathbf{r}} = C_r P_r \frac{A}{m} \frac{\mathbf{r}_\odot}{r_\odot^3} a_\odot^2, \tag{3.10}$$

where P_r is the pressure profile, C_r is the coefficient of reflectivity (dimensionless) and $a_\odot$ is the mean distance from the Sun to the Earth, which equals 1 astronomical unit (AU)[3].

3.3.5 Drag effect

The drag effect is a dissipative force acting on an object at low altitude from the Earth. As in the case of the Solar radiation pressure, the drag effect also depends on the cross-section of the object, and on the atmospheric density at the altitude of the object. The acceleration due to this force is given by (see (Delhaise, 1991)):

$$\ddot{\mathbf{r}} = -\frac{1}{2}\rho(\mathbf{r}) C_D \frac{A}{m} |\mathbf{v}_r| \cdot \mathbf{v}_r, \tag{3.11}$$

where C_D is the drag coefficient[4], $\rho(\mathbf{r})$ is the atmospheric density and $\mathbf{v}_r$ is the relative velocity of the object with respect to the atmosphere.

Assuming that the atmosphere rotates with the angular velocity of the Earth (ω_E) and denoting by ρ_{ip} the density at the initial perigee, $\mathbf{r}_{ip}$ the initial distance of the satellite from the Earth, we have that

$$\mathbf{v}_r = \mathbf{v} - \omega_E \cdot \mathbf{r}$$

and

$$\rho(\mathbf{r}) = \rho_{ip} \exp\left(\frac{\mathbf{r}_{ip} - \mathbf{r}}{H}\right),$$

where H is the scale height.

3.3.6 Equations of motion up to 2nd order

Using the formulas (3.2), (3.3.2), (3.9), (3.10) and denoting by $CS^- = C_{22}\cos(2\theta) - S_{22}\sin(2\theta)$ and $CS^+ = C_{22}\cos(2\theta) + S_{22}\sin(2\theta)$, we provide the equations of motion of an object around the Earth in the J2000 system:

$$\begin{aligned}
\ddot{x} = &-\frac{\mu_E x}{r^3} + \frac{\mu_E R_E^2}{r^5}\left\{C_{20}\left(\frac{3}{2}x - \frac{15}{2}\frac{xz^2}{r^2}\right) + 6CS^- x + 6CS^+ y \right.\\
&\left. + \frac{15x}{r^2}[CS^-(y^2 - x^2) - 2xyCS^+]\right\} - \mu_\odot\left(\frac{x - x_\odot}{|x - x_\odot|^3} + \frac{x_\odot}{|x_\odot|^3}\right)\\
&- \mu_\leftmoon\left(\frac{x - x_\leftmoon}{|x - x_\leftmoon|^3} + \frac{x_\leftmoon}{|x_\leftmoon|^3}\right) + C_r P_r a_\odot^2 \frac{A}{m}\frac{x - x_\odot}{|\mathbf{r} - \mathbf{r}_\odot|^3},
\end{aligned}$$

$$\begin{aligned}
\ddot{y} = &-\frac{\mu_E y}{r^3} + \frac{\mu_E R_E^2}{r^5}\left\{C_{20}\left(\frac{3}{2}y - \frac{15}{2}\frac{yz^2}{r^2}\right) + 6CS^+ x - 6CS^- y \right.\\
&\left. + \frac{15y}{r^2}[CS^-(y^2 - x^2) - 2xyCS^+]\right\} - \mu_\odot\left(\frac{y - y_\odot}{|y - y_\odot|^3} + \frac{y_\odot}{|y_\odot|^3}\right)\\
&- \mu_\leftmoon\left(\frac{y - y_\leftmoon}{|y - y_\leftmoon|^3} + \frac{y_\leftmoon}{|y_\leftmoon|^3}\right) + C_r P_r a_\odot^2 \frac{A}{m}\frac{y - y_\odot}{|\mathbf{r} - \mathbf{r}_\odot|^3}
\end{aligned}$$

[3] See Table 3.2 for the value in proper units.

[4] The value $B^* = C_D\frac{A}{m}$ is called the ballistic coefficient and it is usually given in the TLE datasets.

$$\ddot{z} = -\frac{\mu_E z}{r^3} + \frac{\mu_E R_E^2}{r^5}\left\{C_{20}\left(\frac{9}{2}z - \frac{15}{2}\frac{z^3}{r^2}\right). + \frac{15z}{r^2}\left[CS^-(y^2-x^2) - 2xyCS^+\right]\right\}$$
$$-\mu_\odot\left(\frac{z-z_\odot}{|z-z_\odot|^3} + \frac{z_\odot}{|z_\odot|^3}\right) - \mu_{\leftmoon}\left(\frac{z-z_{\leftmoon}}{|z-z_{\leftmoon}|^3} + \frac{z_{\leftmoon}}{|z_{\leftmoon}|^3}\right) + C_r P_r a_\odot^2 \frac{A}{m}\frac{z-z_\odot}{|\mathbf{r}-\mathbf{r}_\odot|^3}.$$

We will use these equations in the numerical computations as an accurate representation of the motion of an object around the Earth.

3.4 Hamiltonian formulation

In this section we will provide two methods to construct the Hamiltonian description of the dynamical system. The first one is done by deriving the Hamiltonian functions for J_2, Moon, Sun from the corresponding potential in Cartesian formulation, and the second one by using the so-called Kaula-Lane expansion (see (Kaula, 2000), (Lane, 1989)). For the Keplerian part, SRP and drag effect, we will give only one procedure to describe these forces in the Hamiltonian framework.

3.4.1 Keplerian part

Starting from the Cartesian formulation of the problem we have that the Hamiltonian as a function of position and velocity can be written as:

$$\mathcal{H}_{Kep} = \frac{v^2}{2} - \frac{\mu_E}{r}.$$

In terms of the Keplerian elements we obtain that:

$$\mathcal{H}_{Kep} = -\frac{\mu_E}{2a}.$$

3.4.2 Non-spherical Earth perturbation

Here, we firstly want to describe the perturbation due to the averaged J_2 term starting from the spherical harmonics described in Section 3.3.2. Dropping the Keplerian part and the C_{22} terms from equation (3.8) we have that:

$$V_{J_2}(X,Y,Z) = -J_2\mu_E R_E^2\left(\frac{1}{2r^3} - \frac{3Z^2}{2r^5}\right).$$

The transformation between the fixed reference frame (X,Y,Z) and the reference frame of the orbital plane, say (x_t, y_t, z_t), is obtained by rotating by Ω around the Z axis and by i around the line of the nodes (the intersection between the XOY plane and the orbital plane). These rotations are simply performed by using the matrix

$$\begin{pmatrix} \cos(\Omega) & -\cos(i)\sin(\Omega) & \sin(i)\sin(\Omega) \\ \sin(\Omega) & \cos(i)\cos(\Omega) & -\sin(i)\cos(\Omega) \\ 0 & \sin(i) & \cos(i) \end{pmatrix}.$$

To get the position of the satellite on the orbital plane, we have to implement the following transformation

$$\begin{aligned} x_t &= r\cos(\omega + f) \\ y_t &= r\sin(\omega + f) \\ z_t &= 0. \end{aligned}$$

Here, f stands for the true anomaly. After this transformation, we get the first form of the Hamiltonian function for the J_2 perturbation:

$$\begin{aligned} H_{J_2}^{first} = \frac{3J_2\mu_E R_E^2\cos(2f+2i+2\omega)}{16r^3} + \frac{3J_2\mu_E R_E^2\cos(2f-2i+2\omega)}{16r^3} \\ -\frac{3J_2\mu_E R_E^2\cos(2f+2\omega)}{8r^3} - \frac{3J_2\mu_E R_E^2\cos(2i)}{8r^3} - \frac{J_2\mu_E R_E^2}{8r^3}. \end{aligned}$$

In order to take the average, we must compute the integral

$$\frac{1}{2\pi}\int_0^{2\pi} H_{J_2}^{first} dM;$$

since M does not appear in $H_{J_2}^{first}$, we use the relation $dM = \frac{r^2}{a^2\sqrt{1-e^2}}df$ (which comes from $\dot{f}r^2 = h = \sqrt{\mu_E a\,(1-e^2)}$ and $M = \sqrt{\frac{\mu_E}{a^3}}\,(t-t_0)$) to obtain

$$\frac{1}{2\pi}\int_0^{2\pi} H_{J_2}^{first}\frac{r^2}{a^2\sqrt{1-e^2}}df,$$

where $r = \frac{a\sqrt{1-e^2}}{1-e\cos(f)}$. After the substitution and computation of the integral we end up with the averaged Hamiltonian

$$H_{J_2}(a,e,i) = J_2\mu_E R_E^2\left(\frac{1}{8a^3\left(1-e^2\right)^{3/2}} + \frac{3\cos^2(i)}{8a^3\left(1-e^2\right)^{3/2}} - \frac{3\sin^2(i)}{8a^3\left(1-e^2\right)^{3/2}}\right). \quad (3.12)$$

Now, the same expansion can be performed by following (Kaula, 2000). In the synodic reference frame, we have the following expansion in series of the orbital elements:

$$\mathcal{H}_{Earth} = -\frac{\mu_E}{a}\sum_{n=2}^{\infty}\sum_{m=0}^{n}\left(\frac{R_E}{a}\right)^n F_{nmp}(i)\sum_{q=-\infty}^{\infty} G_{npq}(e)S_{nmpq}(M,\omega,\Omega,\theta), \quad (3.13)$$

where

$$\begin{aligned} F_{nmp}(i) = \sum_{w=0}\frac{(2n-2w)!}{w!(n-w)!(n-m-2w)!w^{2n-2w}}\sin(i)^{n-m-2w}\sum_{s=0}^{m}\binom{m}{s}\cos(i)^s \\ \sum_{m=0}^{n}\binom{n-m-2w+s}{c}\binom{m-s}{p-w-c}(-1)^{c-k}, \quad (3.14) \end{aligned}$$

$$G_{npq}(e) = (-1)^{|q|}(1+\beta^2)^n\beta^{|q|}\sum_{k=0}^{\infty}P_{npqk}Q_{npqk}\beta^{2k},$$

$$\beta = \frac{e}{1+\sqrt{1-e^2}},$$

$$P_{npqk} = \sum_{r=0}^{h} \binom{2p'-2n}{h-r} \frac{(-1)^r}{r!} \left(\frac{(n-2p'+2q')e}{2\beta}\right)^r, \begin{cases} h = k+q', q' > 0 \\ h = k, q' < 0 \end{cases},$$

$$Q_{npqk} = \sum_{r=0}^{h} \binom{-2p'}{h-r} \frac{1}{r!} \left(\frac{(n-2p'+2q')e}{2\beta}\right)^r, \begin{cases} h = k, q' > 0 \\ h = k-q', q' < 0 \end{cases},$$

while $p' = p$ and $q' = q$ when $p < n/2$, $p' = n-p$ and $q' = -q$ when $p > n/2$, and

$$S_{nmpq} = \begin{cases} -J_{nm}\cos(\Psi_{nmpq}), (n-m)mod2 = 0 \\ -J_{nm}\sin(\Psi_{nmpq}), (n-m)mod2 = 1 \end{cases}$$

where

$$\Psi_{nmpq} = (n-2p)\omega + (n-2p+q)M + m(\Omega-\theta) - m\lambda_{nm}. \tag{3.15}$$

The quantities J_{nm} and λ_{nm} are introduced through the following relations:

$$\lambda_{nm} = \frac{\arccos(-\frac{C_{nm}}{J_{nm}})}{m}, \qquad J_{nm} = \begin{cases} \sqrt{C_{nm}^2 + S_{nm}^2}, m \neq 0 \\ -C_{n0}, m = 0 \end{cases}$$

In order to obtain the secular part of the expansion (3.13), we average over the fast angles M and θ, by choosing $m = 0$ and $n-2p+q = 0$ in (3.15). For example, the expansion up to order $n = 2$ has the following form:

$$\mathcal{H}_{J_2} = \mu_E R_E^2 J_2 \frac{1+3\cos(2i)}{8a^3\left(1-e^2\right)^{3/2}}, \tag{3.16}$$

which is the simplified form of Eq. (3.12).

3.4.3 Third body perturbation

As third body perturbations, we will consider only the attraction of the Moon and the Sun. We start from the same expansion and, later, we will distinguish the elements of the Moon and the Sun. The potential of the pertuber body has the form

$$V_b = -\mu_b\left(\frac{1}{|\mathbf{r}-\mathbf{r}_b|} - \frac{\mathbf{r}\cdot\mathbf{r}_b}{|\mathbf{r}_b|^3}\right),$$

which can be written as

$$V_b = -\mu_b\left(\frac{1}{\sqrt{r_b^2 - 2r\cdot r_b + r^2}} - \frac{\mathbf{r}\cdot\mathbf{r}_b}{|\mathbf{r}_b|^3}\right). \tag{3.17}$$

Remark 9 *The first term in the parenthesis of formula (3.17) is the potential of the third body with respect to the object and the second term comes from the potential of the third body with respect to the center of the Earth.*

Now we expand the potential (3.17) with respect to $\frac{r}{r_b}$ around 0 and using the coordinate formulation of $\mathbf{r}\cdot\mathbf{r}_b$,we get an expression of V_b that depends on x_b, y_b, z_b, the parameters of

the third body, the distance r from the Earth to the object, and the angles i, f, ω, Ω. To average this expression over the mean anomaly M, we will make a similar change of coordinates as for the J_2 problem by expressing dM as function of dE, where E is the eccentric anomaly. Using the following formulas

$$\begin{aligned}\cos(f) &= \frac{a(\cos(E)-e)}{r}\\ \sin(f) &= \frac{a\sqrt{1-e^2}\sin(E)}{r}\\ r &= a(1-e\cos(E))\\ M &= E - e\sin(E)\\ dM &= (1-e\cos(E))dE,\end{aligned}$$

we keep in the averaged Hamiltonian those terms that are independent on E. The last step is to compute x_b, y_b, z_b as a function of orbital elements of the Moon and of the object. To this end, we use the same approach as in the case of the object around the Earth. In this case, we first transform from the fixed reference frame to the ecliptic plane and, with respect to the ecliptic plane, we look at the position of the third body as an object around the Earth (using the same transformation matrix as before). More precisely, the position of the Moon with respect to the fixed reference frame is given by:

$$\begin{aligned}x_b =& -\frac{1}{4}r_b\cos(i_b - M_b + 2\Omega_b) - \frac{1}{4}r_b\cos(i_b + M_b - 2\Omega_b) + \frac{1}{4}r_b\cos(i_b - M_b)\\ &+ \frac{1}{4}r_b\cos(i_b + M_b) + \frac{1}{2}r_b\cos(M_b - 2\Omega_b) + \frac{1}{2}r_b\cos(M_b)\\ y_b =& -\frac{1}{4}\cos(i_0)r_b\sin(i_b - M_b + 2\Omega_b) + \frac{1}{4}\cos(i_0)r_b\sin(i_b + M_b - 2\Omega_b)\\ &- \frac{1}{4}\cos(i_0)r_b\sin(i_b - M_b) + \frac{1}{4}\cos(i_0)r_b\sin(i_b + M_b) - \frac{1}{2}\cos(i_0)r_b\sin(M_b - 2\Omega_b)\\ &+ \frac{1}{2}\cos(i_0)r_b\sin(M_b) + \frac{1}{2}r_b\sin(i_0)\cos(i_b + M_b - \Omega_b) - \frac{1}{2}r_b\sin(i_0)\cos(i_b - M_b + \Omega_b)\\ z_b =& -\frac{1}{2}\cos(i_0)r_b\cos(i_b + M_b - \Omega_b) + \frac{1}{2}\cos(i_0)r_b\cos(i_b - M_b + \Omega_b)\\ &- \frac{1}{4}r_b\sin(i_0)\sin(i_b - M_b + 2\Omega_b) + \frac{1}{4}r_b\sin(i_0)\sin(i_b + M_b - 2\Omega_b) - \frac{1}{4}r_b\sin(i_0)\sin(i_b - M_b)\\ &+ \frac{1}{4}r_b\sin(i_0)\sin(i_b + M_b) - \frac{1}{2}r_b\sin(i_0)\sin(M_b - 2\Omega_b) + \frac{1}{2}r_b\sin(i_0)\sin(M_b).\end{aligned}$$

Here i_0 is the inclination of the ecliptic plane with respect to the equatorial plane and we can substitute $r_b = a_b\sqrt{1-e_b^2}$. The last step is to use the above transformation and then to average over M_b, which implies the reduction of the terms depending on M_b. Up to this point, if the expansion w.r.t $\frac{r}{r_b}$ has been done up to second order, the Hamiltonian of the third body will depend on the orbital elements of the object $(a, e, i, \omega, \Omega)$, as well as on the orbital elements $(a_b, e_b, i_b, \Omega_b)$, and the gravitational parameter of the third body μ_b. From the general expression of a third body perturber, one can substitute and obtain the Hamiltonian functions for the perturbations due to the Moon and the Sun, using the constants given in the Table 3.2.

Remark 10 *Taking into account the constancy of Ω_S and that $i_S = i_0$, the Hamiltonian function of the Sun has 2 degrees of freedom. On the other hand, since the Moon is inclined*

w.r.t the ecliptic plane, and it shows a little linear variation in time of Ω_M, the Hamiltonian function of the Moon has 2 degrees of freedom and it is time-dependent.

The `Mathematica`© code to generate the functions for these two perturbations is given in Appendix B.1.

In the following subsection we will consider an alternative expansion using the Kaula-Lane formulation (see (Lane, 1989),(Hughes, 1980)).

3.4.4 Moon perturbation

The perturbation of a space object due to the Moon's attraction can be written as an expansion in orbital elements of the Moon and the object, using the following formula (see (Lane, 1989)):

$$\mathcal{R}_M = \mu_M \sum_{l\geq 2}\sum_{m=0}^{l}\sum_{p=0}^{l}\sum_{s=0}^{l}\sum_{q=0}^{l}\sum_{j=-\infty}^{\infty}\sum_{r=-\infty}^{\infty}(-1)^{[m/2]}\frac{\epsilon_m\epsilon_s}{2a_M}\frac{(l-s)!}{(l+m)!}\left(\frac{a}{a_M}\right)^l F_{lmp}(i)$$
$$F_{lsq}(i_M)H_{lpj}(e)G_{lqr}(e_M)\{(-1)^{t(m+s-1)+1}U_l^{m,-s}\cos(\phi_{lmpj}+\phi'_{lsqr}-y_s\pi)+$$
$$(-1)^{t(m+s)}U_l^{m,-s}\cos(\phi_{lmpj}-\phi'_{lsqr}-y_s\pi)\}, \quad (3.18)$$

where $y_s = 0$, if s mod 2 = 0, $y_s = \frac{1}{2}$, if s mod 2 = 1, $t = (l-1) \bmod 2$,

$$\epsilon_m = \begin{cases} 1, & m = 0 \\ 2, & m \in \mathbb{Z}\backslash\{0\} \end{cases}$$

$$\phi_{lmpj} = (l-2p)\omega + (l-2p+j)M + m\Omega \quad (3.19)$$

$$\phi'_{lsqr} = (l-2q)\omega_M + (l-2q+r)M_M + s(\Omega_M - \frac{\pi}{2}). \quad (3.20)$$

The functions $F_{lmp}(i)$ and $F_{lsq}(i_M)$ have been introduced in (3.14), $H_{lpj}(e)$ and $G_{lqr}(e_M)$ are the Hansen coefficients and the function $U_l^{m,s}$ has the following form

$$U_l^{m,-s} = \sum_{r=\max(0,s-m)}^{\min(l+s,l-m)}(-1)^{l-m-r}\binom{l+m}{m-s+r}\binom{l-m}{r}\cos^{m-s+2r}(\epsilon/2)\sin^{-m+s+2(l-r)}(\epsilon/2),$$

where $\epsilon = 23^o26'21.45''$. In our model, we have $\mathcal{H}_{Moon} = -\mathcal{R}_M$.

3.4.5 Sun pertubation and Solar radiation pressure

A similar expansion, in the orbital elements of the Sun and space object, is defined for the Solar perturbation in the following way (see (Lane, 1989))

$$\mathcal{R}_S = \mu_S \sum_{l\geq 2}\sum_{m=0}^{l}\sum_{p=0}^{l}\sum_{h=0}^{l}\sum_{q=-\infty}^{\infty}\sum_{j=-\infty}^{\infty}\frac{a^l}{a_S^{l+1}}\epsilon_m\frac{(l-m)!}{(l+m)!}$$
$$F_{lmp}(i)F_{lmh}(i_S)H_{lpq}(e)G_{lhj}(e_S)\cos(\phi_{lmphqj}), \quad (3.21)$$

where

$$\phi_{lmphqj} = (l-2p)\omega + (l-2p+q)M - (l-2h)\omega_S - (l-2h+j)M_S + m(\Omega - \Omega_S). \quad (3.22)$$

In our model, we have $\mathcal{H}_{Sun} = -\mathcal{R}_S$.
Following (Hughes, 1980), the contribution to the Hamiltonian due to the Solar radiation pressure is given by:

$$\mathcal{H}_{SRP} = C_r P_r \frac{A}{m} a_S^2 \sum_{l=1}^{1} \sum_{s=0}^{l} \sum_{p=0}^{l} \sum_{h=0}^{l} \sum_{q=-\infty}^{\infty} \sum_{j=-\infty}^{\infty} \frac{a^l}{a_S^{l+1}} \epsilon_s \frac{(l-s)!}{(l+s)!} F_{lsp}(i) F_{lsh}(i_S) H_{lpq}(e) G_{lhj}(e_S) \cos(\phi_{lsphqj}), \quad (3.23)$$

where A/m is the area-to-mass ratio of the object, C_r is the reflectivity coefficient, and P_r is the radiation pressure for an object located at $1\,AU$.

3.4.6 Dissipative forces - Drag effect

The atmospheric drag is a force that affects only the evolution of the semi-major axis and the eccentricity of the orbit. Following the formulation of (Chao, 2005), the additional variation of the orbital elements due to the atmospheric drag is given by the following formulas

$$\frac{d}{dt}a(t) = -\frac{1}{2\pi}\int_0^{2\pi} B\rho v \frac{a}{1-e^2}\left[1 + e^2 + 2e\cos(f) - \omega_E \cos(i)\sqrt{\frac{a^3(1-e^2)^3}{\mu_E}}\right] dM$$

$$\frac{d}{dt}e(t) = -\frac{1}{2\pi}\int_0^{2\pi} B\rho v \left[e + \cos(f) - \frac{r^2\omega_E\cos(i)}{2\sqrt{\mu_E a(1-e)^2}}\left(2(e+\cos(f)) - e\sin^2(f)\right)\right] dM$$

$$\frac{d}{dt}i(t) = 0,$$

where

$$\rho(h) = \rho_0 \exp\left(-\frac{h-h_0}{H_0}\right)$$

and

$$v = \sqrt{\frac{\mu_E}{a(1-e^2)}(1+e^2+2e\cos(f))}\left(1 - \frac{(1-e^2)^{\frac{3}{2}}}{1+e^2+2e\cos(f)}\frac{\omega_E}{n^*}\cos(i)\right),$$

where n^* is the mean motion of the space object. To obtain the equations depending only on the orbital elements, we use the following approximations:

$$f = M + 2e\sin(M) + \frac{5e^2}{4}\sin(2M), \quad (3.24)$$

$$h = a\left[1 - e\cos(M) + \frac{e^2}{2}(1-\cos(2M))\right] - R_E. \quad (3.25)$$

A detailed description of the atmospheric drag can be found in (Celletti and Galeş, 2017).

Chapter 4

Analysis of the Secular and Resonant Effects

In this chapter we will study the analysis of secular and resonant effects due to the different perturbations at different altitudes. This analysis will give us some insights about the structure of the Hamiltonian functions that we intend to normalize. The present chapter is split into two sections. The first one describes some theoretical aspects related to the long and short effects due to the non-spherical Earth perturbation, the secular changes in eccentricity and inclination due to the Lunar and Solar effects, and the additional corrections due to the solar radiation pressure for objects with a high area-over-mass ratio. The second section provides the numerical results that emphasize the difference in evolution of the orbital elements when only some of these perturbations are considered.

4.1 Theoretical aspects

In order to clearly separate the contribution of the different terms in the perturbation, let us denote by $\overline{H_{J_2}}$, $\overline{H_{J_3}}$, $\overline{H_{res2:1}}$, $\overline{H_{res1:1}}$, $\overline{H_M}$, $\overline{H_S}$, $\overline{H_{SRP}}$, $\overline{F_L}$, $\overline{F_G}$, $\overline{F_H}$ the perturbations due to the secular effect of J_2 and J_3, the tesseral resonances 2:1 and 1:1, the secular effect of the Moon and the Sun gravitational influence, the Solar radiation pressure, and the components of the dissipative effect F_L, F_G, F_H, respectively.

We will use the same notation $\overline{H}$ for the sum of the perturbations in different cases. We also introduce here the Delaunay's variables, the modified Delaunay's variables and the Poincaré's variables as follows:

Delaunay's variables:

$$\begin{aligned} l &= M & L &= \sqrt{\mu_E a} \\ g &= \omega & G &= \sqrt{\mu_E a(1-e^2)} \\ h &= \Omega & H &= \sqrt{\mu_E a(1-e^2)}\cos(i) \end{aligned} \tag{4.1}$$

Modified Delaunay's variables:

$$\begin{aligned} \lambda &= M+\omega+\Omega & \Lambda &= \sqrt{\mu_E a} \\ p &= -\omega-\Omega & P &= \sqrt{\mu_E a}(1-\sqrt{1-e^2}) \\ q &= -\Omega & Q &= \sqrt{\mu_E a}\sqrt{1-e^2}(1-\cos(i)) \end{aligned} \tag{4.2}$$

Poincaré's variables:

$$\begin{aligned} X_1 &= \lambda & Y_1 &= \Lambda \\ X_2 &= \sqrt{2P}\sin(p) & Y_2 &= \sqrt{2P}\cos(p) \\ X_3 &= \sqrt{2Q}\sin(q) & Y_3 &= \sqrt{2Q}\cos(q) \end{aligned} \tag{4.3}$$

Every set above contains conjugate pairs of variables, and we will make use of the desired set depending on the case we are considering.

4.1.1 Secular effects due to the Earth's perturbation

In this subsection we want to analyze the evolution of the orbital elements e, i, ω, Ω when only the Earth's perturbations H_{J_2} and H_{J_3} are considered. Firstly, let us analyze the system defined by the following Hamiltonian function in the Delaunay variables:

$$\overline{H} = \overline{H_{J_2}} = \frac{J_2 \mu_E^4 R_E^2 \left(G^2 - 3H^2\right)}{4G^5 L^3}. \tag{4.4}$$

The system is integrable since it does not depend on any angle. The time derivatives of the angles ω and Ω are given by the following equations:

$$\begin{aligned} \dot{\omega}(t) &= 3J_2 R_E^2 \sqrt{a_0 \mu_E} \frac{(5\cos(2i_0) + 3)}{8a_0^4 \left(e_0^2 - 1\right)^2}, \\ \dot{\Omega}(t) &= 3J_2 R_E^2 \sqrt{a_0 \mu_E} \frac{\cos(i_0)}{2a_0^4 \left(e_0^2 - 1\right)^2}, \end{aligned} \tag{4.5}$$

while the time derivatives of the eccentricity and inclination are 0.

When $5\cos(2i) + 3 = 0$ the angle ω will be constant and when $\cos(i) = 0$ the angle Ω will be constant. This leads to the following definition.

Definition 34 *The initial values $i_0 = 90°$, $i_0 \approx 63.4°$ and $i_0 \approx 116.5°$ are called **critical inclinations** for the secular problem.*

The structure of the system around $i_0 \approx 63.4°$ will be analyzed in detail in the following subsections. In the case $\overline{H} = \overline{H_{J_3}}$ with

$$\overline{H_{J_3}} = \frac{3J_3 \mu_E^5 R_E^3 \sin(g) \left(G^2 - 5H^2\right) \sqrt{G^2 - H^2} \sqrt{L^2 - G^2}}{8G^8 L^4}, \tag{4.6}$$

we notice the presence of the angle g which implies that the system is still integrable, but we cannot find a closed-form solution as in the case of $\overline{H_{J_2}}$. Also, we can see that Hamilton's equation associated to this system will contain terms like $G^2 - H^2$ and $L^2 - G^2$ at the denominator. It means that for values of eccentricity and inclination close to 0, we face singularities. Nevertheless, by making use of the Poincaré variables, we get rid of these singularities and we numerically integrate the system (see (Lyddane, 1963)). This aspect will be emphasized in Section 4.2.1.

4.1.2 Tesseral resonances

We noticed in (4.4) and (4.6) that the semi-major axis is constant in the case of the secular dynamics. Nevertheless, there are some special cases when this orbital element is affected

by the synchronized evolution of the mean anomaly of the particle with the rotation of the Earth. We call this effect a tesseral resonance.

Starting from the definitions in Section 3.4.2, we can see that the function of the combination of angles (3.15) is a constant whenever $\dot{\Psi}_{nmpq} = 0$. This implies that the combination $(n-2p)\dot{\omega} + (n-2p+q)\dot{M} + m(\dot{\Omega} - \dot{\theta}) = 0$. By reordering the terms, denoting by $k = n-2p+q$ and $l = m$, and taking into account that for $\overline{H} = \overline{H_{J_2}} + \overline{H_{J_3}}$, the frequencies $\dot{\omega}$ and $\dot{\Omega}$ are much smaller than $\dot{M}$ and $\dot{\theta}$; in this case we have the following definition.

Definition 35 *We say that an object is in $k : l$ **tesseral resonance**, for some $k, l \in \mathbf{Z}\backslash\{0\}$, with the rotation of the Earth, which means a commensurability between the angles M and θ, whenever $l\dot{M} - k\dot{\theta} = 0$.*

We can obtain an approximation of the region where the tesseral resonance occurs by assuming that $\dot{M} \approx \frac{\partial H_{\text{Kep}}}{\partial L}$. From Proposition 4 we have that $\dot{\theta} = 1$. The Hamiltonian function of the Keplerian part in Delaunay variables and proper units has the following form:

$$H_{\text{Kep}} = -\frac{1}{2L^2}, \tag{4.7}$$

so that we obtain the equation

$$a = \left(\frac{k}{l}\right)^{\frac{2}{3}},$$

in the proper units. For example the $2:1$ resonance occurs at $a \approx 26560$ km, while the $1:1$ resonances occurs at $a \approx 42160$ km.

One can obtain the terms for the tesseral resonance $k : l$ by putting the condition $k(n-2p+q) = lm$ in the expansion (3.13). For $\overline{H_{res2:1}}$, we obtain the expansion up to order 3 by choosing $m \neq 0$ and $2(n-2p+q) = m$, which in the orbital elements has the following form:

$$\begin{aligned}
\overline{H_{res2:1}} &= J_{22}\mu_{\text{E}}R_{\text{E}}^2 \frac{9e\left(2-2\cos^2(i)\right)\cos\left(-2\lambda_{22}+2(\Omega-\theta)+M\right)}{8a^3} \\
&- J_{22}\mu_{\text{E}}R_{\text{E}}^2 \frac{3e\left(\cos^2(i)+2\cos(i)+1\right)\cos\left(-2\lambda_{22}+2(\Omega-\theta)+M+2\omega\right)}{8a^3} \\
&+ J_{32}\mu_{\text{E}}R_{\text{E}}^3 \frac{165e^2\sin(i)\left(3\cos^2(i)-2\cos(i)-1\right)\sin\left(-2\lambda_{32}+2(\Omega-\theta)+M-\omega\right)}{64a^4} \\
&+ J_{32}\mu_{\text{E}}R_{\text{E}}^3 \frac{15\left(2e^2+1\right)\sin(i)\left(-3\cos^2(i)-2\cos(i)+1\right)\sin\left(-2\lambda_{32}+2(\Omega-\theta)+M+\omega\right)}{8a^4} \\
&+ J_{32}\mu_{\text{E}}R_{\text{E}}^3 \frac{15e^2\sin(i)\left(\cos^2(i)+2\cos(i)+1\right)\sin\left(-2\lambda_{32}+2(\Omega-\theta)+M+3\omega\right)}{64a^4}.
\end{aligned} \tag{4.8}$$

As it is described in detail in (Celletti and Galeş, 2014), we remark that the terms depending on the eccentricity at the 1st and 0th power are the ones that mainly affect the evolution of the semi-major axis, namely

$$\begin{aligned}
\overline{H^t_{res2:1}} &= J_{22}\mu_{\text{E}}R_{\text{E}}^2 \frac{9e\left(2-2\cos^2(i)\right)\cos\left(-2\lambda_{22}+2(\Omega-\theta)+M\right)}{8a^3} \\
&- J_{22}\mu_{\text{E}}R_{\text{E}}^2 \frac{3e\left(\cos^2(i)+2\cos(i)+1\right)\cos\left(-2\lambda_{22}+2(\Omega-\theta)+M+2\omega\right)}{8a^3} \\
&+ J_{32}\mu_{\text{E}}R_{\text{E}}^3 \frac{15\sin(i)\left(-3\cos^2(i)-2\cos(i)+1\right)\sin\left(-2\lambda_{32}+2(\Omega-\theta)+M+\omega\right)}{8a^4}.
\end{aligned} \tag{4.9}$$

In the case of $\overline{H_{res1:1}}$, there are several terms appearing in the expansion, given by the following expression

$$\begin{aligned}
\overline{H_{res1:1}} &= -J_{21}\mu_E R_E^2 \frac{9e\sin(i)\cos(i)\sin(-\lambda_{21}-\theta+M+\Omega)}{4a^3} \\
&- J_{21}\mu_E R_E^2 \frac{3e\sin(i)(\cos(i)+1)\sin(-\lambda_{21}-\theta+M+2\omega+\Omega)}{8a^3} \\
&+ J_{22}\mu_E R_E^2 \frac{3\left(1-\frac{5e^2}{2}\right)\left(\cos^2(i)+2\cos(i)+1\right)\cos(-2\lambda_{22}+2(\Omega-\theta)+2M+2\omega)}{4a^3} \\
&+ J_{31}\mu_E R_E^3 \frac{15e^2\sin^2(i)(-\cos(i)-1)\cos(-\lambda_{31}-\theta+M+3\omega+\Omega)}{128a^4} \\
&+ J_{31}\mu_E R_E^3 \frac{\left(2e^2+1\right)\left(\frac{3}{4}(-\cos(i)-1)+\frac{15}{16}\sin^2(i)(3\cos(i)+1)\right)\cos(-\lambda_{31}-\theta+M+\omega+\Omega)}{a^4} \\
&+ J_{31}\mu_E R_E^3 \frac{11e^2\left(\frac{3}{4}(\cos(i)-1)+\frac{15}{16}\sin^2(i)(1-3\cos(i))\right)\cos(-\lambda_{31}-\theta+M-\omega+\Omega)}{8a^4} \\
&+ J_{32}\mu_E R_E^3 \frac{45e\sin(i)\left(-3\cos^2(i)-2\cos(i)+1\right)\sin(-2\lambda_{32}+2(\Omega-\theta)+2M+\omega)}{8a^4} \\
&- J_{32}\mu_E R_E^3 \frac{15e\sin(i)\left(\cos^2(i)+2\cos(i)+1\right)\sin(-2\lambda_{32}+2(\Omega-\theta)+2M+3\omega)}{8a^4} \\
&+ J_{33}\mu_E R_E^3 \frac{795e^2\left(-3\cos^3(i)-3\cos^2(i)+3\cos(i)+3\right)\cos(-3\lambda_{33}+3(\Omega-\theta)+3M+\omega)}{64a^4} \\
&+ J_{33}\mu_E R_E^3 \frac{15\left(1-6e^2\right)\left(\cos^3(i)+3\cos^2(i)+3\cos(i)+1\right)\cos(-3\lambda_{33}+3(\Omega-\theta)+3M+3\omega)}{8a^4}.
\end{aligned} \tag{4.10}$$

Since J_{22} and J_{31} are one order of magnitude greater than the other ones, one might make a truncation, keeping only those terms depending on J_{22} and J_{31} and including the terms starting with order 0 in the eccentricity, i.e.:

$$\begin{aligned}
\overline{H^t_{res1:1}} &= J_{22}\mu_E R_E^2 \frac{3\left(1-\frac{5e^2}{2}\right)\left(\cos^2(i)+2\cos(i)+1\right)\cos(-2\lambda_{22}+2(\Omega-\theta)+2M+2\omega)}{4a^3} \\
&+ J_{31}\mu_E R_E^3 \frac{\left(\frac{3}{4}(-\cos(i)-1)+\frac{15}{16}\sin^2(i)(3\cos(i)+1)\right)\cos(-\lambda_{31}-\theta+M+\omega+\Omega)}{a^4}.
\end{aligned} \tag{4.11}$$

Keeping a simple, but accurate, expansion is necessary both in the analysis of the geometrical insights of the Hamiltonian structure and in the numerical computations.

4.1.3 Lunisolar effects

Starting from the expansions described in Sections 3.4.2 and 3.4.3, we define the following Hamiltonian function, in Delaunay variables:

$$\overline{H}(G,H,H_M,g,h,h_M;L) = \overline{H_{J_2}}(G,H;L) + \overline{H_S}(G,H,g,h;L) + \overline{H_M}(G,H,H_M,g,h,h_M;L), \tag{4.12}$$

	Sun	Moon
Mean daily motion	$1^o/day$	$13.06^o/day$
Semi-major axis	$1.496 \cdot 10^8$ km	384478 km
Eccentricity	0.0167	0.0549
Inclination	$23^o26'21.406''$	$5^o15'$
$\dot{\omega}_{S/M}$	$282.94^o/day$	$0.164^o/day$
$\dot{\Omega}_{S/M}$	$0^o/day$	$-0.0529^o/day$

TABLE 4.1: Orbital elements of Sun and Moon.

which will describe a 2.5-DoF Hamiltonian system, where the expression of the Moon and the Sun can be written as

$$\begin{aligned}\overline{H_M}(G,H,H_M,g,h,h_M;L) &= \sum_{\substack{k_1=0\\k_2=0\\k_3\in\{1,2\}}} \mathcal{M}_{0,0,k_3}(G,H,H_M;L)\cos(k_3h_M)\\ &+ \sum_{\substack{k_1=0\\k_2=1\\k_3\in\{-2,-1,0,1,2\}}} \mathcal{M}_{0,1,k_3}(G,H,H_M;L)\cos(h+k_3h_M)\\ &+ \sum_{\substack{k_1=0\\k_2=2\\k_3\in\{-2,-1,0,1\}}} \mathcal{M}_{0,2,k_3}(G,H,H_M;L)\cos(2h+k_3h_M) \qquad (4.13)\\ &+ \sum_{\substack{k_1=2\\k_2\in\{-2,-1,0,1,2\}\\k_3\in\{-2,-1,0,1,2\}}} \mathcal{M}_{k_1,k_2,k_3}(G,H,H_M;L)\cos(k_1g+k_2h+k_3h_M)\end{aligned}$$

and

$$\overline{H_S}(G,H,g,h;L) = \sum_{\substack{k_1=2\\k_2\in\{-2,-1,0,1,2\}}} \mathcal{S}_{k_1,k_2}(G,H;L)\cos(k_1g+k_2h), \qquad (4.14)$$

where the functions $\mathcal{M}$ and $\mathcal{S}$ are polynomials in the action variables.

We want to analyze how the two external perturbers, Moon and Sun, affect the orbital evolution of the eccentricity. As in the case of Earth's perturbation, the most interesting effects occurs when we approach a resonant region, which in this case is defined as follows.

Definition 36 *A lunisolar resonance of order k_1:k_2:k_3, for $k_1,k_2,k_3 \in \mathbf{Z}\backslash\{0\}$, with $k_1 \in \{-2,0,2\}$ and $k_2,k_3 \in [-2,2]^2$ occurs whenever the following equation is satisfied*

$$k_1\dot{\omega} + k_2\dot{\Omega} + k_3\dot{\Omega}_M = 0, \qquad \forall k_1 \in \{-2,0,2\} \text{ and } k_2,k_3 \in [-2,2]^2.$$

Let us distinguish, for the moment, between two different cases, one with the Moon on the ecliptic plane, namely when $i_M = 0$, and the other one with the Moon inclined w.r.t. the ecliptic plane. While the Hamiltonian function that describes the Moon with inclination is given in (4.13), the expression for the Moon on the ecliptic plane is given by

$$\overline{H_M^{ecliptic}}(G,H,g,h;L) = \sum_{\substack{k_1=2\\k_2\in\{-2,-1,0,1,2\}}} \mathcal{M}_{k_1,k_2}^{ecliptic}(G,H;L)\cos(k_1g+k_2h), \qquad (4.15)$$

which does not depend on the angle h_M anymore. The function $\mathcal{M}^{ecliptic}$ is polynomial in the action variables.
Let us take as a study case the region of $2\dot{\omega} = 0$ resonance, namely $k_1 = 2$, $k_2 = k_3 = 0$. In section 4.1.1 we already obtained that the equation $2\dot{\omega} = 0$ is satisfied when $i \approx 63.4°$. Around this value we start to analyze the structure of the manifolds that are in this region, by playing with the orbital parameters a and e. We start with the model in which the Moon is not inclined w.r.t. the ecliptic plane, by setting $i_M = 0$, and considering also only the orbits that are circular, namely $e = 0$. In this way the Hamiltonian reduction to the center manifold[1] leads to a system with one degree of freedom, and the following Hamiltonian function H_{MECO} (Moon Ecliptic Circular Orbits) is obtained:

$$\overline{H_{MECO}}(H,h;L) = \overline{H_{J_2}}(H;L) + \overline{H_S}(H,h;L) + \overline{H_M^{ecliptic}}(H,h;L). \tag{4.16}$$

As shown in Figure 4.1, the phase space of the center manifold is foliated by one-dimensional

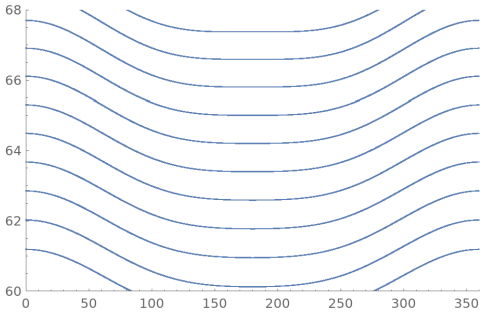

FIGURE 4.1: Phase portrait of the center manifold (Ω vs i) at $a = 26500$ km for the Hamiltonian function $\overline{H_{MECO}}$

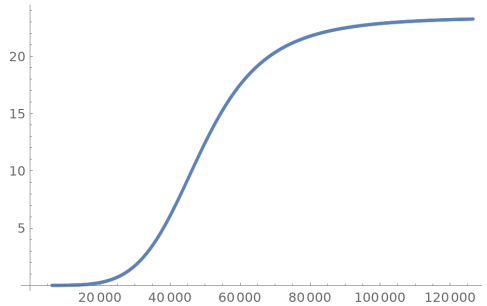

FIGURE 4.2: Inclination of the Laplace plane as a function of the semi-major axis

rotational tori (periodic orbits). These tori correspond to a change in length of the inclination vector, of amplitude equal to the forced inclination, i.e., the local value of the inclination of the Laplace plane (Cook, 1966). Figure 4.2 shows the dependence of the inclination of the Laplace plane on the semi-major axis. This curve is obtained by using the numerical integration of $\dot{h}$ and $\dot{H}$ and approximating the solution of the fixed points given by $\dot{h} = 0$ and $\dot{H} = 0$.
Let us analyze what happens with the tori in Figure 4.1 when the additional angle Ω_M appears in the combinations of angles, i.e. the Moon is set in an inclined orbit with respect to the ecliptic plane. This means, to construct a Hamiltonian, say H_{MICO} (Moon Inclined Circular Orbits), for which we have $e = 0$ and $i_M \neq 0$:

$$\overline{H_{MICO}}(H,h,\Omega_M;L) = \overline{H_{J_2}}(H;L) + \overline{H_S}(H,h;L) + \overline{H_M}(H,h,\Omega_M;L). \tag{4.17}$$

To depict the phase space structure, we then employ a Poincaré surface of section (Ω, i), with the intersection points corresponding to the points for which the angle Ω_M has done a full rotation (with period 18.6 years). In Figure 4.3 we now observe the presence of both rotational and librational tori. The latter are generated by lunisolar resonances transverse to $2g$, which involve the argument of the lunar node Ω_M.
On the other hand, to examine the domain transverse to the center manifold we keep the Moon on the ecliptic plane and leave the orbits to have any possible eccentricity, thus ending

[1] The center manifold is described by the behavior of the orbits nearby an equilibrium point. The definition and the theorem of existence of the center manifold can be found, for example, in (Wiggins, 2003).

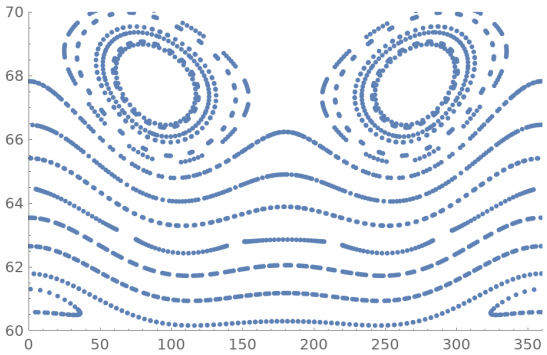

FIGURE 4.3: Ω vs i at $a = 26500$ km for the Hamiltonian function $\overline{H_{MICO}}$

up with the following Hamiltonian function

$$\overline{H_{MEEO}}(G,H,g,h;L) = \overline{H_{J_2}}(H,G;L) + \overline{H_S}(G,H,g,h;L) + \overline{H_M}(G,H,g,h;L). \quad (4.18)$$

It is convenient to write $\overline{H_{MEEO}}$ (Moon Ecliptic Elliptic Orbits) in the Poincaré variable, motivated by the analysis of the phase space $e\sin(\omega)$-$e\cos(\omega)$ around the critical inclination $i_c = 63.4^o$. To get this, we first fix the semi-major axis a and then define the linear transformation $\delta i = i - i_c$.

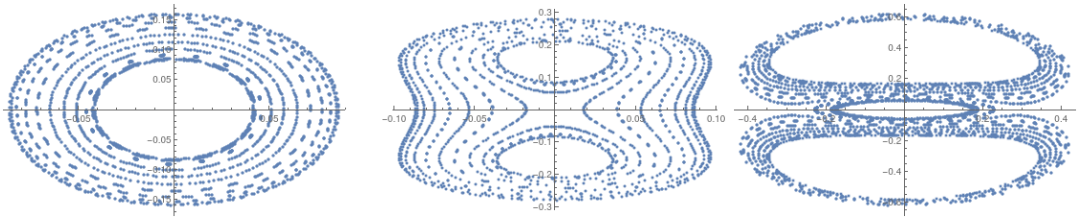

FIGURE 4.4: Stroboscopic plot of the phase space $(X_2, Y_2) = (e\sin(\omega), e\cos(\omega))$ for different values of δi for the Hamiltonian function $\overline{H_{MEEO}}$

In this way we can see how the phase space evolves when we are closer or farther from the center of resonance $2g$. Again we have a 2-DoF Hamiltonian, in the variables (X_2, X_3, Y_2, Y_3), and we plot the stroboscopic surface of section (X_2, Y_2) point whenever $\Omega = 0 \mod 2\pi$. Figure 4.4 shows an example of the sequence of bifurcations characterizing the stability of the central periodic orbit in the direction transverse to the center manifold. We notice a fast eccentricity growth for the orbits with initial conditions close to, or upon the unstable manifolds, which imply an exponential deviation of the orbits far from the circular orbit at the origin.

4.1.4 The effect of the solar radiation pressure

While the expansion of the perturbation due to the Sun in (3.21) up to order 2 does not show the presence of the semi-fast angle M_S, in the case of the expansion of the solar radiation pressures (3.23) we obtain an expression that has the following structure:

$$\overline{H_{SRP}} = \frac{A}{m} C_r P_r a e \left(\mathcal{T}_1 + \mathcal{T}_2 + \mathcal{T}_3\right), \quad (4.19)$$

where

$$\begin{aligned}
\mathcal{T}_1 &= \sum_{\substack{k_1\in\{-1,1,2,3\}\\ k_2\in\{-1,1\}\\ k_3\in\{-1,1\}}} A_{k_1k_2k_3}\cos(k_1\cdot M_s + k_2\cdot\omega + k_3\cdot\Omega),\\
\mathcal{T}_2 &= \cos(i)\sum_{\substack{k_1\in\{-1,1,2,3\}\\ k_2\in\{-1,1\}\\ k_3\in\{-1,1\}}} B_{k_1k_2k_3}\cos(k_1\cdot M_s + k_2\cdot\omega + k_3\cdot\Omega),\\
\mathcal{T}_3 &= \sin(i)\sum_{\substack{k_1\in\{-1,1,2,3\}\\ k_2\in\{-1,1\}}} C_{k_1k_2}\cos(k_1\cdot M_s + k_2\cdot\omega),
\end{aligned} \tag{4.20}$$

where $A_{k_1k_2k_3}$, $B_{k_1k_2k_3}$, $C_{k_1k_2}$ are real coefficients. The presence of M_S in the expression (4.20) leads us to the following definition.

Definition 37 *We say that an object is in $k_1 : k_2 : k_3$ **semi-secular resonance** with the Sun, for $k_1, k_2, k_3 \in \mathbf{Z}\backslash\{0\}$, which means a commensurability between the angles M_s, ω and Ω, whenever $k_1\dot{M}_S + k_2\dot{\omega} + k_3\dot{\Omega} = 0$, $\forall k_1 \in \{-1,1,2,3\}, k_2 \in \{-1,1\}, k_3 \in -1,0,1$.*

The semi-secular effects will be numerically analyzed in Section 4.2.2.

4.2 Numerical analysis of the dynamics

The integration of the Cartesian equations described in Section 3.3.6 and the Hamilton's equation for the different systems analyzed in Section 4.1 is done using a *Runge-Kutta* 4th order integrator. The plots obtained in this section are obtained by using `Mathematica`© and `SIMPRO`, a software which is briefly described in the Appendix B.

4.2.1 Evolution of the orbital elements in different regimes

The purpose of this section is to numerically validate the construction of different Hamiltonian models in several cases. Let us start by comparing the evolution of the mean orbital elements obtained by integrating Hamilton's equations with the evolution of the osculating elements obtained by integrating the Cartesian equations. For this comparison, we included all forces described in Chapter 3, namely J_2, J_3, Moon, Sun, SRP and drag effect for objects in LEO. Since the semi-major axis is constant in the model of secular dynamics, we are interested in comparing the evolution of the mean eccentricity and the mean inclination with the evolution of the corresponding osculating elements.
We present in the Figures 4.5, 4.6, and 4.7 how the elements evolve in time for different altitudes, different eccentricities and different inclinations, respectively, fixing the initial values for the other elements. In Figure 4.5 we observe that the discrepancy between the two integration methods increases as the altitude gets higher. Also, we can notice here that the Hamilton's equations solution is able to catch both the semi-secular and secular effects even at high altitudes.

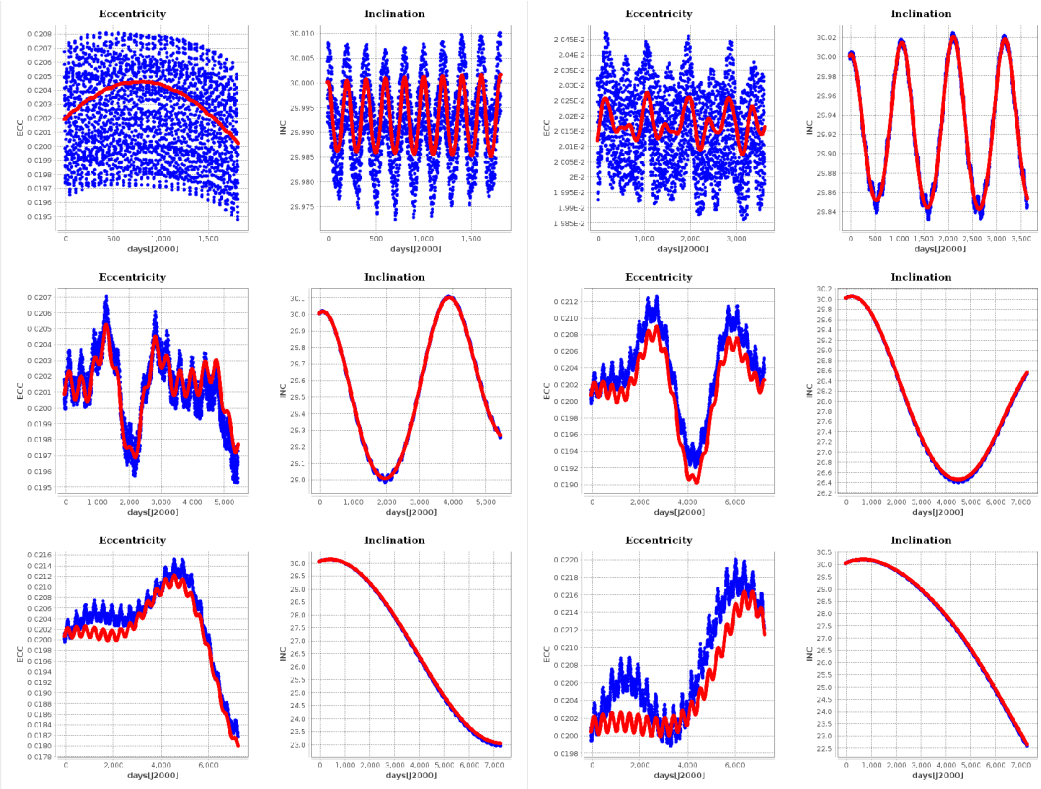

FIGURE 4.5: Comparison of the eccentricity evolution (columns 1 and 3) and inclination evolution (columns 2 and 4) at different altitudes $a = 10000$ km (top-left), $a = 16000$ km (top-right), $a = 23000$ km (middle-left), $a = 29000$ km (middle-right), $a = 35000$ km (bottom-left), $a = 40000$ km (bottom-right). The initial conditions for the other orbital elements are: $e = 0.02$, $i = 30°$, $\omega = 30°$, $\Omega = 20°$. Both the Cartesian (blue curves) and the Hamiltonian (red curves) solutions are obtained for a model that includes J_2, J_3, Moon, Sun, SRP and drag effect (for objects in LEO).

By fixing the initial altitude, namely $a = 21600$ km, in Figure 4.6, we remark a good agreement also for eccentricity greater that 0.5 (right bottom plot of Figure 4.6), for which the semi-secular effects are slightly different. This happens because the terms that produce this effect are not included in the Hamiltonian of the Moon (3.18) and the Sun (3.21), when the expansion in eccentricity is up to order 2. Another point to note here is that the evolution of the inclination is not very much affected by different shapes of the orbit.

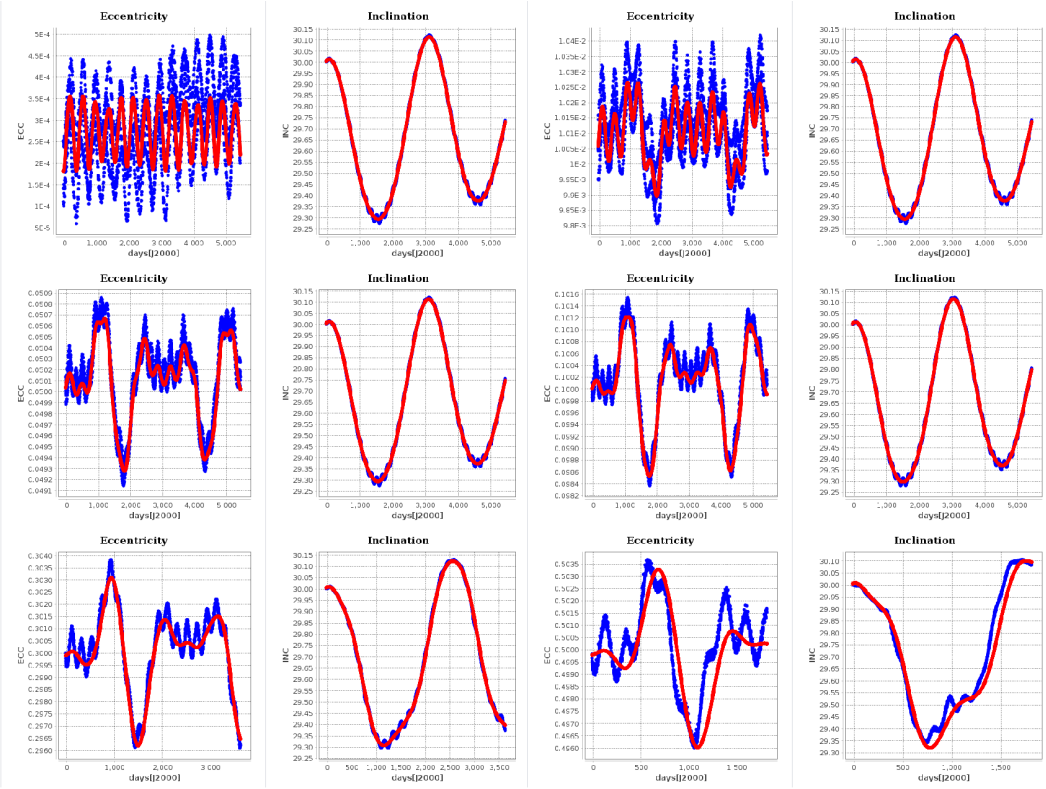

FIGURE 4.6: Comparison of the eccentricity evolution (columns 1 and 3) and inclination evolution (columns 2 and 4) at different initial eccentricities $e = 0$, $e = 0.01$, $e = 0.05$, $e = 0.1$, $e = 0.3$, $e = 0.5$. The initial conditions for the other orbital elements are: $a = 21600$ km, $i = 30°$, $\omega = 20°$, $\Omega = 20°$. Both the Cartesian (blue curves) and the Hamiltonian (red curves) solutions are obtained for a model that includes J_2, J_3, Moon, Sun, SRP and drag effect (for objects in LEO).

In the last comparison between the two integration models, we are interested to see if the orbital elements evolutions behave well also at different inclinations. This is shown in Figure 4.7, where apart from the polar orbits (right-bottom plot), the secular dynamics is in agreement with the evolution of the osculating elements. An interesting aspect here appears in the left-bottom plot, at $i = 63.4°$ (critical inclination), where we notice a growth in eccentricity as explained in the Section 4.1.3. This type of orbits are analyzed in detail in the remaining part of this section.

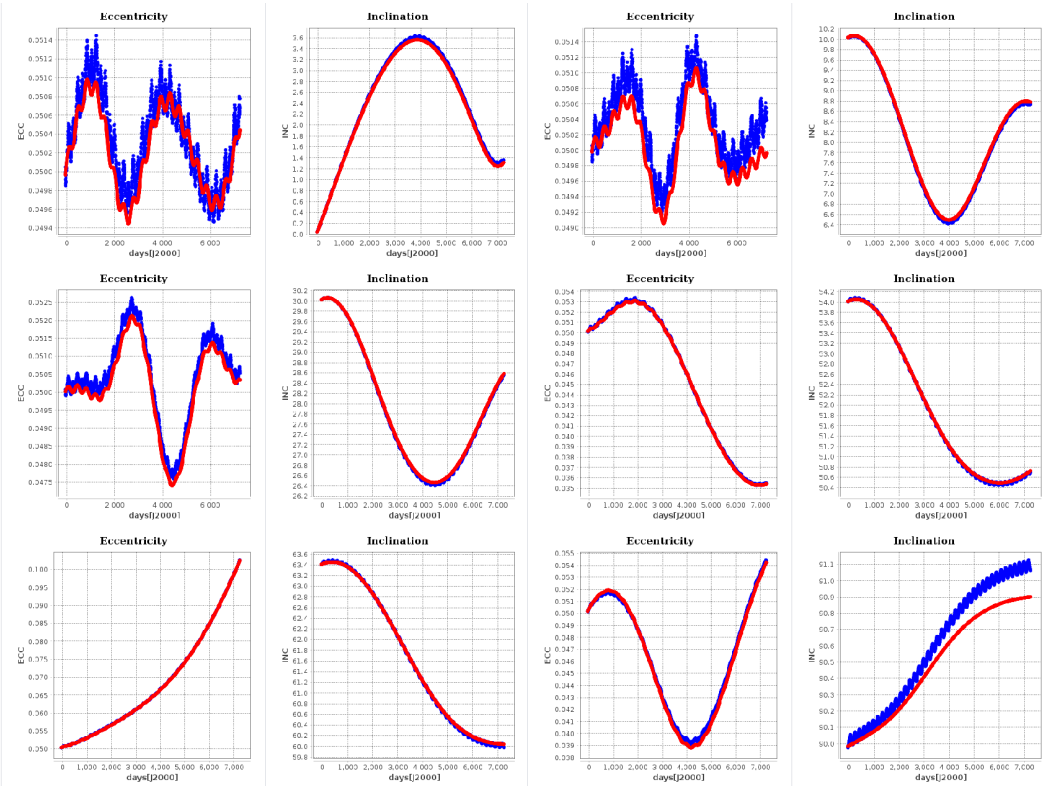

FIGURE 4.7: Comparison of the eccentricity evolution (columns 1 and 3) and inclination evolution (columns 2 and 4) at different initial inclinations $i = 0°$, $i = 10°$, $i = 30°$, $i = 54°$, $i = 63.4°$, $i = 90°$. The initial conditions for the other orbital elements are: $a = 29000$ km, $e = 0.05$, $\omega = 20°$, $\Omega = 20°$.

Since the numerical integration of the Hamiltonian model is now validated for several regions, we will continue the numerical analysis of the secular effects without including the evolution of the osculating elements.

4.2.2 Secular evolution of the eccentricity under different effects

It was shown in Section 4.1.1 that the mean eccentricity and the mean inclination are constants for the J_2 secular problem. An important point of this analysis is to understand what happens if we perturb more and more the constancy of these elements by progressively introducing other effects.

As a first example, let us see in what region the J_3 perturbation becomes significant. Since this is an effect of the non-sphericity of the Earth, we expect to see changes in the evolution of the eccentricity for low altitude orbits. Let us take for example a grid of initial semi-major axis $a = [7000\,km, 17000\,km, 27000\,km, 37000\,km]$ and initial inclinations $i = [0°, 30°, 63.4°, 116°]$. Since the grid includes also low altitudes, we take as an initial eccentricity the value $e = 0.05$ (to avoid the re-entry of the objects).

Let us analyze the several phenomena observed in Figure 4.8 by starting with the low altitude orbits, namely the column 1. As it is expected, the most important factor in this region (600 km above the Earth surface) is the air drag force. This is the main reason of the "circularization" of the ellipse, since $e \to 0$, when $t \to \infty$. Comparing the magenta and blue curves in these columns, we remark that the decreasing speed highly depends on the A/m ratio. As well, the plots in these columns show for low inclinations: a semi-secular oscillations of the evolution, which is caused by to the strong effect of J_3 (close to the Earth), and by the weak

influence of the lunisolar effects. On the other hand, for the critical values of the inclination, the J_3 effect becomes negligible, due to the lunisolar resonances.

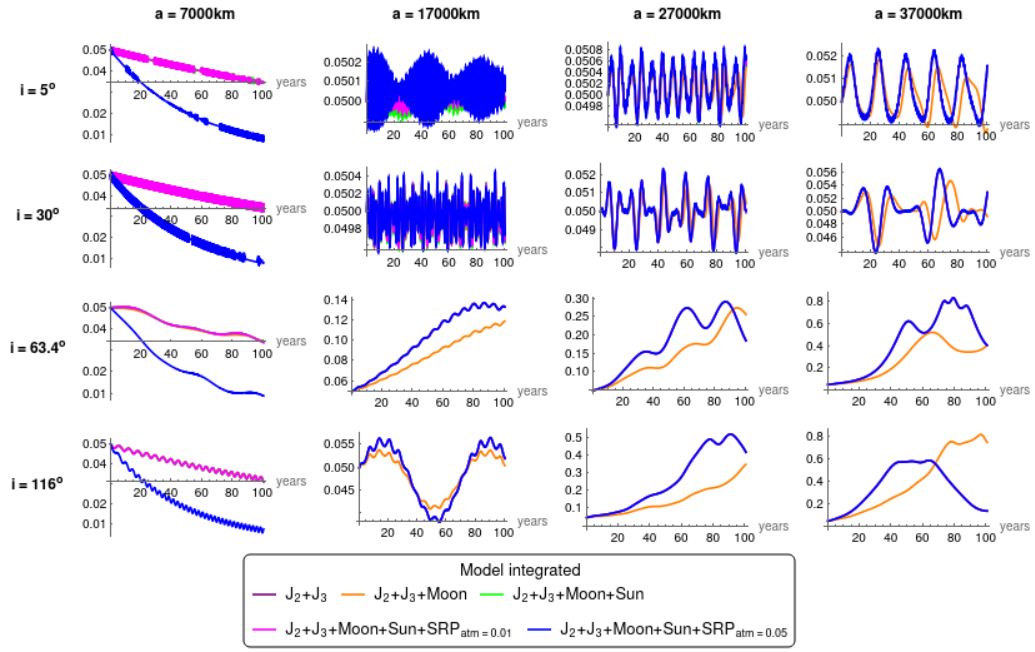

FIGURE 4.8: Comparison of the eccentricity evolution at different initial inclinations $i = 5°$, $i = 30°$, $i = 63.4°$, $i = 116°$ and different initial altitudes $a = 7000$ km, $a = 17000$ km, $a = 27000$ km, $a = 37000$ km. The initial conditions for the other orbital elements are: $e = 0.05$, $\omega = 30°$, $\Omega = 10°$.

For the second column, the dominant terms are represented by J_2 and J_3, far from lunisolar resonances, and by the lunar terms for the last two plots. In this case, since the atmospheric drag is not present anymore, we notice a significant growth in eccentricity, for the models that include the lunar terms (all, but no purple curve). It is worth mentioning that the Sun does not have a clear importance in the secular growth. As it can be seen in the plots from (line 3, column 2) and (line 3, column 4) of Figure 4.8, the orange and green curves overlap, and also the magenta and blue ones. This implies only a semi-secular effect due to the solar radiation pressure.

The third and the forth columns show how the lunisolar effects become the most important perturbation over a long time-scale. Even for values of the inclination far from the lunisolar resonances, the evolution of the eccentricity shows only oscillations of order of years, which is an effect of the Moon and Sun attraction; also the Solar radiation highlights that the orbits are almost re-entry, which means very eccentric orbits, with a low level of perigee ($(1-0.8)\cdot 37000 = 7400$ km). This effect was mathematically described in Section 4.1.3.

Chapter 5

Proper Elements for Space Debris

This chapter is dedicated to the theoretical description of the normalization procedure in different contexts. We start by presenting the simplest case, namely a 2-DoF system including the J_2, J_3, Moon and Sun perturbations, mentioning that in the first section we consider the approximation that the orbital plane of the Moon is the same as the ecliptic plane. This restriction is made just for simplifying the notations, while focusing on the steps of the procedure. In the second section, the tesseral and lunisolar resonant cases are analyzed and a modification of the original procedure is presented. At this point we want also to see the influence of the nodes of the Moon during the normalization, so we will drop the restriction of the Moon on the ecliptic plane. The last section will approach the case of dissipative systems, where a semianalytic method for the computation of the proper elements is presented.

5.1 Proper elements for the non-resonant case - analytic solutions

Let us start by defining the Hamiltonian function which describes a system perturbed by J_2, J_3, Sun and Moon, with the Moon on the ecliptic plane, precisely with $i_M = 0$ in (3.18). We denote this Hamiltonian function by H_{NR}, that we express as

$$\begin{aligned} H_{NR}(G,H,g,h;L) &= \overline{H_{J_2}}(G,H;L) + \overline{H_{J_3}}(G,H,g;L) + \overline{H_S}(G,H,g,h;L) \\ &+ \overline{H_M^{ecliptic}}(G,H,g,h;L), \end{aligned} \tag{5.1}$$

where $\overline{H_{J_2}}(G,H;L)$, $\overline{H_{J_3}}(G,H,g;L)$, $\overline{H_S}(G,H,g,h;L)$, $\overline{H_M^{ecliptic}}(G,H,g,h;L)$ are given in (4.4), (4.6), (4.14), and (4.15), respectively.

5.1.1 Proper semi-major axis

Since H_{NR} does not depend on the mean anomaly l, its conjugated action L will be constant over time. Taking into account this aspect, we give the following definition.

Definition 38 *We call **proper semi-major axis**, for the Hamiltonian system defined by the function H_{NR}, the initial value of the mean semi-major axis.*

While the Delaunay action L is constant, the mean semi-major axis $a = \frac{L^2}{\mu}$ will be also constant, and therefore the definition is consistent.

Remark 11 *We mention that the normalization procedure is presented in this framework, because in most of the cases the elements mainly affected by perturbations are the eccentricity and the inclination. The semi-major axis is affected only by tesseral resonances and drag effects, which we consider as peculiar cases.*

5.1.2 Before the normalization

Once the proper semi-major axis is determined, we focus on the computation of the remaining two proper elements. Before applying the theoretical algorithm described in Section 2.3, we need to make some preparation of the Hamiltonian function that has to be normalized.
Let us start with some initial values for the mean orbital elements, say $(a_0, e_0, i_0, M_0, \omega_0, \Omega_0)$. We will denote by $(L_0, G_0, H_0, l_0, g_0, h_0)$ the corresponding initial conditions in Delaunay's variables obtained by using (4.1).
The first canonical transformation applied to H_{NR} is a linear change in the actions, described as follows

$$P = G - G_0, \qquad Q = H - H_0, \qquad p = g, \qquad q = h. \tag{5.2}$$

Substituting also L with L_0, we obtain the new Hamiltonian function H_{NR}^{lin} having the following form

$$\begin{aligned} H_{NR}^{lin}(P,Q,p,q;\quad L_0,G_0,H_0) &= \overline{H_{J_2}}(P,Q;L_0,G_0,H_0) + \overline{H_{J_3}}(P,Q,p;L_0,G_0,H_0) \\ &+\overline{H_S}(P,Q,p,q;L_0,G_0,H_0) + \overline{H_M^{ecliptic}}(P,Q,p,q;L_0,G_0,H_0). \end{aligned} \tag{5.3}$$

We are interested now in splitting H_{NR}^{lin} in 3 different parts, namely a part that contains only the actions at the first power (H_{NR}^0), a part that is free of angles and excludes H_{NR}^0 (h_{NR}^0) and a remainder that contains combinations of actions with sine or cosine of angles (R_{NR}^0).
Taking into account the non-linear form of the functions involved in this Hamiltonian we need to perform an expansion in power series. Since the new action variables P and Q of H_{NR}^{lin} are very small, we can make this expansion around the values $P = 0$ and $Q = 0$. At this point we can define the Hamiltonian function that will be normalized as follows:

$$\begin{aligned} H_{NR}^{expanded}(P,Q,p,q;L_0,G_0,H_0) &= H_{NR}^0(P,Q;L_0,G_0,H_0) + \lambda\Big(h_{NR}^0(P,Q;L_0,G_0,H_0) \\ &+R_{NR}^0(P,Q,p,q;L_0,G_0,H_0)\Big), \end{aligned} \tag{5.4}$$

where we intend that H_{NR}^0, h_{NR}^0 are expanded around $P = 0$ and $Q = 0$.
Since H_{NR}^0 is a function linear in the actions P and Q, we easily find the frequency vector $\nu = (\nu_P, \nu_Q)$, where

$$\begin{aligned} \nu_P &= \frac{9.2690\cdot 10^{-5}H_0^2}{G_0^6L_0^3} - \frac{1.8538\cdot 10^{-5}}{G_0^4L_0^3} + \frac{3.3928\cdot 10^{-5}H_0^2L_0^4}{G_0^3} - 0.6785\cdot 10^{-5}G_0L_0^2, \\ \nu_Q &= -\frac{3.7076\cdot 10^{-5}H_0}{G_0^5L_0^3} - \frac{3.3928\cdot 10^{-5}H_0L_0^4}{G_0^2} + 2.0356\cdot 10^{-5}H_0L_0^2. \end{aligned} \tag{5.5}$$

On the other hand, the remainder R_{NR}^0 has the following form

$$\begin{aligned} R_{NR}^0 &= \sum_{\substack{k_1=2\\ k_2\in\{-2,-1,0,1,2\}}} f_{\{k_1,k_2\}}(P,Q;L_0,G_0,H_0)\cos(k_1p+k_2q) \\ &+ \sum_{\substack{k_1=0\\ k_2\in\{1,2\}}} f_{\{k_1,k_2\}}(P,Q;L_0,G_0,H_0)\cos(k_1p+k_2q) \\ &+ f_{\{1,0\}}(P,Q;L_0,G_0,H_0)\sin(p), \end{aligned} \tag{5.6}$$

where $f_{\{k_1,k_2\}}$ is a function which depends on P, Q and the initial values L_0, G_0, H_0.
The function h_{NR}^0 is a polynomial depending only on the actions with the degree equal to the

order of the power series expansion. The symbol λ introduced in (5.4) is a parameter, the so-called 'book-keeping', that is used to keep track of the terms at each order of normalization.

5.1.3 Normal form procedure

To compute the normal form using the procedure described in Section 2.3, we need to transform the remainder R^0_{NR} in a Fourier series, like the function in (2.14).

Proposition 5 *The steps of the normalization procedure described in Section 2.3.1 are well-defined for the initial Hamiltonian function $H^{expanded}_{NR}$ if and only if the inclination $|i_0 - i_c| > \delta$, where $i_c \in \{46.3°, 56°, 63.4°, 69°, 73.1°, 90°, 106.8°, 111°, 116.5°, 123.9°, 133.6°\}$ and δ is a tolerance value.*

Proof 3 In the equations (2.13)-(2.22), only the computation of the new coefficients (2.21) might provoke singularities. This would happen if the scalar product between the vector obtained with the angles' coefficients in the remainder and the frequency vector $\boldsymbol{\nu}$ is zero. Taking into account the form of H^0_{NR}, we define the set of all possible coefficient vectors that appear inside the sine or cosine function, $\mathcal{K} = \{\{2,0\},\{2,-2\},\{2,-1\},\{0,1\},\{0,2\},\{2,1\},\{2,2\},\{1,0\}\}$.
Using the transformations (4.1), after some algebraic computations, the frequency vector $\boldsymbol{\nu}$ is defined in orbital elements as follows:

$$\begin{aligned} \nu_P &= \frac{c_1 \cos^2(i_0) - c_2}{a^{7/2}\left(e^2-1\right)^2}, \\ \nu_Q &= -\frac{c_3 \cos(i_0)}{a^{7/2}\left(e^2-1\right)^2}, \end{aligned} \tag{5.7}$$

where $c_1 = 1.42672 \cdot 10^{12}, c_2 = -2.8534 \cdot 10^{11}, c_3 = -5.70688 \cdot 10^{11}$ are constants in proper units. By taking any scalar product $\boldsymbol{\nu} \cdot \boldsymbol{k}$, $\forall \boldsymbol{k} \in \mathcal{K}$, one obtains the equation

$$\frac{1}{a^{7/2}\left(e^2-1\right)^2}\left(k_1 c_1 \cos^2(i_0) - k_1 c_2 - k_2 c_3 \cos(i_0)\right), \tag{5.8}$$

which vanishes when $k_1 c_1 \cos^2(i_0) - k_1 c_2 - k_2 c_3 \cos(i_0) = 0$. After substituting $\boldsymbol{k} = (k_1, k_2) \in \mathcal{K}$ and solving the quadratic equation in $\cos(i_0)$, the solutions are given by the values of i_c. A threshold δ, according to the specific value of the inclination, is needed since in a vicinity of i_c the scalar product $\boldsymbol{\nu} \cdot \boldsymbol{k}$ tends to zero. □

Far from the values of i_c in Proposition 5, the procedure described in Section 2.3.1 is applied straight-forward to obtain the generating function χ^1_{NR} and the new Hamiltonian H^1_{NR} after the first order normalization of the Hamiltonian function $H^{expanded}_{NR}$, where

$$\begin{aligned} \chi^1_{NR} &= \sum_{\substack{k_1=2 \\ k_2\in\{-2,-1,0,1,2\}}} g_{\{k_1,k_2\}}(P,Q;L_0,G_0,H_0)\cos(k_1 p + k_2 q) \\ &+ \sum_{\substack{k_1=0 \\ k_2\in\{1,2\}}} g_{\{k_1,k_2\}}(P,Q;L_0,G_0,H_0)\cos(k_1 p + k_2 q) \\ &+ g_{\{1,0\}}(P,Q;L_0,G_0,H_0)\sin(p), \end{aligned} \tag{5.9}$$

and

$$\begin{aligned} H^1_{NF}(P^1,Q^1,p^1,q^1 \quad ; \quad & L_0,G_0,H_0) = H^0_{NR}(P^1,Q^1;L_0,G_0,H_0) \\ + \quad & \lambda H^1_{NR}(P^1,Q^1;L_0,G_0,H_0) \\ + \quad & \lambda^2\left(h^1_{NR}(P^1,Q^1;L_0,G_0,H_0) + R^2_{NR}(P^1,Q^1,p^1,q^1;L_0,G_0,H_0)\right). \end{aligned} \tag{5.10}$$

The relation between the function $g_{\{k_1,k_2\}}$ in (5.9) and the function $f_{\{k_1,k_2\}}$ in (5.6) is given by the formula (2.21). The superscript "1" in (5.10) indicates the Hamiltonian function obtained after the first order normalization. Thus, if we remove the terms that depend on λ^2 and set λ to be 1 in (5.10), we obtain a function that contains only the actions.

Definition 39 *We call the* ***normal form at the first order*** *of the system described by the Hamiltonian function $H^{expanded}_{NR}$ in (5.4), the function $H_{NF}(P^1,Q^1;L_0,G_0,H_0)$ which is defined as*

$$H_{NF}(P^1,Q^1;L_0,G_0,H_0) = H^0_{NR}(P^1,Q^1;L_0,G_0,H_0) + H^1_{NR}(P^1,Q^1;L_0,G_0,H_0). \tag{5.11}$$

5.1.4 Proper eccentricity and proper inclination

In Section 5.1.3, we ended up with a Hamiltonian function H_{NF} that depends only on the action variables, which means that the new system is integrable, and even more, its solution can be obtained from Hamilton's equation:

$$\begin{aligned} P^1(t) &= P^1_0, \\ Q^1(t) &= Q^1_0, \\ p^1(t) &= p^1_0 + \frac{\partial H_{NF}}{\partial P^1}(P^1_0,Q^1_0)t, \\ q^1(t) &= q^1_0 + \frac{\partial H_{NF}}{\partial Q^1}(P^1_0,Q^1_0)t\,, \end{aligned} \tag{5.12}$$

where P^1_0, Q^1_0, p^1_0, and q^1_0 are the initial conditions for the normalized system, which are unknowns. Nevertheless, it is possible to obtain these values from the initial conditions of the initial Hamiltonian system, by using the generating function χ^1_{NR}. The relation between the new and the old variables is given by

$$\begin{aligned} P^1(P,Q,p,q) &= (S^{\lambda}_{\chi^1_{NR}})^{-1}P, \\ Q^1(P,Q,p,q) &= (S^{\lambda}_{\chi^1_{NR}})^{-1}Q, \\ p^1(P,Q,p,q) &= (S^{\lambda}_{\chi^1_{NR}})^{-1}p, \\ q^1(P,Q,p,q) &= (S^{\lambda}_{\chi^1_{NR}})^{-1}q, \end{aligned} \tag{5.13}$$

where $S^{\lambda}_{\chi^1_{NR}}$ is the Lie series operator defined in (2.9). Since the new variables can be written as functions of the old variables, once we have the values of the old variables (P_t,Q_t,p_t,q_t) at a certain time t, the values of the new variables are obtained by

$$\begin{aligned} P^1_t &= P^1(P_t,Q_t,p_t,q_t), \\ Q^1_t &= Q^1(P_t,Q_t,p_t,q_t), \\ p^1_t &= p^1(P_t,Q_t,p_t,q_t), \\ q^1_t &= q^1(P_t,Q_t,p_t,q_t). \end{aligned} \tag{5.14}$$

Definition 40 *We say that the values $P_t^1, Q_t^1, p_t^1, q_t^1$ are **proper elements** of the initial Hamiltonian system at time t.*

Once the proper elements are known, we can compute the proper eccentricity and inclination of the orbit, by using the inverse of the transformations used to obtain $H_{NR}^{expanded}$. Namely, we first shift back the actions to obtain the proper Delaunay actions, $G_t = P_t + G_0$ and $H_t = Q_t + H_0$. Then, we can compute the proper eccentricity (e_t) and proper inclination (i_t) by using the formulas in (4.1).
The analysis of the accuracy and stability of the proper elements computed in this chapter is presented in Chapter 6.

Remark 12 *In the same manner, the computation of proper eccentricity and proper inclination can be done also for a Hamiltonian system that takes into account the inclination of the Moon w.r.t the ecliptic plane, and the effect of the Solar radiation pressure. Far from any resonance (either secular or semi-secular), the procedure described here (with some consideration explained in details in Section 5.2) is able to compute the proper elements. Nevertheless, once included these two effects, the set of small divisors becomes larger and so it needs a dedicated method.*

5.2 Proper elements in the resonant cases - semi-analytic solutions

We already notice in Chapter 4 that there are several situations when the dynamics of the Hamiltonian system is affected by some resonant effects. This Section analyzes the computation of the proper elements in the resonant case.

5.2.1 Tesseral resonance

Let us analyse the case of a 2:1 tesseral resonance (1:1 or other tesseral resonances could be similarly approached), which is described in Section 4.1.2 and let us consider the Hamiltonian function that describes the system:

$$\begin{aligned} H_{R21}(L,G,H,l,g,h;\theta) &= \overline{H_{J_2}}(L,G,H) + \overline{H_{J_3}}(L,G,H) + \overline{H^t_{res2:1}}(L,G,H,l,g,h;\theta) \\ &+ \overline{H_S}(L,G,H,g,h) + \overline{H_M^{ecliptic}}(L,G,H,g,h) + H_{Kep}(L) \end{aligned} \quad (5.15)$$

where the expansions $\overline{H_{J_2}}(G,H;L)$, $\overline{H_{J_3}}(G,H,g;L)$, $H_{Kep}(L)$, $\overline{H^t_{res2:1}}(L,G,H,l,g,h;\theta)$, $\overline{H_S}(G,H,g,h;L)$, and $\overline{H_M^{ecliptic}}(G,H,g,h;L)$ are given in (4.4), (4.6), (4.7), (4.9), (4.14), and (4.15), respectively.
In this case we have a 3-DoF time-dependent Hamiltonian system, where the time-dependency comes from the angle θ (sidereal time), which in the proper units is exactly the proper time t. The preparation of the Hamiltonian for the normalization will follow the same steps as in Section 5.1, after we consider the angle θ as a new angle and introduce its conjugated action Θ. In this way we extend the phase space by one fictitious dimension. The extension of the phase space is consistent if the Hamilton's equation of the new system are the same as in the original system. This means that we add the new action Θ with the coefficient being equal to the frequency of the angle θ, namely equal to 1. In this way, we

obtain the extended Hamiltonian function, written as

$$\begin{aligned} H^{ext}_{R21}(L,G,H,\Theta,l,g,h,\theta) &= \overline{H_{J_2}}(L,G,H)+\overline{H_{J_3}}(L,G,H)+\overline{H^t_{res2:1}}(L,G,H,l,g,h,\theta) \\ &+ \overline{H_S}(L,G,H,g,h)+\overline{H^{ecliptic}_M}(L,G,H,g,h) \\ &+ H_{Kep}(L)+\Theta. \end{aligned} \tag{5.16}$$

Remark 13 *The definition of the proper semi-major axis given in Section 5.1 is no more valid for this case, since the mean semi-major axis is not constant in the case of a Hamiltonian including tesseral resonances.*

At this point, the steps presented in Section 5.1 will be implemented similarly, but with the additional expansion of R around the initial Delaunay action L_0 and with Θ as a dummy variable.
An important aspect of this case is that the remainder, R^0_{R21}, depends now on more combinations of angles, which include of course the combination of the resonant angle $2\theta - l$ (r in the shifted variables). This combination of angles, alongside with the interaction with the other angles, will provoke the appearance of the small divisors. In this case the small divisors are not obtained only by changing the inclination, but they will occur as a combination of a_0, e_0 and i_0, as it is described in Section 2.3.2. The form of the remainder function R^0_{R21} is the following:

$$\begin{aligned} R^0_{R21} &= c_1\cos(2\theta-2q-r+2.62049)+c_2\cos(2\theta-2p-2q-r+2.62049) \\ &+ c_3\sin(2\theta-p-2q-r+2.54159)+f_{\{0,1,0,0\}}(R,P,Q;L_0,G_0,H_0)\sin(p) \\ &+ \sum_{\substack{k_1=0\\ k_2\in\{1,2\}}} f_{\{0,k_1,k_2,0\}}(R,P,Q;L_0,G_0,H_0)\cos(k_1p+k_2q) \\ &+ \sum_{\substack{k_1=2\\ k_2\in\{-2,-1,0,1,2\}}} f_{\{0,k_1,k_2,0\}}(R,P,Q;L_0,G_0,H_0)\cos(k_1p+k_2q). \end{aligned} \tag{5.17}$$

As in the case of the non-resonant normalization (5.6), $f_{\{k_1,k_2,k_3,k_4\}}$ is a function that depends on the actions and the initial values. Since we encounter the small divisors during the computation of χ^1_{R21}, we need to take into account the remarks in Section 2.3.2 such that the resonant terms will not be part of the generating function, but they will appear in the new Hamiltonian obtained, as follows

$$\begin{aligned} H^1_{RNF}(R^1,P^1,Q^1,\Theta^1,r^1,p^1,q^1,\theta^1;L_0,G_0,H_0) &= H^0_{R21}(R^1,P^1,Q^1;L_0,G_0,H_0) \\ &+ \lambda\left(H^1_{R21}(R^1,P^1,Q^1,r^1,p^1,q^1;L_0,G_0,H_0)\right) \\ &+ \lambda^2\left(h^1_{R21}(R^1,P^1,Q^1;L_0,G_0,H_0)\right. \\ &+ \left.R^2_{R21}(R^1,P^1,Q^1,r^1,p^1,q^1;L_0,G_0,H_0)\right), \end{aligned} \tag{5.18}$$

where H^0_{R21} is the part containing only the action at the first power; H^1_{R21} is the part of the normal obtained after the first order normalization and which contains the resonant combination of the angles r^1, p^1, q^1; h^1_{R21} and R^2_{R21} are the reminders obtained after the first step of the procedure. Once we neglect the terms depending on λ^2 and setting λ equal to 1 in (5.18), we obtain a function H_{RNF}, that is a 1-DoF Hamiltonian, which is still integrable, although

usually it is not possible to find a closed-form solution:

$$\begin{aligned} H_{RNF}(R^1,P^1,Q^1,\Theta^1,r^1,p^1,q^1,\theta^1;L_0,G_0,H_0) &= H^0_{R21}(R^1,P^1,Q^1;L_0,G_0,H_0) \\ &+ H^1_{R21}(R^1,P^1,Q^1,r^1,p^1,q^1;L_0,G_0,H_0). \end{aligned} \tag{5.19}$$

In the resonant case, we adopt a different methodology to compute the proper values taking into account also the resonant effects. Since the resulting system depends only on one combination of the angles, we can make a canonical transformation such that the new system will depend only on the resonant angle, say σ, and its conjugated action, Σ. The other momenta obtained after the transformation, say Ψ, Φ, Υ, will be constant for the new Hamiltonian. Having this transformation, the Hamiltonian function can be written as:

$$\overline{H_{RNF}}(\Sigma,\sigma;\Psi,\Phi,\Upsilon) = \overline{H^0_{R21}}(\Sigma;\Psi,\Phi,\Upsilon) + \overline{H^1_{R21}}(\Sigma,\sigma;\Psi,\Phi,\Upsilon). \tag{5.20}$$

Since the variables Ψ, Φ, Υ are constant, we can fix some of their values and compute Hamilton's equations as follows:

$$\begin{aligned} \frac{d\Sigma}{dt}(t) &= -\frac{\partial\overline{H_{RNF}}}{\partial\sigma}, \\ \frac{d\sigma}{dt}(t) &= \frac{\partial\overline{H_{RNF}}}{\partial\Sigma}. \end{aligned} \tag{5.21}$$

One can solve this system of equations by using interpolation methods (see (Morbidelli, 1993)). For this task, it is needed to know the initial values of Σ and σ, which are obtained from the initial values of $R^1,P^1,Q^1,\Theta^1,r^1,p^1,q^1,\theta^1$. The latter $(R^1,P^1,Q^1,\Theta^1,r^1,p^1,q^1,\theta^1)$ can be computed in the same way described in (5.13) and (5.14). Once obtained the evolution of the resonant variables Σ and σ, it is a matter of implementing an inverse transformation to obtain the proper semi-major axis, proper eccentricity and proper inclination.

5.2.2 Lunisolar resonance

The computation of the proper elements in the case of a lunisolar resonance is conceptually the same as in the case of tesseral resonances. The steps of the procedure are basically the following:

1. Define the model before normalization in Delaunay variables;
2. Transform the time-dependent Hamiltonian into an autonomous Hamiltonian by introducing the dummy variables (in case it is needed);
3. Apply the algorithm presented in Section 5.2 to compute the generating function;
4. Using the generating function, compute the new Hamiltonian function, and then the normal form;
5. Since the normal form will depend on the resonant angle, we need to define the resonant variables;
6. Compute the evolution of the resonant variables by using interpolating (or numerical) methods;
7. Compute the proper elements at the initial time using the formulas (5.13) and (5.14);

8. Once the evolution of the resonant variables is obtained, the computation of the proper elements is done by using the inverse transformations.

These steps can be applied whenever a resonant angle is present. Nevertheless, there are some special cases to be mentioned in the case of a lunisolar resonance. In the case when the Moon is not inclined with respect to the ecliptic, there are only some regions where we need to apply the resonant normalization procedure. In those cases, one just follows the steps listed above.
On the other hand, when we take into account the inclination of the Moon with respect to the ecliptic plane, the model is different from the very beginning. We first need to understand if the critical inclinations from Proposition 5 are the same for this case. To this end, let us see which is the Hamiltonian that has to be normalized. Since i_M is not equal to 0 anymore, and taking into account the expression (4.13), we end-up with the following Hamiltonian:

$$\begin{aligned} H_{LSR}(G,H,g,h,h_M;L) &= \overline{H_{J_2}}(G,H;L)+\overline{H_{J_3}}(G,H,g;L)+\overline{H_S}(G,H,g,h;L) \\ &+ \overline{H_M}(G,H,g,h,h_M;L), \end{aligned} \tag{5.22}$$

which depends on the angle $h_M(=\Omega_M)$ (the argument of the ascending node of the Moon). However, we can numerically approximate the evolution of this angle by $-0.0529918^\circ/day$ (see Table (4.1)), which in the proper units is equal to -0.000146798. This implies an extended Hamiltonian of the form

$$\begin{aligned} H_{LSR}(G,H,H_M,g,h,h_M;L) &= \overline{H_{J_2}}(G,H;L)+\overline{H_{J_3}}(G,H,g;L)+\overline{H_S}(G,H,g,h;L) \\ &+ \overline{H_M}(G,H,g,h,h_M;L)-0.000146798H_M. \end{aligned} \tag{5.23}$$

Then, the expanded Hamiltonian around G_0 and H_0 will be written as

$$\begin{aligned} H_{LSR}^{expanded} & (P,Q,Q_M,p,q,q_M;L_0,G_0,H_0) = H^0_{LSR}(P,Q,Q_M;L_0,G_0,H_0) \\ &+\lambda\left(h^0_{LSR}(P,Q;L_0,G_0,H_0)+R^0_{LSR}(P,Q,p,q,q_m;L_0,G_0,H_0)\right), \end{aligned} \tag{5.24}$$

with H^0_{LSR}, h^0_{LSR}, R^0_{LSR} denoting the linear part in actions, namely the part that will be kept in the normal form and the remainder that depends on the angles, respectively. In this case, the frequency vector is $\boldsymbol{\nu}=(\nu_P,\nu_Q,\nu_{Q_M})$, where

$$\begin{aligned} \nu_P &= \frac{9.2690\cdot10^{-5}H_0^2}{G_0^6L_0^3}-\frac{1.8538\cdot10^{-5}}{G_0^4L_0^3}+\frac{3.3928\cdot10^{-5}H_0^2L_0^4}{G_0^3}-0.6785\cdot10^{-5}G_0L_0^2, \\ \nu_Q &= -\frac{3.7076\cdot10^{-5}H_0}{G_0^5L_0^3}-\frac{3.3928\cdot10^{-5}H_0L_0^4}{G_0^2}+2.0356\cdot10^{-5}H_0L_0^2, \\ \nu_{Q_M} &= -1.46798\cdot10^{-4}, \end{aligned} \tag{5.25}$$

and the remainder R^0_{NR} has the following form

$$\begin{aligned} R^0_{LSR} &= \sum_{\substack{k_1\in\{0,2\}\\ k_2\in\{0,1,2\}\\ k_3\in\{-2,-1,0,1,2\}}} f_{\{k_1,k_2,k_3\}}(P,Q;L_0,G_0,H_0)\cos(k_1p+k_2q+k_3q_M) \\ &+ f_{\{1,0,0\}}(P,Q;L_0,G_0,H_0)\sin(p), \end{aligned} \tag{5.26}$$

where $f_{\{k_1,k_2,k_3,k_4\}}$ is a function that depends on the actions and the initial values. Following the proof of Proposition 5, in a similar way we can show that the critical inclination set for

the Hamiltonian system defined by the function H_{LSR} is the following

$$\begin{aligned}\mathcal{R}_{i_c} = \{&23.8^\circ, 31.7^\circ, 39.1^\circ, 43.3^\circ, 46.3^\circ, 49.5^\circ, 51.7^\circ, 54.1^\circ, 56.0^\circ, 57.3^\circ, 58.2^\circ, 62.7^\circ, 63.2^\circ,\\ &63.3^\circ, 63.4^\circ, 63.6^\circ, 63.9^\circ, 67.9^\circ, 69.0^\circ, 70.7^\circ, 73.1^\circ, 74.6^\circ, 75.8^\circ, 76.7^\circ, 79.3^\circ, 82.4^\circ,\\ &86.3^\circ, 90.0^\circ, 92.2^\circ, 93.6^\circ, 97.5^\circ, 100.6^\circ, 103.2^\circ, 104.1^\circ, 105.3^\circ, 106.8^\circ, 109.2^\circ,\\ &110.9^\circ, 112.0^\circ, 116.3^\circ, 116.5^\circ, 116.6^\circ, 116.7^\circ, 117.2^\circ, 121.7^\circ, 122.6^\circ, 123.9^\circ, 125.8^\circ,\\ &128.2^\circ, 130.4^\circ, 133.6^\circ, 136.6^\circ, 140.8^\circ, 148.2^\circ, 156.1^\circ\}. \end{aligned} \tag{5.27}$$

As it can be seen, there are more regions where the resonant normalization procedure is needed, when we take into account the inclination of the Moon w.r.t. the ecliptic plane. This effect is also explained in Section 4.1.3, and it is caused by the apparition of the argument of the nodes of the Moon in the initial Hamiltonian.
With these aspects in mind, we can follow the steps presented in 5.2.2 to compute the generating function, and hence the proper elements.

Remark 14 *The methods of computing the proper elements for some resonant cases do not take into account the possible appearance of the resonance overlapping. This phenomenon might appear for example in case of an orbit close to a* $2:1$ *tesseral resonance, but in the same time having a critical inclination. To solve this problem, one needs a special analysis and a relative importance of the resonant effects.*

5.3 Proper elements for dissipative systems

As it is exposed in Section 4.2, the dissipative effects have an important role in the evolution of the mean semi-major axis and the mean eccentricity for orbits close to the surface of the Earth. The drag effect will provoke a visible decay in these two elements, even over a short period of time.
Since the normalization algorithm described in Section 2.3.1 is based on the assumption that the initial Hamiltonian is preserved, one needs to find an alternative method to compute the proper elements for this case. Moreover, since the drag forces are added to Hamilton's equation, and they are not part of the Hamiltonian function, this is also an issue in the computation of the normal form.
Since the effect of the drag forces is quite predictable, a possibility for the computation of the proper elements would be to split the problem into sub-problems, as follows:

1. Starting from the initial Hamiltonian function which does not contain the drag forces, we can compute the normal form as it is described in Sections 2.3.1, 5.1 and 5.2.
2. Compute the new Hamiltonian and the initial values for the new variables by using the generating function χ obtained at the first step.
3. Compute Hamilton's equation for the new Hamiltonian.
4. Transform the dissipative effects into the new variables.
5. Add the new dissipative effects to the new Hamilton's equation and compute the evolution of the elements in the new variables.
6. Use the inverse transformation to obtain the dissipative proper values and hence the proper semi-major axis, proper eccentricity and proper inclination.

Remark 15 *It is important to mention that the proper elements are no more constant, but their variability is still very small along the drift given by the drag effect.*

5.3.1 Normal forms

Let us consider, as in the conservative case, a simple model to illustrate the procedure, say

$$\begin{aligned} H_C(G,H,g,h;L) &= \overline{H_{J_2}}(G,H;L) + \overline{H_{J_3}}(G,H,g;L) + \overline{H_S}(G,H,g,h;L) \\ &+ \overline{H_M^{ecliptic}}(G,H,g,h;L). \end{aligned} \tag{5.28}$$

Even if the drag effects provoke a change in the mean semi-major axis and the mean eccentricity, by starting from the conservative system, we can expand the Hamiltonian (5.28) only around G_0 and H_0. After we repeat the steps from (5.2) to (5.10), we obtain a generating function χ_C, and a corresponding normal form H_{CNF} in the new variables P^1, Q^1, which has the following form:

$$H_{CNF}(P^1,Q^1;L_0,G_0,H_0) = H^0_{CNF}(P^1,Q^1;L_0,G_0,H_0) + H^1_{CNF}(P^1,Q^1;L_0,G_0,H_0). \tag{5.29}$$

5.3.2 Computation of the proper elements

In the case of non-resonant regions, the Hamiltonian function H_{CNF} in (5.29) depends only on the action variables, which means that one can find a solution by solving Hamilton's equations as:

$$\begin{aligned} P^1(t) &= P^1_0, \\ Q^1(t) &= Q^1_0, \\ p^1(t) &= p^1_0 + \frac{\partial H_{CNF}}{\partial P^1}(P^1_0,Q^1_0)t, \\ q^1(t) &= q^1_0 + \frac{\partial H_{CNF}}{\partial Q^1}(P^1_0,Q^1_0)t\,, \end{aligned} \tag{5.30}$$

where P^1_0, Q^1_0, p^1_0, and q^1_0 are the initial conditions for the normalized system, which are unknowns. Nevertheless, this system does not include the effect of the dissipative forces, which need to be added to Hamilton's equation of the normalized system. Since the dissipative forces F_L, F_G, and F_H in Section 3.4.6 are described in Delaunay variables, we need to implement the same transformation that we applied to function H_C, so to express the dissipative terms in the variables R, P, Q, r, p, and q. Hence, we make a linear change of coordinates, $R = L - L_0$, $P = G - G_0$, $Q = H - H_0$, $r = l$, $p = g$, $q = h$, and an expansion in power series around $R = 0$, $P = 0$ and $Q = 0$. After that, we transform the dissipative effects into the new variables R^1, P^1, Q^1, r^1, p^1, and q^1 as follows[1]: We use the generating function χ_C to compute the relation between the old variables and the new variables, as follows:

$$\begin{aligned} R(R^1,P^1,Q^1,r^1,p^1,q^1) &= S^{\lambda}_{\chi_C} R^1, \\ P(R^1,P^1,Q^1,r^1,p^1,q^1) &= S^{\lambda}_{\chi_C} P^1, \\ Q(R^1,P^1,Q^1,r^1,p^1,q^1) &= S^{\lambda}_{\chi_C} Q^1, \\ r(R^1,P^1,Q^1,r^1,p^1,q^1) &= S^{\lambda}_{\chi_C} r^1, \\ p(R^1,P^1,Q^1,r^1,p^1,q^1) &= S^{\lambda}_{\chi_C} p^1, \\ q(R^1,P^1,Q^1,r^1,p^1,q^1) &= S^{\lambda}_{\chi_C} q^1, \end{aligned} \tag{5.31}$$

[1] An alternative method to obtain the transformation of the dissipative effects is done in (Ferraz-Mello, 2007). One can transform the dissipative vector field $\boldsymbol{F} = (F_L, F_G, F_H)$ by using the formula $\boldsymbol{F}^1 = \boldsymbol{F} \cdot \frac{\partial \boldsymbol{\varphi}}{\partial \boldsymbol{\varphi}^1}$, where we denote the old angles by $\boldsymbol{\varphi}$ and the new angles by $\boldsymbol{\varphi}^1$.

where $(S^{\lambda}_{\chi_C})^{-1}$ is the Lie series operator in (2.9). By substituting the variables obtained in (5.31) in F_L, F_G, and F_H, we obtain the drag effect in the new variables, namely F^1_L, F^1_G, F^1_H as functions of the new action-angles variables R^1, P^1, Q^1, r^1, p^1, and q^1. Since the equations (5.30) do not define the real evolution of the dissipative normalized system, we compute Hamilton's equation as follows:

$$\begin{aligned}
\frac{dR^1}{dt}(t) &= -F^1_L,\\
\frac{dP^1}{dt}(t) &= -F^1_G,\\
\frac{dQ^1}{dt}(t) &= -F^1_H,\\
\frac{dr^1}{dt}(t) &= \frac{\partial H_{CNF}}{\partial R^1},\\
\frac{dp^1}{dt}(t) &= \frac{\partial H_{CNF}}{\partial P^1},\\
\frac{dq^1}{dt}(t) &= \frac{\partial H_{CNF}}{\partial Q^1}.
\end{aligned} \tag{5.32}$$

It is clear that the system (5.32) is not integrable, which means that it is not possible to find an analytical solution of the proper elements. Nevertheless, by a numerical integration, one can find the solution of the system (5.32), once the initial conditions are known. These initial conditions for the new variables can be found by using the following transformation

$$\begin{aligned}
R^1(R,P,Q,r,p,q) &= (S^{\lambda}_{\chi^1_C})^{-1}R,\\
P^1(R,P,Q,r,p,q) &= (S^{\lambda}_{\chi^1_C})^{-1}P,\\
Q^1(R,P,Q,r,p,q) &= (S^{\lambda}_{\chi^1_C})^{-1}Q,\\
r^1(R,P,Q,r,p,q) &= (S^{\lambda}_{\chi^1_C})^{-1}r,\\
p^1(R,P,Q,r,p,q) &= (S^{\lambda}_{\chi^1_C})^{-1}p,\\
q^1(R,P,Q,r,p,q) &= (S^{\lambda}_{\chi^1_C})^{-1}q,
\end{aligned} \tag{5.33}$$

and replace R,P,Q,r,p,q with R_0,P_0,Q_0,r_0,p_0,q_0. The function $(S^{\lambda}_{\chi^1_C})^{-1}$ is the inverse of Lie series operator defined in (2.9).

Definition 41 *We call **dissipative proper elements** at time t for the dissipative system (5.32), the values $R^1(t),P^1(t),Q^1(t),\ r^1(t),p^1(t),q^1(t)$ obtained by the numerical integration of system (5.32).*

Using the proper elements in the transformed coordinates, one can obtain the proper values in the Delaunay variables by computing $L_t = R(t)+L_0$, $G_t = P(t)+G_0$ and $H_t = Q(t)+H_0$. Finally, we can compute the proper semi-major axis (a_t), the proper eccentricity (e_t) and proper inclination (i_t) by using the formulas (4.1).

Chapter 6

An Implementation of the Analytic Method and an Application to Simulated and Real Data

The analytic method to compute the normal form of a Hamiltonian system and, hence, to find the proper elements, as is described in Chapter 5, can be implemented fully symbolically, by using an algebraic manipulator like Mathematica©. The program that computes the normal form of the Hamiltonian system for space debris (satellite) dynamics is described in detail in Appendix A so that it can be reproduced by the reader. In this chapter, we want to analyze the results obtained by the analytic method and to highlight the benefits of computation the proper elements and the normal form of the Hamiltonian system. The first section shows the behavior of the proper elements, and a comparison between mean and proper elements of the objects in different regimes. This analysis gives us a general idea of the space regions where the proper elements highlight important aspects of the dynamics. The second section is devoted to the analysis of the evolution of space debris groups and to show how the proper elements can be used to find the ancestor body of space debris. We apply the analytic method both to simulated space debris and to the real objects in space.

6.1 Analysis of the proper elements computation

The computation of the proper elements might be affected by the presence of resonances (either tesseral or luni-solar), and thus we need to adapt the procedure with respect to the approaches described in Chapter 5. The Mathematica© notebook presented in Appendix A is making automatically this selection, so that the Hamiltonian function is created taking into account the most important forces in the region chosen and the normalization algorithm is adapted to the initial Hamiltonian. Nevertheless, in this section we want to present the results of the comparison between mean and proper elements of the objects in different regimes, by splitting the space regions in stable region, higher-altitude region, lunisolar resonant region, tesseral resonant region and low-altitude regions.

6.1.1 Stable regions

In this chapter, by stable region we mean that set of initial conditions that provokes only small changes in the orbital elements a, e, i over a long period of time. For example, a region where $a \in [10000, 20000]$ km and the initial inclination is far from a critical value is a stable region due to the weak effect of the Laplace plane (see Section 4.1.3, Figure 4.2). In this case, we model the dynamics of space debris by an averaged Hamiltonian function of the form:

$$\begin{aligned} H(G,H,H_M,R_S,g,h,h_M,r_S;L) &= \overline{H_{J_2}}(G,H;L)+\overline{H_{J_3}}(G,H,g;L)+\overline{H_S}(G,H,g,h;L) \\ &+ \overline{H_M}(G,H,H_M,g,h,h_M;L)+\overline{H_{SRP}}(G,H,L_S,g,h,l_s;L), \end{aligned} \tag{6.1}$$

that includes the perturbations due to J_2, J_3, Moon, Sun and Solar radiation pressure, whose expressions are described in Chapter 2 and Chapter 3. Thus, the Hamiltonian system that we want to normalize has 4 DoF. Choosing the initial conditions far away from any kind of resonances, we can apply the analytic method presented in Section 5.1 to find the proper elements.
Let us consider three different orbits in the stable region defined by the random initial conditions (mean elements):

$$\begin{aligned}
\{a, e, i, M, \omega, \Omega, A/m\} &= \{11319.30\,km, 0.08, 19.84^\circ, 196.00^\circ, 243.85^\circ, 63.15^\circ, 0.34\,m^2/kg\},\\
\{a, e, i, M, \omega, \Omega, A/m\} &= \{19590.9\,km, 0.05, 23.46^\circ, 155.63^\circ, 62.14^\circ, 354.19^\circ, 0.21\,m^2/kg\},\\
\{a, e, i, M, \omega, \Omega, A/m\} &= \{20319.2\,km, 0.08, 23.66^\circ, 158.26^\circ, 61.84^\circ, 352.62^\circ, 0.27\,m^2/kg\}.
\end{aligned}$$

For each set of initial conditions, we compute the evolution of the mean elements, by integrating numerically Hamilton's equation of (6.1), as well as the evolution of proper elements computed as described in (5.13) and (5.14). We want also to analyze the behavior when we increase the area-to-mass ratio (A/m) of the space debris.
Let us start with the first orbit,

$$\{a, e, i, M, \omega, \Omega, A/m\} = \{11319.30\,km, 0.08, 19.84^\circ, 196.00^\circ, 243.85^\circ, 63.15^\circ, 0.34\,m^2/kg\},$$

for which we want to give more details during the normalization process. Thus, a linear change of coordinates as in (5.2) leads to the new actions (P, Q, Q_M, R_S) and the new angles (p, q, q_M, r_S). The Hamiltonian depending on the shifted variable and the constants $L_0 = 0.5181$, $G_0 = 0.5164$, $H_0 = 0.4857$ (obtained by using Delaunay variables (4.1)), is expanded in actions P, Q around the origin. The frequencies of the ascending nodes of the Moon $\nu_{q_M} = -0.000146798$ and the mean anomaly of the Sun $\nu_{r_S} = 0.0027303$ are computed in proper units from the values of Table 4.1.

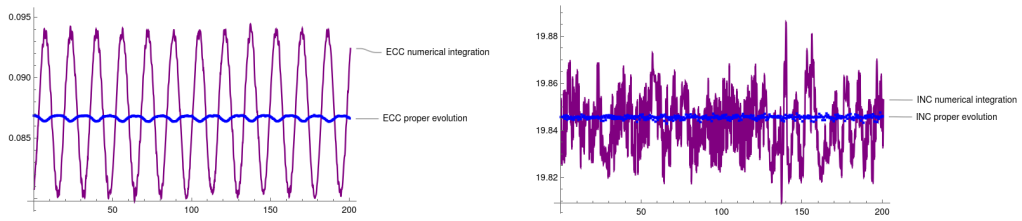

FIGURE 6.1: The evolution, over 200 years, of the mean elements (purple lines) and the proper elements (blue lines) for eccentricity (left) and inclination (right) for the Hamiltonian (6.1) and initial conditions $\{a, e, i, M, \omega, \Omega, A/m\} = \{11319.30\,km, 0.08, 19.84^\circ, 196.00^\circ, 243.85^\circ, 63.15^\circ, 0.34\,m^2/kg\}$.

The generating function is then computed by using the formula (2.22), since the scalar product frequency vector $\nu = (0.00641779, -0.00352645, -0.000146798, 0.0027303)$ and the coefficients' vector of the angles inside the sine and cosine functions do not produce small divisors. The smallest value of the dot products is obtained with the vector $(0, 0, -1, 0)$, which stands for $0 \cdot p + 0 \cdot q - 1 \cdot q_M + 0 \cdot r_S$, providing the value 0.000146798.
Having the generating function, we compute the normal form at the first order, which, in this

case, has the following form:

$$\begin{aligned} H_{NF}(P_1, Q_1, Q_{1M}, R_{1S}) &= -0.7744P_1^4 + 0.8956P_1^3Q_1 + 0.1941P_1^3 - 0.2040P_1^2Q_1^2 - 0.1982P_1^2Q_1 \\ &- 0.0409P_1^2 + 0.0351P_1Q_1^2 + 0.0341P_1Q_1 + 0.0064P_1 - 0.0036Q_1^2 \\ &- 0.0035Q_1 - 0.0001Q_{M1} + 0.0027R_{S1} - 0.0005. \end{aligned} \tag{6.2}$$

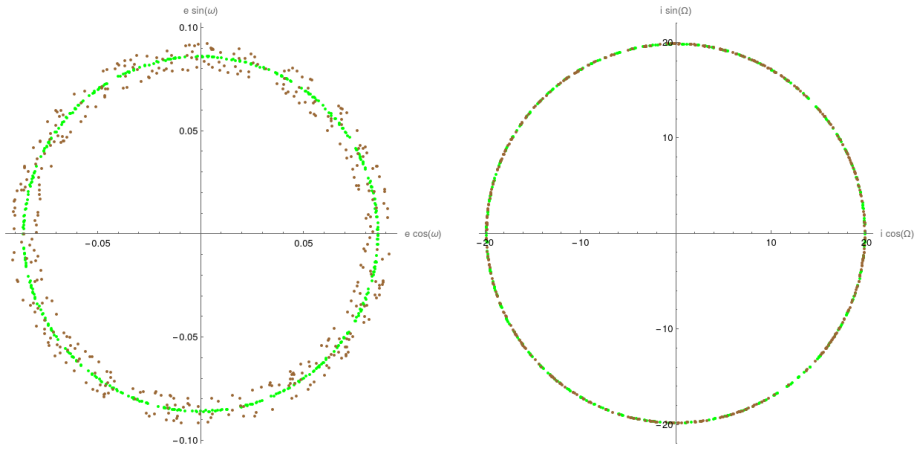

FIGURE 6.2: The evolution of the mean elements (brown dots) and the proper elements (green dots) in Poincarè variables for $(e\cos(\omega), e\sin(\omega))$ (left) and $(i\cos(\Omega), i\sin(\Omega))$ (right) for the Hamiltonian (6.1) and initial conditions $\{a, e, i, M, \omega, \Omega, A/m\} = \{11319.30\,km, 0.08, 19.84°, 196.00°, 243.85°, 63.15°, 0.34\,m^2/kg\}$.

Also, by using the generating function we compute the expression of the new variables as a function of old variables as in (5.13). The resulting expressions give us the transformation from old values (P, Q, Q_M, R_S) to the new values $(P_1, Q_1, Q_{1M}, R_{1S})$, and hence the proper elements.

In Figure 6.1 we show the evolution of the mean and proper eccentricity (left) and the evolution of mean and proper inclination (right) over a time period of 200 years. The proper values are computed every 6 months, and as it can be seen in Figure 6.1, they are almost constant over the time-span and they are located close to the middle of the corresponding mean elements range.

We can highlight the constancy of the proper elements also plotting the Poincarè variables as in Figure 6.2. These plots give us the intuition of the importance of the proper elements in comparison with the mean elements. If the variance of the mean elements is way larger than the variance of the proper elements, then the proper elements can be used as an indicator of orbit position over a long period of time.

We are interested to see now what happens with the orbit and, hence, the proper elements when we increase the A/m ratio from $0.34\,m^2/kg$ to $1.34\,m^2/kg, 5.34\,m^2/kg$ and $10.34\,m^2/kg$. The results, in terms of the comparison between mean and proper evolution, are presented in Figure 6.3. As we expect from the results in Section 4.2, a higher A/m ratio will produce a significant effect in mean eccentricity over a semi-secular horizon, and so in the proper eccentricity. Nevertheless, as it can be seen in all plots of Figure 6.3, the blue lines (proper elements) still have a smaller variance than the green lines (mean elements).

Let us see now a second advantage of the normalization procedure, that is the possibility of computing the so-called analytic solution (or analytic form) of the mean elements. These are basically closed-form solutions for the mean elements, that depend only on time. They

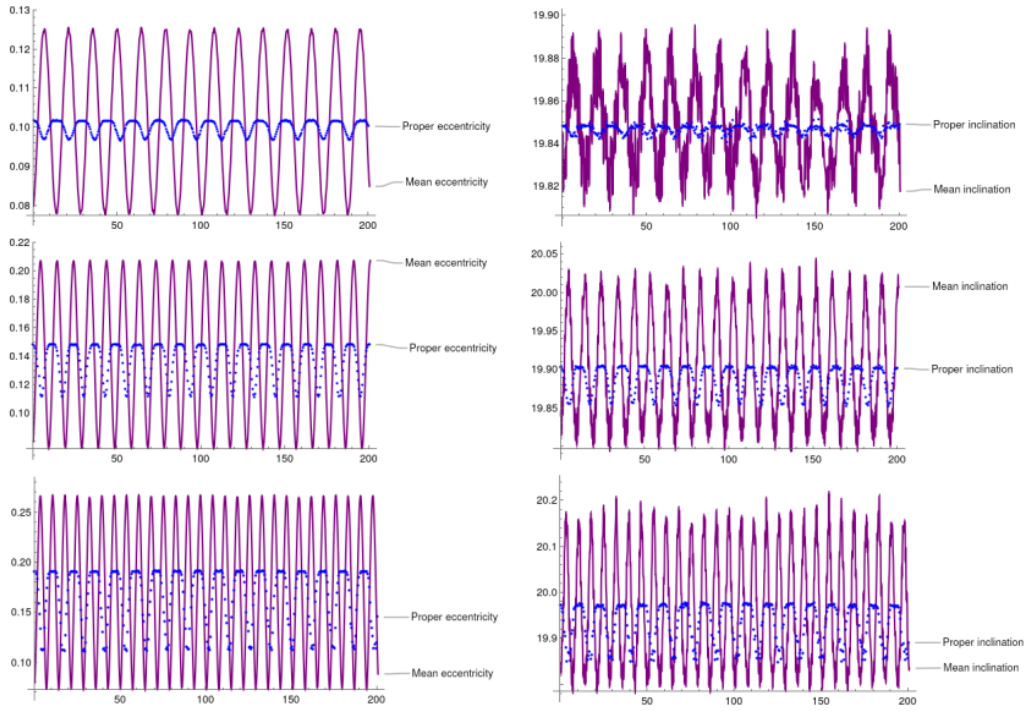

FIGURE 6.3: The evolution, over 200 years, of the mean elements (purple lines) and the proper elements (blue dots) for eccentricity (left) and inclination (right) for the Hamiltonian (6.1) and initial conditions: Row 1 - $A/m = 1.34\,m^2/kg$, Row 2 - $A/m = 5.34\,m^2/kg$, Row 3 - $A/m = 10.34\,m^2/kg$.

can be obtained by using the inverse of the generating function as in (2.29) such that the old variables are functions of the new variables. Since the new actions are constant and the new angles depend only on time, we obtain the old variables as functions of time.
The comparison of the eccentricity between the numerical integration of Hamilton's equations of system (6.1) and the analytic solution obtained after the normalization procedure is shown in Figure 6.4. The accuracy of the analytic solution of the eccentricity is kept over a long period due to the stability of the orbit.
The plots shown in Figure 6.5 and Figure 6.6 correspond to the initial conditions

$$\{a, e, i, M, \omega, \Omega, A/m\} = \{19590.9\,km, 0.05, 23.46^\circ, 155.63^\circ, 62.14^\circ, 354.19^\circ, 0.21\,m^2/kg\}$$

and

$$\{a, e, i, M, \omega, \Omega, A/m\} = \{20319.2\,km, 0.08, 23.66^\circ, 158.26^\circ, 61.84^\circ, 352.62^\circ, 0.27\,m^2/kg\}$$

, respectively. They highlight the same behavior as in the case of Figure 6.1, namely the constancy of the proper elements over a long period of time (200 years) for orbits in stable regions.

6.1.2 Higher-altitude regions

Once we increase the orbital altitude, the secular effects start to be significant in the inclination's evolution. Thus, the difference between mean and proper elements becomes larger and larger, at least in the case of inclination.
For the examples presented in this section, we still keep the initial inclination far from any lunisolar resonances, and we progressively increase the semi-major axis for different orbits.

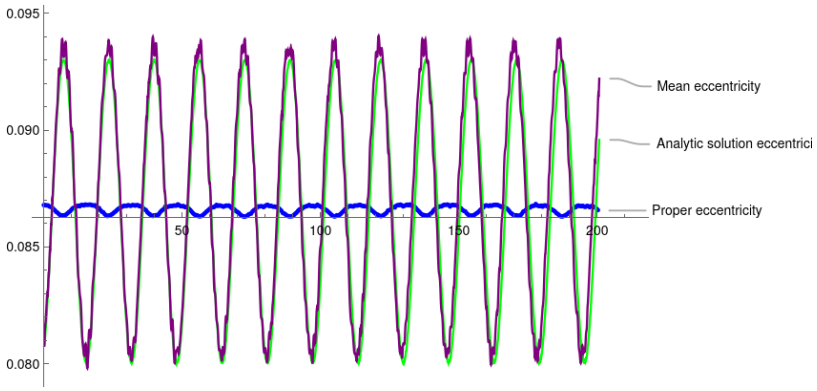

FIGURE 6.4: The evolution, over 200 years, of the mean elements (purple line) and the proper elements (blue line) and the analytic solution (green line) of the eccentricity for the Hamiltonian (6.1) and initial conditions: $\{a, e, i, M, \omega, \Omega, A/m\} = \{11319.30\,km, 0.08, 19.84°, 196.00°, 243.85°, 63.15°, 1.34\,m^2/kg\}$.

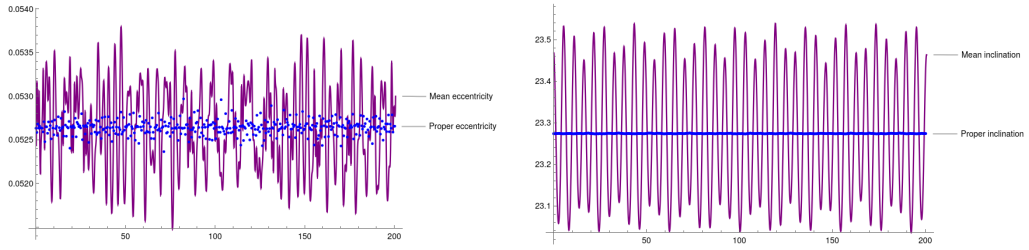

FIGURE 6.5: The evolution, over 200 years, of the mean elements (purple lines) and the proper elements (blue lines) for eccentricity (left) and inclination (right) for the Hamiltonian (6.1) and initial conditions $\{a, e, i, M, \omega, \Omega, A/m\} = \{19590.9\,km, 0.05, 23.46°, 155.63°, 62.14°, 354.19°, 0.21\,m^2/kg\}$.

In this case, we can use the same Hamiltonian (6.1) and the same procedure (non-resonant normalization) as in Section 6.1.1.
The series of plots in Figure 6.7 show the evolution of three different elements for the eccentricity and the inclination: mean elements obtained by numerical integration of Hamilton's equation of (6.1) (purple line), proper elements obtained by using the procedure described in Section 5.1.3 (blue line), and the analytic solution obtained with the inverse transformation (2.29) (green line). The initial conditions used are the following:

$$\{a, e, i, M, \omega, \Omega, A/m\} = \{22493.3\,km, 0.19, 19.64°, 54.44°, 302.44°, 241.34°, 0.06\,m^2/kg\},$$
$$\{a, e, i, M, \omega, \Omega, A/m\} = \{28138.5\,km, 0.16, 12.69°, 142.25°, 352.71°, 98.95°, 0.22\,m^2/kg\},$$
$$\{a, e, i, M, \omega, \Omega, A/m\} = \{35611.2\,km, 0.29, 29.73°, 259.99°, 63.35°, 194.42°, 0.28\,m^2/kg\},$$
$$\{a, e, i, M, \omega, \Omega, A/m\} = \{42683.0\,km, 0.07, 18.87°, 277.13°, 219.69°, 245.11°, 0.13\,m^2/kg\}.$$

In Figure 6.7 we remark that the variability of the proper inclination is much smaller (being almost 0) than the variability of mean inclination, and we notice that the proper eccentricity becomes more irregular as we increase the altitude. As well, the analytic solution of both orbital elements is less accurate for higher altitudes. This phenomenon is due to the effect of the Laplace plane that provokes large secular oscillations in the mean inclination. In the last

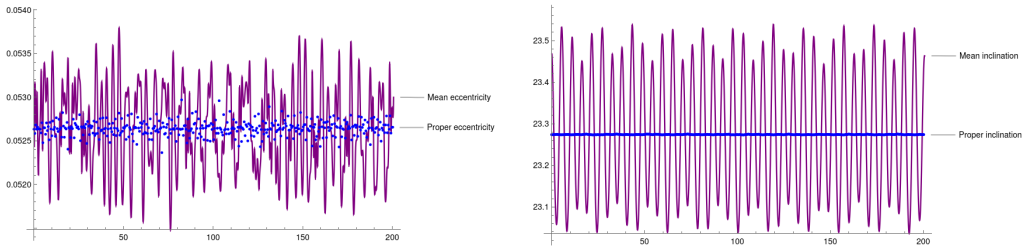

FIGURE 6.6: The evolution, over 200 years, of the mean elements (purple lines) and the proper elements (blue lines) for eccentricity (left) and inclination (right) for the Hamiltonian (6.1) and initial conditions $\{a, e, i, M, \omega, \Omega, A/m\} = \{20319.2\,km, 0.08, 23.66°, 158.26°, 61.84°, 352.62°, 0.27\,m^2/kg\}$.

two lines of Figure 6.7, the large oscillations lead to values of inclinations close to the critical ones (namely, 23.8° and 31.7° respectively), and thus to large oscillations in eccentricity (as described in Section 4.1.3). Nevertheless, the variability of the proper eccentricity is still smaller than the variability of the mean eccentricity.

6.1.3 Tesseral resonant regions

Let us analyze now what happens in the case that an object is in a tesseral resonance region. We show here how the implementation of the methods described in Section 2.3.2 and Section 5.1.3 works for two different orbits, one in a 2:1 resonance and the other one in a 1:1 resonance. Before showing the numerical results, we must mention that the initial Hamiltonian is different from (6.1) and has the following form:

$$\begin{aligned} H(L,G,H,H_M,R_S,\Theta,g,h,h_M,r_S,\theta) &= \overline{H_{J_2}}(G,H;L) + \overline{H_{J_3}}(G,H,g;L) \\ &+ \overline{H_M}(G,H,H_M,g,h,h_M;L) + \overline{H_S}(G,H,g,h;L) \\ &+ \overline{H_{SRP}}(G,H,L_S,g,h,l_s;L) \\ &+ \overline{H_{res2:1}}(L,G,H,\Theta,l,g,h,\theta) + H_{Kep}(L), \end{aligned} \tag{6.3}$$

where the expression of $\overline{H_{res2:1}}$ is given in Section 4.1.2. That leads to a 6 DoF Hamiltonian system. After the shifting of the actions w.r.t the initial values L_0, G_0, H_0, and the expansion around the origin, we obtain a Hamiltonian function in the new action angle variables $(R, P, Q, Q_M, R_S, \Theta, r, p, q, q_M, r_S, \theta)$ that can be written as:

$$\begin{aligned} H^{expanded}(R,P,Q,Q_M,R_S,\Theta,r,p,q,q_M,r_S,\theta) &= Z_0(R,P,Q,Q_M,R_S,\Theta) \\ &+ R_0(R,P,Q,Q_M,R_S,\Theta,r,p,q,q_M,r_S,\theta), \end{aligned} \tag{6.4}$$

where

$$Z_0(R,P,Q,Q_M,R_S,\Theta) = \boldsymbol{\nu}\cdot(R,P,Q,Q_M,R_S,\Theta), \tag{6.5}$$

and

$$\begin{aligned} R_0(R,P,Q,Q_M,R_S,\Theta,r,p,q,q_M,r_S,\theta) &= \mathcal{F}(R,P,Q,Q_M,R_S,\Theta) \\ &+ \mathcal{G}(R,P,Q,Q_M,R_S,\Theta,r,p,q,q_M,r_S,\theta). \end{aligned} \tag{6.6}$$

In (6.5), $\boldsymbol{\nu}$ is the frequency vector. In the equation (6.6), $\mathcal{F}$ is a polynomial function in action variables, while the $\mathcal{G}$ function is a sum of products between action variables and cosine or

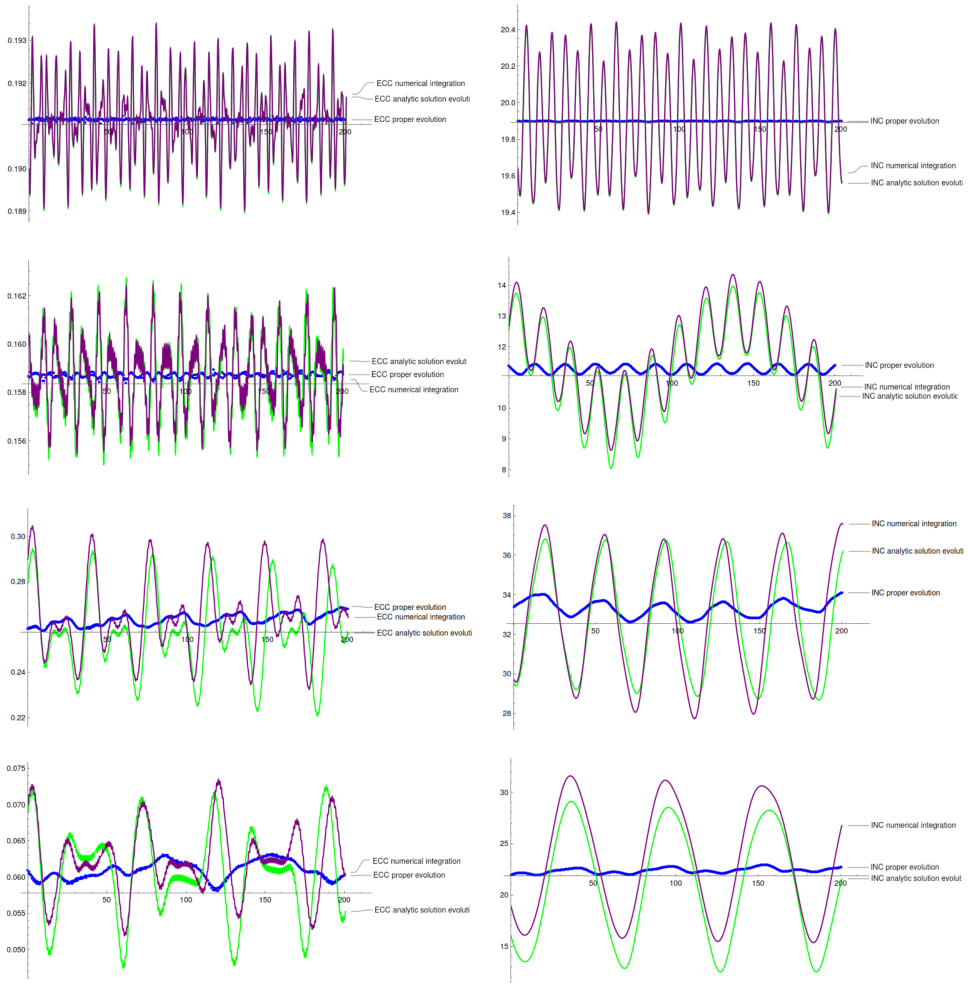

FIGURE 6.7: The evolution, over 200 years, of the mean elements (purple line), the proper elements (blue line) and the analytic solution (green line) of eccentricity for the Hamiltonian (6.1) and initial conditions: First line - $\{22493.3\,km, 0.19, 19.64°, 54.44°, 302.44°, 241.34°, 0.06\,m^2/kg\}$, second line - $\{28138.5\,km, 0.16°, 12.69°, 142.25°, 352.71°, 98.95°, 0.22\,m^2/kg\}$, third line - $\{35611.2\,km, 0.29, 29.73°, 259.99°, 63.35°, 194.42°, 0.28\,m^2/kg\}$, fourth line - $\{42683.0\,km, 0.07, 18.87°, 277.13°, 219.69°, 245.11°, 0.13\,m^2/kg\}$.

sine of angle variables.

Let us start with a concrete example of 2:1 resonance. Starting from the following initial conditions

$$\{a, e, i, M, \omega, \Omega, A/m\} = \{26560\,km, 0.07, 15°, 120°, 100°, 50°, 0.05\,m^2/kg\},$$

we obtain the frequency vector $\boldsymbol{\nu} = (2.00035, 0.00035, -0.00018, -0.00014, 0.00273, 1)$ and during the resonant normalization procedure (see Section 5.1.3), we get small divisors when we compute the dot product between $\boldsymbol{\nu}$ and the angles' coefficients vector $(1, 0, 2, 0, 0, -2)$. The latter corresponds exactly to the angle $2q + r - 2\theta (= l - 2\theta + 2\Omega)$, which provokes the oscillations in semi-major axis, since it depends on the angle l. Then the obtained normal form will depend on the above combination of angles and the normalized Hamiltonian has

the following form:

$$\begin{aligned} H_{NF}(R^1,P^1,Q^1,Q^1_M,R^1_S,\Theta^1,r^1,q^1,\theta^1) &= \mathcal{F}^1(R^1,P^1,Q^1,Q^1_M,R^1_S,\Theta^1) \\ &+ \mathcal{G}^1(R^1,P^1,Q^1,Q^1_M,R^1_S)\cdot \begin{matrix}\cos\\ \sin\end{matrix}(2q^1+r^1-2\theta^1), \end{aligned} \tag{6.7}$$

where $\mathcal{F}^1$ and $\mathcal{G}^1$ are polynomial functions in the action variables. The function H_{NF} describes a 1 DoF Hamiltonian system, since it contains only one combination of the angles. This is an integrable system, but it implies cumbersome computations to compute a closed form solution. In this case, we use a semi-analytic approach to compute the normal form, by computing first the numerical solution of Hamilton's equation of (6.7) and then by computing the numerical evolution of the proper elements as described in (5.20) and (5.21).
The comparison between mean and proper elements (semi-major axis, eccentricity and inclination) is shown in Figure 6.8. We notice that the constancy of the proper elements is affected both in semi-major axis and eccentricity, due to the presence of the resonant angle in the normal form, while the proper inclination still has a very small variability. A similar

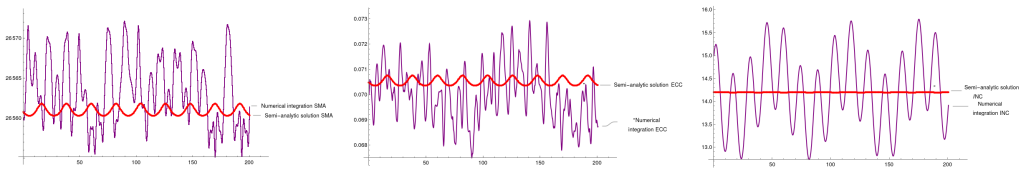

FIGURE 6.8: The evolution, over 200 years, of the mean elements (purple lines) and the proper elements (red lines) for semi-major axis (left), eccentricity (middle), and inclination (right) for the Hamiltonian (6.3) and initial conditions $\{a,e,i,M,\omega,\Omega,A/m\} = \{26560\,km, 0.07, 15°, 120°, 100°, 50°, 0.05\,m^2/kg\}$, which is located in a $2:1$ tesseral resonance.

behavior happens for an orbit in the 1:1 tesseral resonance. For instance, if we choose the initial conditions

$$\{a,e,i,M,\omega,\Omega,A/m\} = \{42155\,km, 0.02, 25°, 50°, 20°, 60°, 0.01\,m^2/kg\},$$

we obtain the evolution of the mean elements and the proper elements as is shown in Figure 6.9. In this case the small divisors appear for the combination of angles $r-\theta+p-q$, that involves also the argument of perigee ω. In the case of $2:1$ tesseral resonance, shown

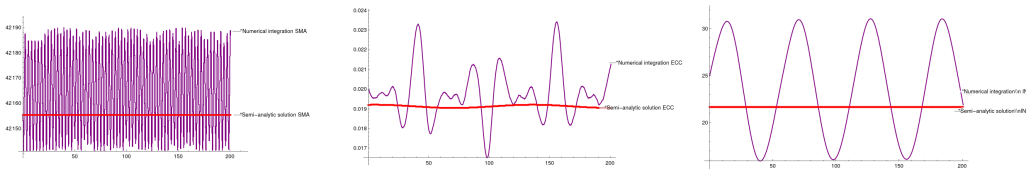

FIGURE 6.9: The evolution, over 200 years, of the mean elements (purple lines) and the proper elements (red lines) for semi-major axis (left), eccentricity (middle), and inclination (right) for the Hamiltonian (6.3) and initial conditions $\{a,e,i,M,\omega,\Omega,A/m\} = \{42155\,km, 0.02, 25°, 50°, 20°, 60°, 0.01\,m^2/kg\}$, which is located in a $1:1$ tesseral resonance.

in Figure 6.8, the terms that depend on the resonant angle in the normal form have a remarkable magnitude, that provokes small oscillations in the evolution of the semi-analytic proper semi-major axis and semi-analytic proper eccentricity. In the case of $1:1$ resonance, the oscillations are barely noticed for the same values of the elements. On the other hand, the semi-analytic proper inclination has a similar behavior in both examples, even if the mean inclination has a larger amplitude in the case of the $1:1$ resonance.

6.1.4 Lunisolar resonant regions

As we have seen in Section 5.2.2, the values of the critical inclinations set (5.27) start with $23.8°$; in the proximity of each value of this set, we can see the influence of the resonant angle. This means that, as we increase the inclination, the stability of the orbit is affected more and more by the 3rd body perturber. This affects also the computation of the proper elements, since we must apply a resonant normal form procedure as it is described in 5.2.2, which provides semi-analytic solutions. Since we are not in a tesseral region, we use the dynamical model described by the Hamiltonian function (6.1).
As in the case of tesseral resonances, we do not expect to see a small variability in the

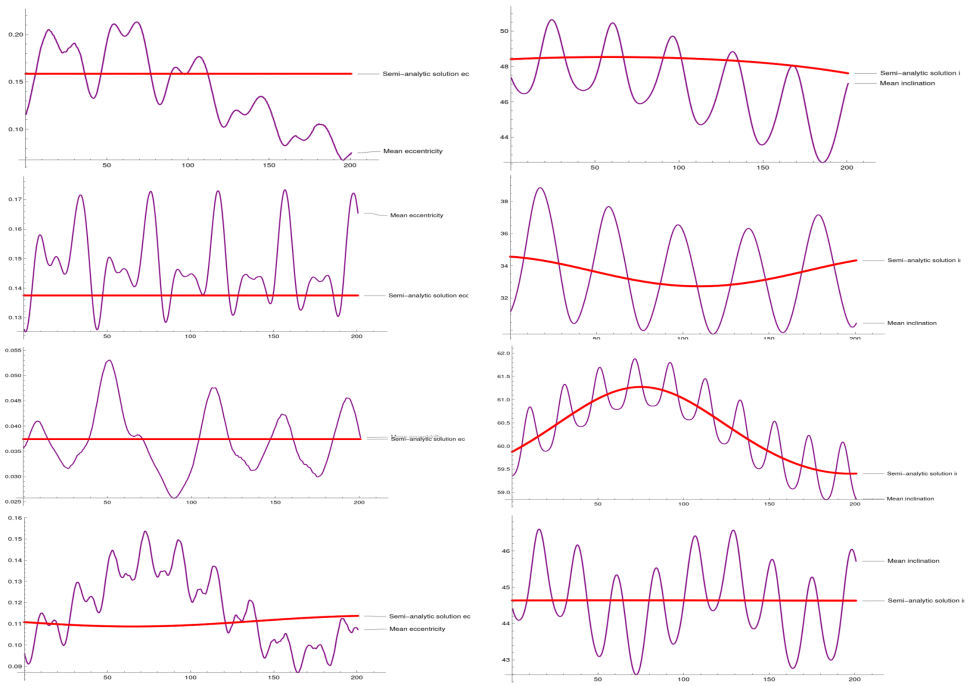

FIGURE 6.10: The evolution, over 200 years, of the mean elements (purple lines) and the semi-analytic proper elements (red lines) for semi-major axis (left) eccentricity (middle) and inclination (right) for the Hamiltonian (6.1) and initial conditions $\{a, e, i, M, \omega, \Omega, A/m\} = \{31988.8\,km, 0.11, 47.37°, 237.90°, 182.42°, 246.44°, 0.25\,m^2/kg\}$, $\{a, e, i, M, \omega, \Omega, A/m\} = \{35479.2\,km, 0.12, 31.17°, 321.96°, 183.94°, 159.23°, 0.02\,m^2/kg\}$, $\{a, e, i, M, \omega, \Omega, A/m\}=\{23995.2\,km, 0.03, 59.36°, 18.36°, 267.20°, 175.55°, 0.04\,m^2/kg\}$, $\{a, e, i, M, \omega, \Omega, A/m\}=\{27937.2\,km, 0.09, 44.41°, 339.60°, 308.60°, 242.22°, 0.11\,m^2/kg\}$.

proper elements evolution. Nevertheless, depending on the resonant combination of angles, we might see the variation either in the proper eccentricity or in the proper inclination. By analyzing the plots in Figure 6.10, which are obtained by comparing the evolution of the mean elements and the evolution of the proper elements for 4 objects with the following

initial conditions

$$\begin{aligned}
\{a,e,i,M,\omega,\Omega,A/m\} &= \{31988.8\,km, 0.11, 47.37°, 237.90°, 182.42°, 246.44°, 0.25\,m^2/kg\},\\
\{a,e,i,M,\omega,\Omega,A/m\} &= \{35479.2\,km, 0.12, 31.17°, 321.96°, 183.94°, 159.23°, 0.02\,m^2/kg\},\\
\{a,e,i,M,\omega,\Omega,A/m\} &= \{23995.2\,km, 0.03, 59.36°, 18.36°, 267.20°, 175.55°, 0.04\,m^2/kg\},\\
\{a,e,i,M,\omega,\Omega,A/m\} &= \{27937.2\,km, 0.09, 44.41°, 339.60°, 308.60°, 242.22°, 0.11\,m^2/kg\},
\end{aligned}$$

we notice how the semi-analytic solutions for the proper elements are affected by the presence of different resonant angles. For instance, the orbit represented in the last row of Figure 6.10 is close to the lunisolar resonance $2\omega = 0$, and we notice that the evolution of the proper eccentricity is not constant. As well, the proper inclination of the orbit in the second line has a small oscillation, following the trend of the mean inclination evolution due to the resonant angle $2\omega + \Omega + \Omega_M$. The examples shown in Figure 6.10 are far from the regions with overlapping resonances, regions that might provoke a fail in the computation of the generating function.

6.1.5 Low-altitude regions

In this subsection we provide some experiments in the case of objects in LEO, where we need to compute the proper elements taking into account the dissipative effects as described in Section 5.3. Since the semi-major axis decays with the altitude due to the effect of drag, we must take into account the fact that the object could reach the Earth after a period of time. Thus, we choose a smaller period of 20 years for the comparison between the evolution of the mean elements and the evolution of the proper elements. In Figure 6.11 we can see the

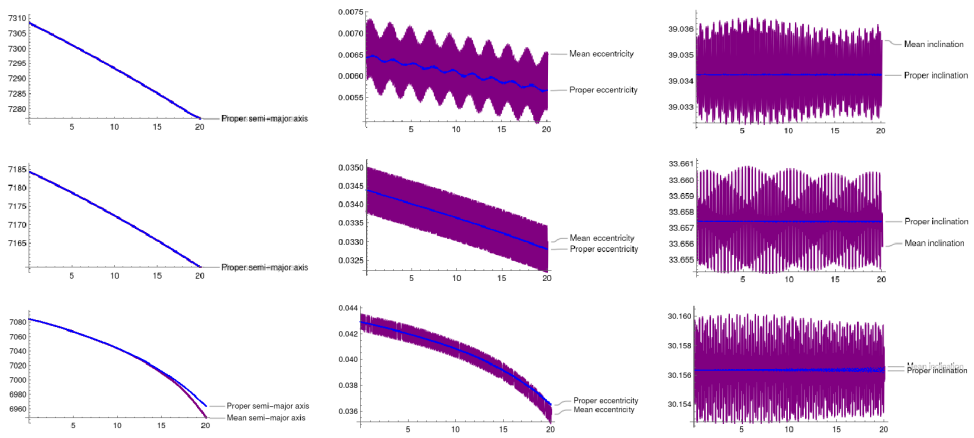

FIGURE 6.11: The evolution, over 20 years, of the mean elements (purple lines) and the proper elements (blue lines) for semi-major axis (left) eccentricity (middle) and inclination (right) for the initial conditions $\{a,e,i,M,\omega,\Omega,A/m\}$=$\{7310.3\,km, 0.006, 30.033°, 78.543°, 124.654°, 54.543°, 0.007\,m^2/kg\}$, $\{a,e,i,M,\omega,\Omega,A/m\}$=$\{7184.9\,km, 0.034, 33.657°, 154.657°, 24.245°, 23.654°, 0.012\,m^2/kg\}$, $\{a,e,i,M,\omega,\Omega,A/m\}$=$\{7084.5\,km, 0.042, 30.159°, 28.395°, 258.849°, 51.971°, 0.005\,m^2/kg\}$.

same behavior as in the conservative case, namely the variability of the proper elements is almost 0 compared with the variability of the mean elements. The additional thing here is the decay in semi-major axis and eccentricity due to the drag effect. As we decrease the initial altitude, we notice a faster decay of the elements. Nevertheless, the proper elements are not

affected very much. The initial conditions for the experiments shown in Figure 6.11 are

$$\{a,e,i,M,\omega,\Omega,A/m\} = \{7310.3\,km, 0.006, 30.033^\circ, 78.543^\circ, 124.654^\circ, 54.543^\circ, 0.007\,m^2/kg\},$$
$$\{a,e,i,M,\omega,\Omega,A/m\} = \{7184.9\,km, 0.034, 33.657^\circ, 154.657^\circ, 24.245^\circ, 23.654^\circ, 0.012\,m^2/kg\},$$
$$\{a,e,i,M,\omega,\Omega,A/m\} = \{7084.5\,km, 0.042, 30.159^\circ, 28.395^\circ, 258.849^\circ, 51.971^\circ, 0.005\,m^2/kg\}.$$

6.2 Simulations and clustering

While in Section 6.1 we analyzed the computational aspects and the evolution of the proper elements for single objects, this section will describe the evolution of a group of objects (space debris) both in the mean elements and in the proper elements. For these experiments we use synthetic data, obtained with the simulator of space debris described in Appendix C, but also some data of real space debris.
The experiments of this section are motivated by the properties of the proper elements to be almost constant over long periods of time. Let us analyze what happens when we have several fragments that have very similar initial conditions and let us make a comparison between their mean elements evolution and their proper elements evolution.

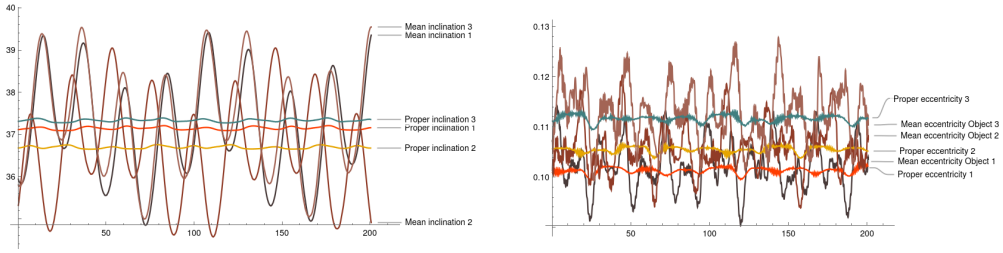

FIGURE 6.12: The evolution, over 200 years, of the mean elements (Light Brown, Brown, Dark Brown colors) and the proper elements (Orange, Red, Green colors) of eccentricity (left) and inclination (right) for 3 different objects with the initial conditions: $\{a,e,i,M,\omega,\Omega,A/m\}$=$\{29130\,km, 0.107, 35.94^\circ, 62.36^\circ, 44.14^\circ, 212.17^\circ, 0.67\,m^2/kg\}$, $\{a,e,i,M,\omega,\Omega,A/m\}$=$\{29074.3\,km, 0.101, 35.32^\circ, 359.38^\circ, 241.68^\circ, 106.95^\circ, 1.13\,m^2/kg\}$, $\{a,e,i,M,\omega,\Omega,A/m\}$=$\{29130.9\,km, 0.107, 35.80^\circ, 4.402^\circ, 20.41^\circ, 198.09^\circ, 1.47\,m^2/kg\}$.

In Figure 6.12 we highlight how the mean elements start from similar values and during the evolution they might get very different values, while the proper elements start close to the average of each orbit, but they remain almost constant (and hence very close) over the period of time. As initial conditions, we take the following values:

$$\{a,e,i,M,\omega,\Omega,A/m\} = \{29130\,km, 0.107, 35.94^\circ, 62.36^\circ, 44.14^\circ, 212.17^\circ, 0.67\,m^2/kg\},$$
$$\{a,e,i,M,\omega,\Omega,A/m\} = \{29074.3\,km, 0.101, 35.32^\circ, 359.38^\circ, 241.68^\circ, 106.95^\circ, 1.13\,m^2/kg\},$$
$$\{a,e,i,M,\omega,\Omega,A/m\} = \{29130.9\,km, 0.107, 35.80^\circ, 4.402^\circ, 20.41^\circ, 198.09^\circ, 1.47\,m^2/kg\}.$$

The property of nearly constancy of the proper elements is used in the last 2 sections of this chapter to analyze the groups of space debris for two kinds of data. The first approach is to make use of the application `SIMPRO` (briefly described in Appendix C and in detail in (Apetrii et al., 2022)) to create a dataset (say $\mathcal{E}_0^M$) based on a break-up event (either collision or explosion) and then to apply the following steps:

1. Propagate the mean elements of each object in the dataset over a period of time T (200 years in most of the cases), say $\mathcal{E}_T^M$;
2. Compute the proper elements of each object by using the mean elements after the evolution (the values of $\mathcal{E}_T^M$), and we obtain the set of proper elements $\mathcal{E}_T^P$;
3. Compare and analyze the distribution of elements for $\mathcal{E}_0^M$ and $\mathcal{E}_T^P$.

This procedure is described in detail in (Celletti, Pucacco, and Vartolomei, 2022), alongside with the results of several break-up events in different region. In the present work, in Section 6.2.1, we use a similar approach, but exposing the full evolution of the proper elements of the group of space debris in comparison with the mean elements' evolution.
The second direction is to use available data from the website SpaceTrack[1], that provides information (orbital elements, properties, etc.) about the trackable objects around the Earth. We use parts of the data to compute the evolution of the mean elements and proper elements for some groups of objects. In Section 6.2.2 we present an example of two groups of real debris and how their mean elements and proper elements evolve. A similar experiment can be found also in (Celletti, Pucacco, and Vartolomei, 2021).

6.2.1 Simulated break-up events

Using `SIMPRO`, we simulated two break-up events, a collision and an explosion, in two different regions. The first one is in a higher altitude region (as it is defined in Section 6.1.2) and the second one is close to the lunisolar resonance $2\Omega - \Omega_M$.
The collision is produced between a spacecraft of 1000 kg and a projectile of 6 kg at a velocity of 5500 m/s. The orbital elements of the spacecraft at the break-up moment are

$$\{a, e, i, M, \omega, \Omega\} \quad = \quad \{34300\,km, 0.1, 15^\circ, 55^\circ, 34^\circ, 26^\circ\},$$

producing a total of 457 fragments. The distribution of the fragments in a, e, i is shown in the top left panel of Figure 6.13, where we can see that the generated fragments have close initial orbital elements. In Figure 6.13 we can also see the evolution of the distribution of fragments

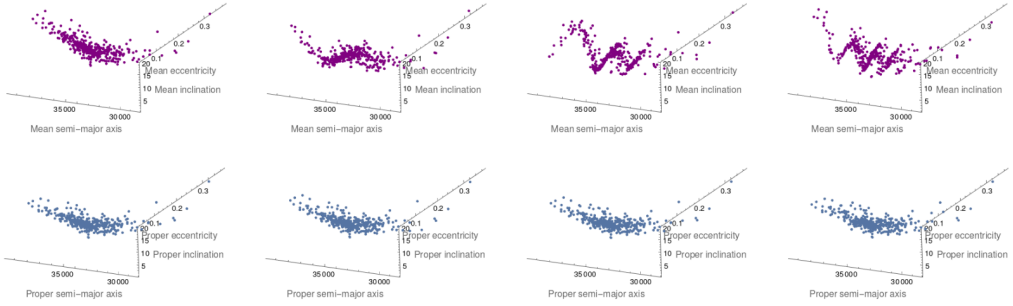

FIGURE 6.13: The evolution of the distribution of mean elements (upper plots) and proper elements (lower plots) at times 0, 60, 120, 180 years, in the 3-D coordinates a - e - i for the fragments generated by a collision between a spacecraft ($\{a, e, i, M, \omega, \Omega\} = \{34300\,km, 0.1, 15^\circ, 55^\circ, 34^\circ, 26^\circ\}$) of 1000 kg and a projectile of 6 kg at a velocity of 5500 m/s.

in the 3-D coordinates a - e - i at every 60 years in mean elements (upper plots, purple dots) and proper elements (lower plots, blue dots). We remark that the distribution in mean elements get spread more and more as the time goes on. On the other hand, the distribution in proper elements tends to be constant at any time. The comparison between mean elements

[1] https://www.space-track.org/

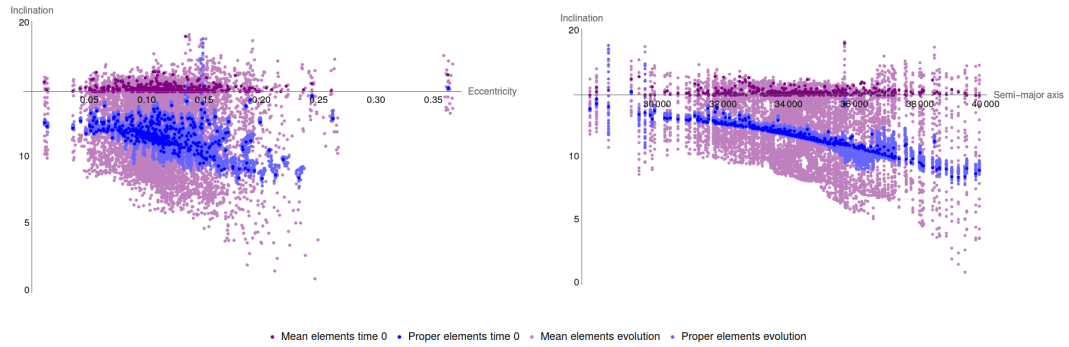

FIGURE 6.14: The comparison between variation of mean elements (purple and light purple dots) and proper elements (blue and light blue dots) for the fragments generated by a collision between a spacecraft ($\{a, e, i, M, \omega, \Omega\} = \{34300\,km, 0.1, 15°, 55°, 34°, 26°\}$) of 1000 kg and a projectile of 6 kg at a velocity of 5500 m/s.

and proper elements variation of each fragment generated is shown in Figure 6.14. The purple dots represent the initial mean elements and the blue dots are the initial proper elements. With light purple and light blue we plot the variation, of each fragment in the planes *e-i* (left) and *a-i* (right), of the mean elements and the proper elements, respectively. Since the variation in proper elements is very small for almost all fragments, we can easily see that at any time the fragments in the proper elements will remain grouped.

The second break-up event is a simulated explosion produced on a spacecraft of "regular body" (see Appendix C) type at the coordinates $\{a, e, i, M, \omega, \Omega\} = \{36000\,km, 0.11, 33°, 110°, 20°, 50°\}$, which produces 178 fragments.

The results of this experiment are summarized in Figure 6.15, where we can see the same behavior of the fragments (in proper elements) as in the non-resonant case of Figure 6.13. The eccentricity is the only orbital element affected by the effect of the resonant terms. Nevertheless, the variability of the fragments computed in proper elements remains very low, compared with the variability of the evolution in mean elements.

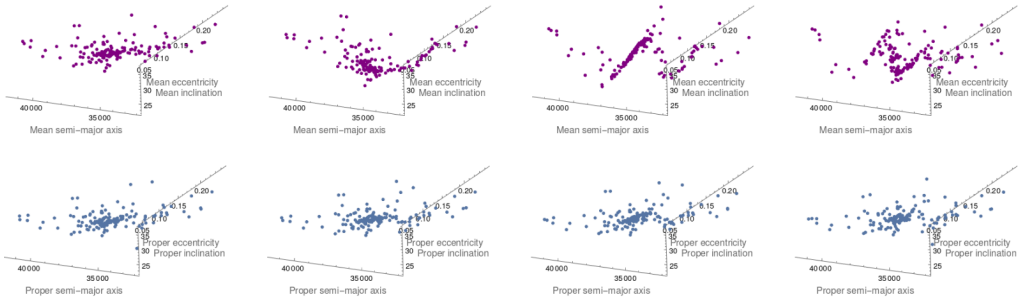

FIGURE 6.15: The evolution of the distribution of mean elements (upper plots) and proper elements (lower plots) at times 0, 60, 120, 180 years, in the 3-D coordinates *a* - *e* - *i* for the fragments generated by an explosion of *regular body* spacecraft ($\{a, e, i, M, \omega, \Omega\} = \{36000\,km, 0.11, 33°, 110°, 20°, 50°\}$) .

A last example, which is also presented in (Celletti, Pucacco, and Vartolomei, 2022), aims to highlight an important application of the proper elements in case of close break-up events. This property will be used in the experiments with real data in Section 6.2.2.

This experiment starts with two nearby (in terms of semi-major axis, eccentricity and inclination) break-up events (explosions) that generate 94 fragments each. The explosions take

place at the same orbital position $\{a, e, M, \omega, \Omega\} = \{24600\,km, 0.02, 54°, 110°, 120°\}$, except for the inclinations which are 20° and 21°, respectively.

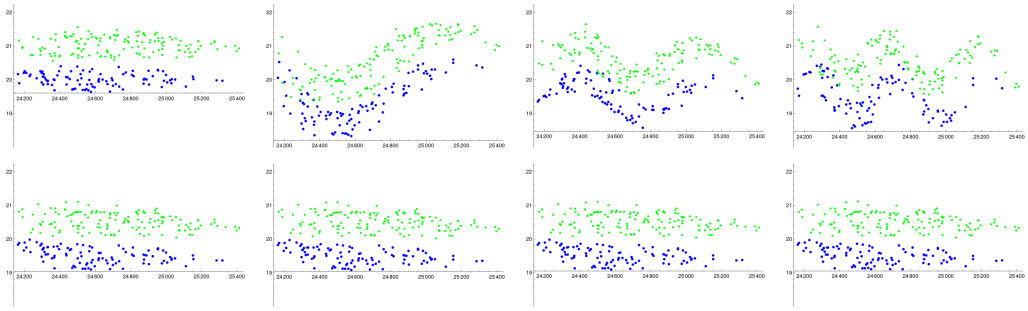

FIGURE 6.16: The evolution of the fragments generated by two nearby explosions in the mean elements (purple dots) and proper elements (blue dots) at every 60 years.

Since the semi-major axis is constant in this region, we reduce the comparison between mean and proper elements to the plane *e-i*. In Figure 6.16 we have the evolution of the 2 groups at every 60 years.
The upper panel of Figure 6.16 shows that the two groups (group 1 - blue dots, group 2- green dots), initially separated, overlap after 60 years, while in the lower panel, represented by the evolution of the proper elements, we are able to recognize the two initial groups at any time. These simple remarks can be checked also by assisted computational methods. In Figure 6.17 we use an algorithm of classification (KMeans) to show that the fragments in the proper elements are easier to be grouped by the machine. The test is based on the following steps: 1 - we classify the initial mean elements and initial proper elements and save the results; 2 - at every time we try to classify again the data in 2 groups and compare the original groups (obtained at step 1) with the groups obtained at current step; 3 - we plot with red dots the wrong classified objects and with purple/blue dots the correct classified objects.

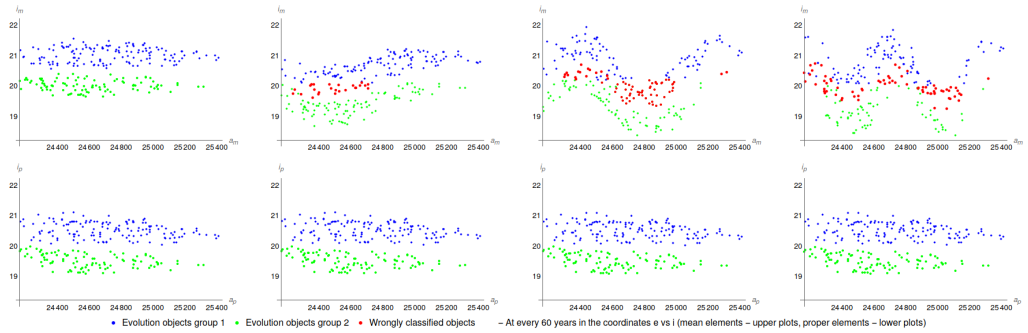

FIGURE 6.17: The evolution of the fragments generated by two nearby explosions (group 1 - blue dots, group 2- green dots) in the mean elements (upper plots) and proper elements (lower) at every 60 years, and the wrongly classified fragments (red dots) at each time following the procedure explained in the text.

As it can be seen in Figure 6.17 the number of wrongly classified objects increases as time increases. On the other hand, there are no miss-classified fragments in the case of proper elements. This result can be explained easily by looking at the evolution of the distribution of mean eccentricity and inclination in comparison to the evolution of the proper elements. Figure 6.18 shows the probability density functions (PDF) of the mean and proper elements

distributions every 5 years. In the case of the proper eccentricity (blue lines - left plot) and proper inclination (blue lines - right plot), we notice an almost perfect overlapping.

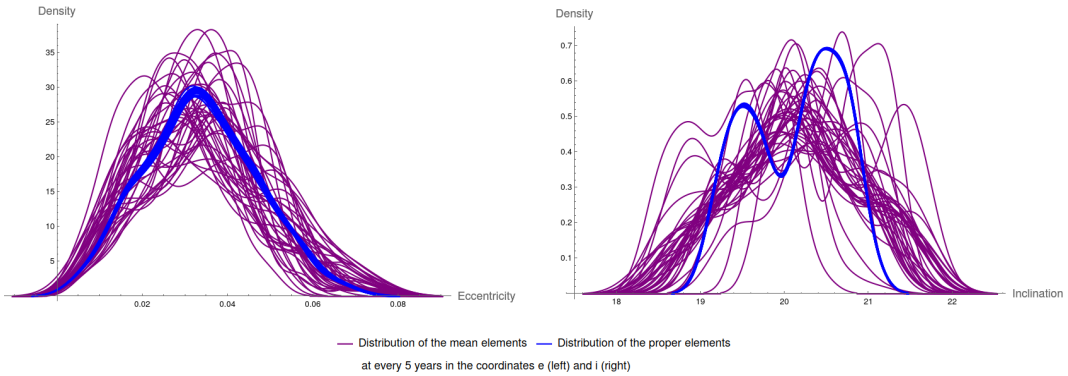

FIGURE 6.18: The probability density functions computed at every 5 years, over 200 years, for the mean (purple lines) and proper (blue lines) eccentricity (left plot) and inclination (right plot) of the fragments generated by two nearby explosions.

6.2.2 Real data experiments

The experiments in this section (and the article (Celletti, Pucacco, and Vartolomei, 2021)) are motivated by the last experiments of Section 6.2.1, namely the constancy of the evolution of the proper elements' distribution. Based on the orbital position of two groups of debris found in the TLE data set from SpaceTrack[2], we compute the evolution of the mean elements of each fragment for a period of 200 years. Using the mean elements, we compute the proper elements at some interval of times, and we plot the distributions in both sets of variables. The space region of the two groups ("Atlas 5 Centaur" and "CZ-3") is bounded by the values of $a \in [26600, 29700]$ km, $e \in [0.45, 0.75]$ and $i \in [20°, 32°]$.

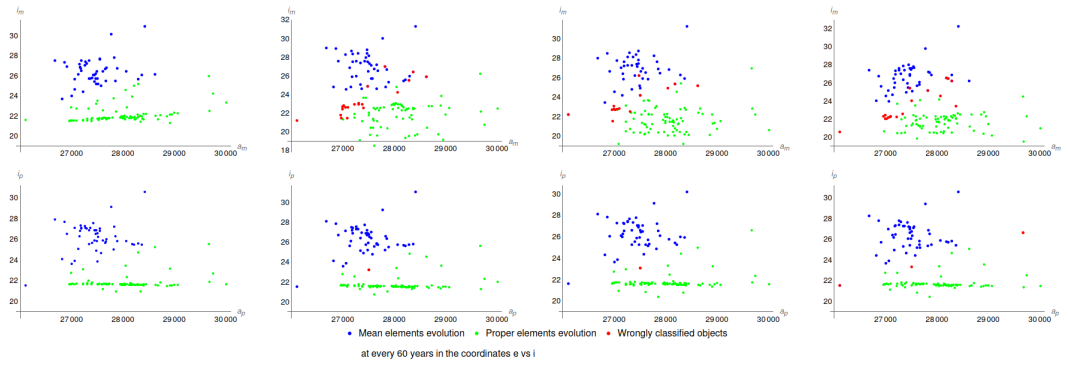

FIGURE 6.19: The evolution of the fragments of two groups of real debris ("Atlas 5 Centaur" - blue dots and "CZ-3" - green dots) in the mean elements (upper plots) and proper elements (lower plots) at every 60 years, and the wrong classified (red dots) fragments at each time following the procedure explained in the text.

We perform here a similar test by checking some well classified objects as in Section 6.2.1 (Figure 6.17). We show in Figure 6.19 the evolution of the mean elements (upper plots) and proper elements (lower plots) in the coordinates a-i at every 60 years. The objects which are

[2] https://www.space-track.org/

wrongly classified are marked in red. We notice that in the cases of real debris we can get miss-classified objects also in the proper elements. Nevertheless, they are much less than in the case of mean element; in fact, the proper elements distribution is nearly constant for all fragments over long periods of time, as it can be seen in Figure 6.20.

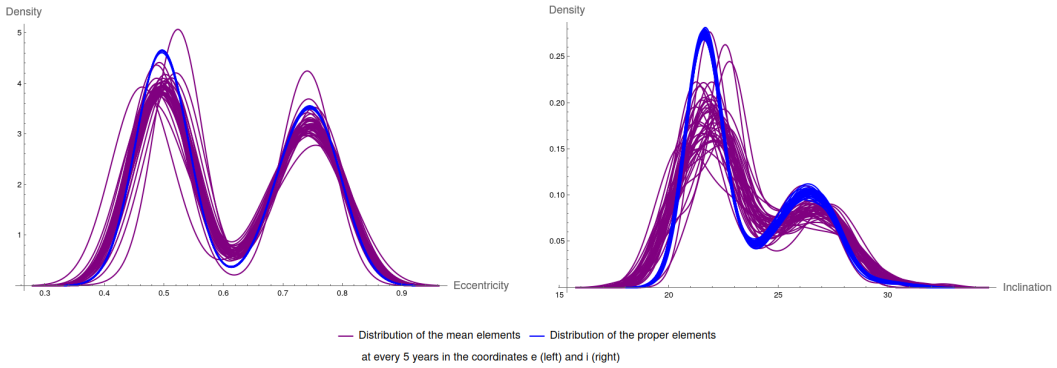

FIGURE 6.20: The probability density functions computed at every 5 years, over 200 years, for the mean (purple lines), and proper (blue lines) eccentricity (left plot), and inclination (right plot) of the fragments of two groups of real debris ("Atlas 5 Centaur" and "CZ-3") .

Chapter 7

Conclusions and Perspectives

In the present work, we developed a method to compute the so-called proper elements for a space object orbiting around the Earth. Together with the presentation of the mathematical framework and the implementation of the desired perturbation theory methods, we also provided some significant applications of the computation of proper elements. We analyzed the behavior of the orbits in different regions and why it is important to make use of adapted techniques in some special cases.

7.1 Conclusions

The main conclusion of the present thesis is that the powerful method of the computation of the proper elements already tested and implemented in the case of asteroids (see (Milani and Knežević, 1998), (Milani and Knežević, 1990), (Knežević and Milani, 2001)) has been successfully developed in the case of artificial Earth's satellites as well as for space debris. We have adapted a Hamiltonian model for an accurate estimation of the dynamics of space debris (numerically compared with the Newtonian model). Based on the normalization procedure with Lie series (as in (Hori, 1966), (Deprit, 1969), (Deprit and Rom, 1970)), we adapted perturbation theory techniques to compute the normal form for the constructed Hamiltonian system, so to find the generating function that gives the transformations from mean elements to proper elements, and vice-versa. Another conclusion is that the proper elements can be used to determine important features of the ancestors of one or more groups of space objects.

7.1.1 Dynamical model

We started by creating the dynamical model that describes the motion of an object around the Earth. The development of the perturbations included in the Hamiltonian system is done in two different ways, so that we can compare the expressions of the results from both methods. As well, we checked the accuracy of the Hamiltonian model by comparing the results with the numerical solutions of the integration of the Cartesian and Hamilton's equations. The theoretical part that describes the model and the perturbation is presented in Chapter 3. It is complemented by a qualitative analysis of the behavior of the orbits in different regions and by the most important effects that occur when using different models (see Chapter 4).

7.1.2 Proper elements computational methods

The main objective of this work was to create the mathematical framework to develop the method to construct the normal form of a Hamiltonian system defined by a complex Hamiltonian function and to compute the proper elements. The mathematical framework and the construction of the normal form are presented in Chapter 5. We started with the development of the method for a simplified case of a 2 DoF Hamiltonian system, that is usually considered for the stable regions (as they are defined in Section 6.1.1), and we showed in detail how the

proper elements are computed. We progressively added more and more perturbations, and analyzed the issues that could appear in some cases, like resonances or rather including the dissipation.
An implementation of the developed method is given in Appendix A in the programming language `Mathematica`©, such that the reader could use it to compute the normal form for a Hamiltonian function defined as in Chapter 3. The results obtained by using the code described in Appendix A, but also using the application `SIMPRO`©, are presented in Chapter 6. From the analysis of the behavior of the proper elements versus the mean elements for objects in different regions, see Section 6.1, we understand the importance of the proper elements constancy and the benefits of the normal form computation.

7.1.3 Applications

The main advantages of the normalization procedure and computation of the proper elements are highlighted in the experiments in Section 6.2, where we showed the validity of the proper elements in the determination of the ancestor body of a group of space debris. The experiments with the simulated data obtained from `SIMPRO`© are complemented with the experiments with the data for real space debris orbiting around the Earth. The results of Chapter 6 described the behavior of the proper elements in a large part of the Earth's space environment. Nevertheless, for peculiar regions like those in which one has an overlapping of resonances, or very chaotic motions nearby separatrices, or even for objects with extremely large A/m values, some new perturbation methods should be implemented.

7.2 Perspectives

We have seen that the computation of the proper elements works better in the stable regions and needs dedicated methods for the special cases, as resonances, dissipation, etc. Hence, we understand that an accurate computation of the proper elements must be applied for a Hamiltonian model that aims to describe the dynamics with much accuracy.

7.2.1 Improving the dynamical model

By developing a more accurate model, we understand the use of more terms in the expansions of the Earth, Moon, Sun and SRP described in Chapter 3, but also the introduction of new forces that might be significant for the dynamics in some regions (for example, Poynting-Robertson drag, Earth's shadowing effects, equinoctial precession of the Earth, etc.). Nevertheless, the additional terms/forces imply a higher complexity of the system and, hence, a very large Hamiltonian function. One needs to understand the trade-off between the accuracy and the complexity, since the computational time of the normalization procedure is proportional to the complexity of the Hamiltonian function.

7.2.2 Algorithm performance

In this work, the computation of normal forms and the computation the proper elements are implemented in a fully symbolic way (in the sense of algebraic operations) and they depend only on the initial conditions of the orbit. In this way we have, for example, to compute two normal forms for two different objects with similar initial conditions. This happens because the Hamiltonian function that has to be normalized is expanded around the initial values of the action variables. These expensive operations could be avoided if the generating functions of two objects in the same regime would have similar properties. This is one direction that can be analyzed and implemented in a future work to reduce the computational time and to

improve the performance of the method.
From the dynamical point of view, the computation of the proper elements highly depends on the understanding of the orbital behavior of the objects in a desired region. Therefore, a well-implemented automatic model selector of the forces involved could be a solution for the trade-off between the complexity of the Hamiltonian function and the accuracy of the motion.

7.2.3 New directions and innovative methods

There are still several objectives to be achieved in future works. From the development of theoretical models and perturbation theory techniques to the optimized implementation of the mathematical methods; besides, from advanced techniques in different fields (e.g., numerical methods, Machine Learning algorithms, etc.), we can get advances in the understanding of the dynamics of the space objects (satellites and space debris) around the Earth.
In our plan of work for the future, the very next steps are:

1. The development of methods for the computation of the proper elements for objects with extreme values for the orbital elements (for example, high eccentricity or very large area-over-mass ratio);
2. The implementation of a similar technique for the synthetic computation of the proper elements as described in (Knežević and Milani, 2001);
3. The study of the behavior of the proper elements for objects within similar regimes (stable regions, close to resonances, etc.);
4. The development of machine learning algorithms for the clusterization of space debris in groups and for the prediction of the ancestor body;
5. The improvement of the computational time for the normalization procedure, by creating dedicated mathematical methods related to those presented in this thesis.

These are just only a few directions for the future work, but it seems that the topic of perturbation theory for space debris (and satellite) dynamics still hides several interesting phenomena, since everytime we find a solution for an existing problem we discover a new challenging problem worth to be studied.

Appendix A

Implementation of the Normalization Algorithm

In this Appendix we describe the `Mathematica`© code used for the normalization procedure with Lie series and for the computation of the proper elements. We give the definition of the functions used, the flow chart of the whole procedure and an example of computation.

A.1 Auxiliary functions

We use some auxiliary functions both in the preparation of the Hamiltonian and during the normalization procedure as well. For the conversion from orbital to Delaunay's variables we use the following code:

Listing A.1: Delaunay's variables

```
ageo = 42164.1696;
LL[a_, e_, i_] := Sqrt[a/ageo];
GG[a_, e_, i_] := Sqrt[a (1 - e^2)/ageo];
HH[a_, e_, i_] := Sqrt[a (1 - e^2)/ageo] Cos[i*Pi/180];
```

Then we create the model depending on the region and on the perturbation chosen. As well, the number of variables are computed with:

Listing A.2: Model construction and number of degrees of freedom

```
{Hj2, Hj3, Hj4, Hmoon, Hsun, Hsrp} = {1, 1, 1, 1, 1, 1};

activeSMA = 0;
activeRes = 0;
activeDrag = 0;
Hkep = 0;
If [SMA < 8000, activeDrag = 1; activeSMA = 1; Hkep = 1,
  activeDrag = 0];
If [26400 < SMA && SMA < 26700, Hres21 = 1; activeSMA = 1;
  activeRes = 1; Hkep = 1, Hres21 = 0];
If [42000 < SMA && SMA < 42300, Hres11 = 1; activeSMA = 1;
  activeRes = 1; Hkep = 1, Hres11 = 0];

HamiltonianTD = (Hkep*HKep + Hj2*HJ2 + Hj3*HJ3 + Hmoon*HMoonTD +
     Hsun*HSun + Hsrp*HSRPTD + Hres21*HRes21TD + Hres11*HRes11TD) /.
   atm -> areaToMass;
HamiltonianPE = (Hkep*HKep + Hj2*HJ2 + Hj3*HJ3 + Hmoon*HMoonPE +
     Hsun*HSun + Hsrp*HSRPPE + Hres21*HRes21PE + Hres11*HRes11PE) /.
   atm -> areaToMass;

dof = 2;
angles = {p, q};
momenta = {P, Q};
```

```
24  If [Hmoon == 1, AppendTo[angles , qM]; AppendTo[momenta, QM];
25    dof = dof + 1];
26  If [Hsrp == 1, AppendTo[angles , rS]; AppendTo[momenta, RS];
27    dof = dof + 1];
28  If [activeSMA == 1, PrependTo[angles , r]; PrependTo[momenta, R];
29    dof = dof + 1];
30  If [activeRes == 1, AppendTo[angles , θ];
31    AppendTo[momenta, Θ]; dof = dof + 1];
32
33  allPossibleVars = {R, P, Q, QM, RS, Θ, r, p, q, qM,
34     rS, θ};
35
36  anglesT = Table[angles[[ii ]][ t ], { ii , 1, dof }];
37  momentaT = Table[momenta[[ii]][t], { ii , 1, dof }];
38  allPossibleVarsT = Table[allPossibleVars [[ ii ]][ t ], { ii , 1, Length[allPossibleVars ]}];
39  anglesTD = Table[D[angles[[ii ]][ t ], t ], { ii , 1, dof }];
40  momentaTD = Table[D[momenta[[ii]][t], t], { ii , 1, dof }];
```

Here is the function used to shift the Delaunay's actions L_0, G_0, H_0 and expand each perturbation up to a given order around the origin:

Listing A.3: Shift expansion function

```
1  ShiftExpansion[HamFunc_, order_] := Chop[Expand[Normal[Series[
2      HamFunc /. {L –> L0 + activeSMA*ebk^2*R, G –> G0 + ebk^2*P, H –> H0 + ebk^2*Q, l –> r, g –>
           p, h –> q, hM –> qM, MS –> rS},
3  {ebk, 0, order }]]]];
```

The computation of the Poisson bracket operator, Lie series operator and the inverse of Lie series operator are given in the following functions:

Listing A.4: Poisson bracket optimized

```
1  poissonBracketComp[H_, χ_, a_, m_, λ_, r_] := Module[{nvars = Length[a]},
2      ss = 0;
3      χ = TrigReduce[ExpToTrig[Coefficient[χ, λ, r]]];
4      For[j = 0, j <= r, j++,
5      Hr = Chop[TrigReduce[ExpToTrig[Coefficient[H, λ, j]]]];
6      ss = ss + λ^(j + r)*
7          Expand[Expand[D[Hr, {a}] . D[χ, {m}]] –
8          Expand[D[Hr, {m}] . D[χ, {a }]]];
9      ];
10     ss
11 ];
```

Listing A.5: Lie series operator optimized

```
1  expLie[H_, χ_, a_, m_, T_, λ_, r_] := Module[{},
2  oldH = poissonBracketComp[H, χ, a, m, λ, r];
3  s = H;
4  For[k = 1, k <= T, k++,
5      s = Sum[Chop[PowerExpand[Expand[Coefficient[s, λ, ii] +
6          TrigToExp[ Coefficient[oldH/Factorial[k], λ, ii ]]]]* λ^ii], { ii , 0, r + 1}];
7      If [k != T,
8          newH = poissonBracketComp[oldH, χ, a, m, λ, r];
9          oldH = newH;
10     ]
11 ];
12 Chop[s]
13 ];
```

Listing A.6: Inverse of Lie series operator optimized

```
expInvLie[H_, χ_, a_, m_, T_, λ_, r_] := Module[{},
oldH = -poissonBracketComp[H, χ, a, m, λ, r];
s = H;
For[k = 1, k <= T, k++,
    s = Sum[Chop[PowerExpand[Expand[Coefficient[s, λ, ii] + TrigToExp[Coefficient[oldH/
        Factorial[k], λ, ii]]]]*λ^ii], {ii, 0, r + 1}];

    If [k != T,
        newH = -poissonBracketComp[oldH, χ, a, m, λ, r];
        oldH = newH;
    ]
];
Chop[s]
];
```

A.2 Hamiltonian preparation

The preparation of the Hamiltonian, which is described in Section 5.1.2, is done in the following code:

Listing A.7: Shift and expansion of the Hamiltonian function

```
orderEarth = 8;
orderMoon = 4;
orderSun = 4;
orderSrp = 0;
orderRes = 4;

HNFinitial = Rationalize[ExpandAll[Chop[(
        ShiftExpansion[Hkep*HKep + Hj2*HJ2, orderEarth] +
        Hmoon*ShiftExpansion[HMoonPE, orderMoon] +
        Hsun*ShiftExpansion[HSun, orderSun] +
        Hsrp*ShiftExpansion[HSRPPE, orderSrp] +
        Hres21*ShiftExpansion[HRes21PE, orderRes] +
        Hres11*ShiftExpansion[HRes11PE, orderRes])
    ]] /. {t -> θ, atm -> areaToMass}] + Hmoon*(-0.05299201*365.242196/(366.242196*360))*QM
      + Hsrp*(35999.04944 365.242196/(36525*366.242196*360))*RS + activeRes*(Θ)
```

A.3 Normalization procedure

We split the normalization procedure in 2 steps. The first one consists in labeling the perturbations involved in the expanded Hamiltonian as follows

Listing A.8: Adding book-keeping parameter

```
Z0 = Chop[HNFinitial /. {ebk^k_ :> 0 /; k > 2} /. {Cos[x_] -> 0, Sin[x_] -> 0}] /. ebk -> 1;
coefZ0 = Coefficient[Z0, momenta];

ZOld = Chop[Expand[Z0]];
ROld = Chop[TrigReduce[TrigExpand[Expand[HNFinitial - ZOld] /. ebk -> 1]]];
HOld = Chop[Collect[TrigToExp[ZOld + λ* ROld], λ]];
```

and the second step is to create the loop in which we compute the generating function and the normal form at each iteration:

Listing A.9: Normalization procedure - for loop

```
For[iterNormalization = 1, iterNormalization <= maxOrderOfNormalization, iterNormalization++,

```

```
3   ROld = Chop[Coefficient[TrigToExp[HOld], λ, iterNormalization]];
4
5   ROldAngleFree = Chop[ROld /. E^x_ -> 0];
6
7   hROld = Chop[ExpandAll[TrigToExp[TrigReduce[ROld - ROldAngleFree]]]];
8
9   chiaux = 0;
10  divisors [[ iterNormalization ]] = {};
11
12  AppendTo[divisors[[iterNormalization]], Level[hROld, 1] /. {A_*E^arg_ :> {Expand[arg/I], Abs[Dot[
        Coefficient[arg/I, angles], coefZ0 ]]}}];
13  minAngleCombination = Coefficient[MinimalBy[divisors[[1, 1]], Last][[1, 1]], angles];
14
15  For[j = 1, j <= Length[hROld], j++,
16      exponentialTerm = hROld[[j]];
17      AppendTo[divisors[[iterNormalization]], exponentialTerm /.{A_*E^arg_ :> {Expand[arg/I], Dot[
            Coefficient[arg/I, angles], coefZ0 ]}}];
18
19      chiaux = chiaux + (exponentialTerm /. {A_*E^arg_ :>
20          If [(Abs[Dot[Coefficient[arg/I, angles], coefZ0]] > eps || Coefficient[arg/I, angles] !=
                minAngleCombination) && (Abs[Dot[Coefficient[arg/I, angles], coefZ0]] > eps ||
                Coefficient[arg/I, angles] != -minAngleCombination), (A*E^arg)/(I*Dot[Coefficient[arg/
                I, angles], coefZ0]), 0]})
21  ];
22
23  χ = AppendTo[χ, λ^iterNormalization*chiaux];
24
25  HNew = Collect[expLie[HOld, χ[[iterNormalization]], angles, momenta, maxOrderTaylor, λ,
        iterNormalization], λ^_]
26
27  HOld = Collect[TrigToExp[Chop[TrigReduce[ExpandAll[ExpToTrig[HNew /. λ^b_ /; b > (
        iterNormalization + maxOrderRemainder) -> 0 ]]]]], λ];
28  ];
29
30  NF = ExpandAll[Chop[TrigReduce[(ExpToTrig[ HOld] /. λ^b_ /; b >= iterNormalization -> 0)] /. λ ->
        1]]
```

A.4 Proper elements computation code

Once we finish the iteration, we use the following code to compute the proper elements for the expanded Hamiltonian:

Listing A.10: Code for computing proper elements

```
1   newVarsAsOldVars = Flatten[{momenta, angles}];
2   For[i = iterNormalization - 1, i >= 1, i--,
3       newVarsAsOldVars = Table[Collect[ expInvLie[ newVarsAsOldVars[[ji]], χ[[i]], angles, momenta,
            maxOrderTaylor, λ, i], λ^_] /. λ^b_ /; b >= iterNormalization -> 0, { ji , 1, Length[
            newVarsAsOldVars]}];
4   ];
5   newVarsAsOldVars = Table[Chop[TrigReduce[ExpToTrig[newVarsAsOldVars[[ji]]]]], {ji, 1, Length[
        newVarsAsOldVars]}];
6
7   properTimes = Table[tp, {tp, t0, tn, N[365*properTimesStep*2 Pi]}];
8
9   substitutionOldInNew = Table[AssociationThread[Keys[numHamVarsSol][[All, 0]], Values[
        numHamVarsSol] /. t -> properTimes[[ji]]], {ji, 1, Length[properTimes]}];
10
11  newInitVarsAsOldInitVars = Table[Chop[TrigReduce[ExpToTrig[Table[Chop[newVarsAsOldVars[[ji]] /.
        {λ -> 1} /. substitutionOldInNew[[ij]]], {ij, 1, Length[properTimes]}]]]], { ji , 1, Length[
        newVarsAsOldVars]}];
```

```
12
13    substitutionNewInit = Table[Append[AssociationThread[Flatten[{momenta, angles}],
          newInitVarsAsOldInitVars[[All, ji]]], AssociationThread[Complement[allPossibleVars, Flatten[{
          momenta, angles}]], Table[0, {ij, 1, Length[Complement[allPossibleVars, Flatten[{momenta,
          angles}]]]}]]], {ji, 1, Length[properTimes]}];
```

and then we use the inverse transformation to get the proper orbital elements:

Listing A.11: Code for computing proper elements

```
1 listSMAproper = ageo*(R + L0)^2 /. substitutionNewInit;
2 listECCproper = Sqrt[1 - (P + G0)^2/(R + L0)^2] /. substitutionNewInit;
3 listINCproper = ArcCos[(Q + H0)/(P + G0)]*180/Pi /. substitutionNewInit;
4 listMANproper = r /. substitutionNewInit;
5 listAOPproper = p /. substitutionNewInit;
6 listAANproper = q /. substitutionNewInit;
```

A.5 Resonant proper elements computation code

For the resonant proper elements we use a different approach, which is described in the following lines of code:

Listing A.12: Resonant proper elements compuation

```
1     resonantAngle =
2     DeleteDuplicates[Cases[NF, Cos[_] | Sin[_], Infinity] /. {Cos[arg_] -> arg, Sin[arg_] -> arg }][[1]]
3     poissonBracket[Q_, P_, q_, p_] := Module[{nvars = Length[q]}, Sum[D[Q, q[[i]]]*D[P, p[[ i ]]] - D[Q, p
          [[ i ]]]* D[P, q[[ i ]]], {i, 1, nvars}]
4     ];
5     oldAngle = angles;
6     oldMomenta = momenta;
7
8     newAngle = Flatten[{resonantAngle, Table[RandomChoice[Range[-2, 1], dof] . angles, {ij, 1, dof -
          1}]}];
9     newMomenta = Table[Table[A[ji, ij], {ji, 1, dof}] . momenta, {ij, 1, dof}];
10    sol = Solve[Table[Simplify[poissonBracket[newAngle[[i]], newMomenta[[j]], oldAngle, oldMomenta]], {i
          , 1, dof}, {j, 1, dof}] == IdentityMatrix[dof], Flatten[Table[Table[A[ji, ij], {ji, 1, dof}], {
          ij, 1, dof }]]];
11    newMomenta = Table[Table[A[ji, ij], {ji, 1, dof}] . momenta, {ij, 1, dof}] /. sol [[1]];
12
13    allResonantNewAngles = {σ[t], τ[t], ϕ[t], γ[t], ρ[t], η[t]};
14    allResonantNewMomenta = {Σ[t], 𝒯[t], Φ[t], Γ[t], P[t], H[t]};
15
16    resonantNewAngles = RandomSample[allResonantNewAngles, dof];
17    indexResNewAngles = Flatten[Table[Position[allResonantNewAngles,resonantNewAngles[[ij]]], {ij, 1,
          dof}]];
18    resonantNewMomenta = allResonantNewMomenta[[indexResNewAngles]];
19    resonantNewVars = Flatten[{resonantNewMomenta, resonantNewAngles}];
20
21    coordsol = Solve[resonantNewVars == Flatten[{newMomenta, newAngle}], Flatten[{momenta, angles
          }]][[1]]
22    eqs = {Append[D[resonantNewAngles, t], D[resonantNewMomenta, t]] == Append[D[NFres, {
          resonantNewMomenta}], -D[NFres, {resonantNewAngles}]]}
23    init = {Flatten[{resonantNewMomenta /. t -> 0, resonantNewAngles /. t -> 0}] == (Flatten[{
          newMomenta, newAngle}] /. substitutionNewInit[[1]])}
24
25    ndsol = NDSolve[{eqs, init}, resonantNewVars, {t, t0, tn}, Method -> {"ExplicitRungeKutta", "
          DifferenceOrder" -> 8, "StiffnessTest" -> False}, StartingStepSize -> step, MaxSteps ->
          Infinity];
26
27    nullAssociation = AssociationThread[Complement[allPossibleVars, Flatten[{momenta, angles}]],
          Table[0, {ij, 1, Length[Complement[allPossibleVars, Flatten[{momenta, angles}]]]}]];
```

```
28
29  nonResonantVarsSol = AssociateTo[nullAssociation, coordsol /. ndsol [[1]]];
30
31  resSMAev = ageo*(R + L0)^2 /. nonResonantVarsSol;
32  resECCev = Sqrt[1 - ((P + G0)/(R + L0))^2] /. nonResonantVarsSol;
33  resINCev = ArcCos[(Q + H0)/(P + G0)] /. nonResonantVarsSol;
34  resMANev = r /. nonResonantVarsSol;
35  resAOPev = p /. nonResonantVarsSol;
36  resAANev = q /. nonResonantVarsSol;
```

A.6 Computation of analytic solution of mean elements

Since we already computed the generating function, we can make use of the function that computes the inverse of the Lie operator to obtain the analytic solution of the mean elements, as follows:

Listing A.13: Analytic solution computation code

```
1   oldVarsAsNewVars = Flatten[{momenta, angles}];
2   For[i = 1, i <= iterNormalization - 1, i++,
3       oldVarsAsNewVars = Table[Collect[ expLie[ oldVarsAsNewVars[[ji]], χ[[i]], angles, momenta,
            maxOrderTaylor, λ, i], λ^_] /. λ^b_ /; b >= iterNormalization -> 0, { ji , 1, Length[
            oldVarsAsNewVars]}];
4   ];
5
6   oldVarsAsNewVars = Table[Chop[TrigReduce[ExpToTrig[oldVarsAsNewVars[[ji]]]]], {ji, 1, Length[
        oldVarsAsNewVars]}];
7
8   oldMomentaAsNewVars = Expand[ExpToTrig[momenta - (D[NF, {angles}])*t] /. substitutionNewInit
        [[1]] /. t -> (t - properTimes[[1]])/myscale]
9   oldAnglesAsNewVars = Expand[ExpToTrig[angles + D[NF, {momenta}]*t] /. substitutionNewInit[[1]] /. t
        -> (t - properTimes[[1]])/myscale]
10
11   substitutionOldInit  = Append[Append[AssociationThread[momenta, oldMomentaAsNewVars],
        AssociationThread[angles, oldAnglesAsNewVars]], AssociationThread[Complement[
        allPossibleVars, Flatten[{momenta, angles}]], Table[0, {ij, 1, Length[Complement[
        allPossibleVars, Flatten[{momenta, angles}]]]}]]];
12
13  oldAnalyticSolutions  = Rationalize[ExpandAll[ExpToTrig[oldVarsAsNewVars /. λ -> 1 /.
        substitutionOldInit]]];
14
15  substitutionOldAS = Append[AssociationThread[Flatten[{momenta, angles}], oldAnalyticSolutions],
        AssociationThread[Complement[allPossibleVars, Flatten[{momenta, angles}]], Table[0, {ij, 1,
        Length[Complement[allPossibleVars, Flatten[{momenta, angles}]]]}]]];
16
17  analyticSMA = ageo*(R + L0)^2 /. substitutionOldAS;
18  analyticECC = Chop[Sqrt[1 - (P + G0)^2/(R + L0)^2] /. substitutionOldAS];
19  analyticINC = Chop[ArcCos[(Q + H0)/(P + G0)]*180/Pi /. substitutionOldAS];
20  analyticMAN = r /.  substitutionOldAS;
21  analyticAOP = p /.  substitutionOldAS;
22  analyticAAN = q /.  substitutionOldAS;
```

A.7 Procedure and a simple example

The scheme of the procedure is summarized in the flow chart in Figure A.1. Let us take as an example, the case presented in Section 6.1.3, Figure 6.8, for an orbit in the 2:1 tesseral resonant region. The model selector will define a Hamiltonian function that contains the following perturbations: J_2, J_3, Moon, Sun, SRP, and the terms of tesseral resonance 2:1

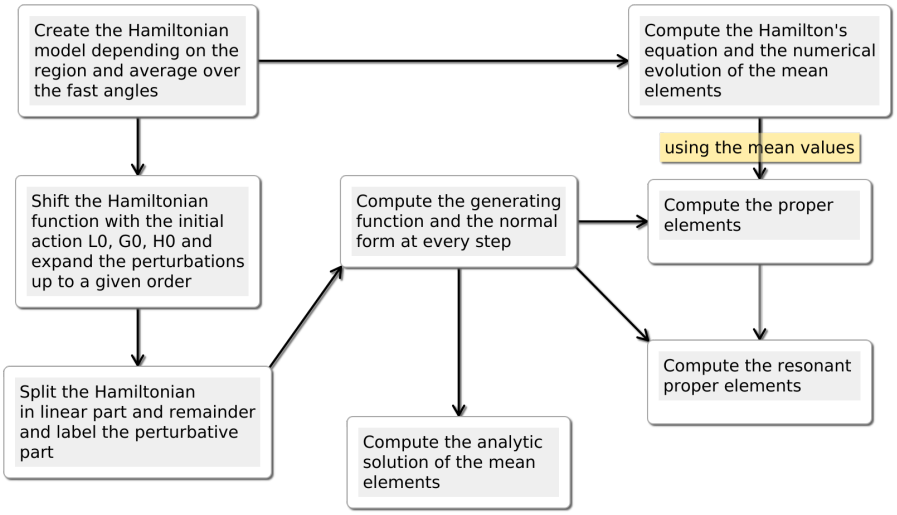

FIGURE A.1: Scheme of the procedure for computing the proper elements and the analytic solution of the mean elements

from equation (4.8).
The next step is to compute the Hamilton's equation for the Hamiltonian function in Delaunay variables and to obtain the evolution of the mean elements. We keep the data of the evolution of the mean elements and we plot it in purple in Figure 6.8. Now, we need to shift and expand the Hamiltonian in Delaunay's variables around the initial actions $L_0 = 0.793674$, $G_0 = 0.791727$, $H_0 = 0.76475$.
The new Hamiltonian has 6 DoF and it depends on the following variables:

$$\{R, P, Q, \mathrm{QM}, \mathrm{RS}, \Theta, r, p, q, \mathrm{qM}, \mathrm{rS}, \theta\}$$

After that, we split the expanded Hamiltonian into 2 parts as in (6.4) where the linear part is given by

$$Z_0 = \Theta + 0.000358248P - 0.000188871Q - 0.000146798\mathrm{QM} + 2.00035R + 0.0027303\mathrm{RS}.$$

The remainder has a huge amount of terms and it is hard to reproduce it here. It has the form described in (6.6). The coefficient vector, ν, is given by

$$\nu = \{2.00035, 0.000358248, -0.000188871, -0.000146798, 0.0027303, 1\}.$$

After the first order normalization we obtained a normal form depending on the resonant angle $r - 2\theta + 2q$ which has the following form:

$$\begin{aligned} H_{NF} = {} & \left(3.58 \cdot 10^{-4}\right) P - \left(1.89 \cdot 10^{-4}\right) Q - \left(1.47 \cdot 10^{-4}\right) \mathrm{QM} + 2R + \left(2.73 \cdot 10^{-3}\right) \mathrm{RS} + \Theta \\ & + \lambda \Big(\left(-1.15 \cdot 10^{-2}\right) P^4 + \left(1.29 \cdot 10^{-2}\right) QP^3 - \left(1.67 \cdot 10^{-2}\right) RP^3 + \left(4.41 \cdot 10^{-3}\right) P^3 \\ & - \left(2.85 \cdot 10^{-3}\right) Q^2P^2 - \left(1.36 \cdot 10^{-2}\right) R^2P^2 - \left(4.36 \cdot 10^{-3}\right) QP^2 + \left(1.65 \cdot 10^{-2}\right) QRP^2 \\ & + \left(5.4 \cdot 10^{-3}\right) RP^2 + \left(6.4 \cdot 10^{-5}\right) \cos(2q + r - 2\theta) P^2 - \left(3.67 \cdot 10^{-5}\right) \sin(2q + r - 2\theta) P^2 \\ & - \left(1.46 \cdot 10^{-3}\right) P^2 - \left(6.92 \cdot 10^{-3}\right) R^3P + \left(7.53 \cdot 10^{-4}\right) Q^2P + \left(1.1 \cdot 10^{-2}\right) QR^2P \end{aligned}$$

$$
\begin{aligned}
&+\left(3.29\cdot10^{-3}\right)R^2P+\left(1.19\cdot10^{-3}\right)QP-\left(2.85\cdot10^{-3}\right)Q^2RP-\left(4.35\cdot10^{-3}\right)QRP\\
&-\left(1.24\cdot10^{-3}\right)RP-\left(1.43\cdot10^{-5}\right)Q\cos(2q+r-2\theta)P-\left(1.17\cdot10^{-4}\right)R\cos(2q+r-2\theta)P\\
&+\left(3.36\cdot10^{-7}\right)\cos(2q+r-2\theta)P+\left(8.22\cdot10^{-6}\right)Q\sin(2q+r-2\theta)P\\
&+\left(6.7\cdot10^{-5}\right)R\sin(2q+r-2\theta)P-\left(1.93\cdot10^{-7}\right)\sin(2q+r-2\theta)P-\left(1.\cdot10^{1}\right)R^4\\
&+\left(3.65\cdot10^{-3}\right)QR^3+6.35R^3-\left(1.23\cdot10^{-4}\right)Q^2-\left(1.14\cdot10^{-3}\right)Q^2R^2-\left(1.74\cdot10^{-3}\right)QR^2\\
&-3.78R^2+\left(4.51\cdot10^{-4}\right)Q^2R+\left(6.32\cdot10^{-4}\right)QR+\left(3.61\cdot10^{-8}\right)Q^2\cos(2q+r-2\theta)\\
&+\left(5.33\cdot10^{-5}\right)R^2\cos(2q+r-2\theta)+\left(5.53\cdot10^{-8}\right)Q\cos(2q+r-2\theta)\\
&+\left(1.37\cdot10^{-5}\right)QR\cos(2q+r-2\theta)-\left(3.77\cdot10^{-7}\right)R\cos(2q+r-2\theta)\\
&-\left(1.52\cdot10^{-9}\right)\cos(2q+r-2\theta)-\left(2.07\cdot10^{-8}\right)Q^2\sin(2q+r-2\theta)\\
&+\left(3.06\cdot10^{-5}\right)R^2\sin(2q+r-2\theta)-\left(3.17\cdot10^{-8}\right)Q\sin(2q+r-2\theta)\\
&-\left(7.88\cdot10^{-6}\right)QR\sin(2q+r-2\theta)+\left(2.16\cdot10^{-7}\right)R\sin(2q+r-2\theta)\\
&+\left(8.71\cdot10^{-10}\right)\sin(2q+r-2\theta)\Big).
\end{aligned}
$$

The generating function at the first step depends on the same combination of angles as the initial Hamiltonian, but not on the resonant angles. This is the reason of having the normal form depending on that resonant angle. The form of the generating function is as large as the initial Hamiltonian, thus it is hard to write all the terms.
The additional terms obtained during the second step of normalization, depending on λ^2, are the following:

$$
\begin{aligned}
\lambda^2\Big(&\left(1.38\cdot10^{-4}\right)\cos(2q+r-2\theta)P^3-\left(7.94\cdot10^{-5}\right)\sin(2q+r-2\theta)P^3-\left(1.2\cdot10^{-3}\right)P^3\\
&+\left(8.49\cdot10^{-4}\right)QP^2+\left(2.94\cdot10^{-3}\right)RP^2\left(1.38\cdot10^{-4}\right)Q\cos(2q+r-2\theta)P^2\\
&-\left(2.73\cdot10^{-4}\right)R\cos(2q+r-2\theta)P^2+\left(4.26\cdot10^{-6}\right)\cos(2q+r-2\theta)P^2\\
&+\left(7.94\cdot10^{-5}\right)Q\sin(2q+r-2\theta)P^2+\left(1.56\cdot10^{-4}\right)R\sin(2q+r-2\theta)P^2\\
&-\left(2.44\cdot10^{-6}\right)\sin(2q+r-2\theta)P^2+\left(1.18\cdot10^{-5}\right)P^2-\left(7.09\cdot10^{-4}\right)Q^2P\\
&-\left(2.78\cdot10^{-3}\right)R^2P-\left(4.8\cdot10^{-5}\right)QP-\left(5.09\cdot10^{-4}\right)QRP\\
&+\left(2.39\cdot10^{-5}\right)RP-\left(7.05\cdot10^{-7}\right)Q^2\cos(2q+r-2\theta)P\\
&+\left(1.23\cdot10^{-4}\right)R^2\cos(2q+r-2\theta)P-\left(4.2\cdot10^{-7}\right)Q\cos(2q+r-2\theta)P\\
&+\left(2.84\cdot10^{-4}\right)QR\cos(2q+r-2\theta)P-\left(8.2\cdot10^{-6}\right)R\cos(2q+r-2\theta)P\\
&+\left(1.03\cdot10^{-8}\right)\cos(2q+r-2\theta)P+\left(4.05\cdot10^{-7}\right)Q^2\sin(2q+r-2\theta)P\\
&-\left(7.08\cdot10^{-5}\right)R^2\sin(2q+r-2\theta)P+\left(2.41\cdot10^{-7}\right)Q\sin(2q+r-2\theta)P\\
&-\left(1.63\cdot10^{-4}\right)QR\sin(2q+r-2\theta)P+\left(4.7\cdot10^{-6}\right)R\sin(2q+r-2\theta)P\\
&-\left(5.94\cdot10^{-9}\right)\sin(2q+r-2\theta)P+\left(4.86\cdot10^{-7}\right)P\\
&+\left(1.94\cdot10^{-4}\right)Q^3+\left(9.41\cdot10^{-4}\right)R^3+\left(2.44\cdot10^{-5}\right)Q^2+\left(2.59\cdot10^{-5}\right)QR^2\\
&-\left(1.43\cdot10^{-5}\right)R^2-\left(2.81\cdot10^{-7}\right)Q+\left(2.39\cdot10^{-4}\right)Q^2R+\left(1.27\cdot10^{-6}\right)QR\\
&-\left(5.7\cdot10^{-7}\right)R+\left(1.07\cdot10^{-9}\right)Q^3\cos(2q+r-2\theta)+\left(1.1\cdot10^{-5}\right)R^3\cos(2q+r-2\theta)\\
&+\left(2.73\cdot10^{-9}\right)Q^2\cos(2q+r-2\theta)-\left(1.46\cdot10^{-4}\right)QR^2\cos(2q+r-2\theta)
\end{aligned}
$$

$$
\begin{aligned}
&+ \left(3.95 \cdot 10^{-6}\right) R^2 \cos(2q + r - 2\theta) \\
&+ \left(1.64 \cdot 10^{-9}\right) Q \cos(2q + r - 2\theta) + \left(6.9 \cdot 10^{-7}\right) Q^2 R \cos(2q + r - 2\theta) \\
&+ \left(4.03 \cdot 10^{-7}\right) QR \cos(2q + r - 2\theta) - \left(1.17 \cdot 10^{-8}\right) R \cos(2q + r - 2\theta) \\
&- \left(6.12 \cdot 10^{-10}\right) Q^3 \sin(2q + r - 2\theta) - \left(6.31 \cdot 10^{-6}\right) R^3 \sin(2q + r - 2\theta) \\
&- \left(1.57 \cdot 10^{-9}\right) Q^2 \sin(2q + r - 2\theta) + \left(8.37 \cdot 10^{-5}\right) QR^2 \sin(2q + r - 2\theta) \\
&- \left(2.27 \cdot 10^{-6}\right) R^2 \sin(2q + r - 2\theta) - \left(9.4 \cdot 10^{-10}\right) Q \sin(2q + r - 2\theta) \\
&- \left(3.96 \cdot 10^{-7}\right) Q^2 R \sin(2q + r - 2\theta) - \left(2.31 \cdot 10^{-7}\right) QR \sin(2q + r - 2\theta) \\
&+ \left(6.73 \cdot 10^{-9}\right) R \sin(2q + r - 2\theta) - 3.99 \cdot 10^{-8}\Big).
\end{aligned}
$$

Since we are in the case of a tesseral resonance, we need to use the semy-analytic method to compute the proper elements. The evolution of the mean elements and the evolution of the proper elements are shown in Figure 6.8; here we give the values of the mean elements and proper elements at 5 different times as follows:

$$
\begin{aligned}
a_\tau^{\text{mean}} &= \{26560., 26568.6, 26572.4, 26566.1, 26564\}, \\
e_\tau^{\text{mean}} &= \{0.07, 0.0690202, 0.0680305, 0.0711677, 0.0686094\}, \\
i_\tau^{\text{mean}} &= \{15, 14.3092, 14.683, 13.4647, 13.8994\},
\end{aligned}
$$

$$
\begin{aligned}
a_\tau^{\text{proper}} &= \{26560.8, 26560.3, 26561.2, 26561.4, 26560.3\}, \\
e_\tau^{\text{proper}} &= \{0.0705481, 0.0704244, 0.0706662, 0.0707184, 0.0704345\}, \\
i_\tau^{\text{proper}} &= \{14.199, 14.2031, 14.1951, 14.1933, 14.2028\},
\end{aligned}
$$

where $\tau = \{0, 50, 100, 150, 200\}$ is the time in years.

Appendix B

Hamiltonian Function Expansion and Cartesian Integration Implementation

B.1 Mathematica©

In this section we give the Mathematica© codes for computing the Hamiltonian expansion for the perturbations due to Earth, Moon, Sun and SRP, respectively obtained by Kaula-Lane (Kaula, 2000), (Lane, 1989) and Hughes (Hughes, 1980) (see Section 3.4).

B.1.1 Auxiliary function

The following code describes the auxiliary function from (3.14)-(3.15) for the Earth's expansion.

Listing B.1: Kaula's Inclination Function

```
F[x_, n_, m_, p_] := Module[ {wmax = Min[p,IntegerPart[(n−m)/2]], IntegerPart[(n−m)/2]},
    Sum[(2n−2w)!/(w! (n−w)! (n−m−2w)! (2^(2n−2w)) ) Sin[x]^(n−m−2w) Sum[Binomial[m,s] Cos[x]^s
    Sum[Binomial[n−m−2w+s,c] Binomial[m−s,p−w−c] (−1)^(c−k),{c,0,n}], {s,0,m}], {w,0,wmax}]
];
```

Listing B.2: Kaula's Eccentricity Functions

```
β[x_] = x/(1 + Sqrt[1 − x^2]) ;

Π[x_, β_, n_, p_, q_, k_] := Module[{h = If[q > 0, k + q, k] }, Sum[Binomial[2 p − 2 n, h − r] (−1)^r/r!
    (((n − 2 p + q) x)/(2 β))^r, {r, 0, h }]];

Θ[x_, β_, n_, p_, q_, k_] := Module[{h = If[q > 0, k, k − q] }, Sum[Binomial[−2 p, h − r] 1/r! (((n − 2 p
    + q) x)/(2 β))^r, {r, 0, h }]];

finiteSum[x_, β_, n_, p_, q_] := Sum[Π[x, β, n, p, q, k] Θ[x, β, n, p, q, k] β^(2 k), {k, 0, 20}];

infiniteSum[x_, β_, n_, p_, q_] = Sum[Π[x, β, n, p, q, k] Θ[x, β, n, p, q, k] β^(2 k), {k, 0, Infinity }];

Γ[x_, β_, n_, p_, q_] := Module[{P = If[p <= n/2, p, n − p], Q = If [p <= n/2, q, −q]},
    If [n − 2*p + q != 0, Normal[ Series[(−1)^Abs[q] (1 + β^2)^n β^Abs[q] finiteSum[x, β, n, P, Q],
        {x, 0, expmax}]], (−1)^Abs[q] (1 + β^2)^n β^Abs[q] infiniteSum[x, β, n, P, Q]
    ]
];
```

Listing B.3: Kaula's Angles Functions

```
Ψ[l_, g_, h_, θ_, n_, m_, p_, q_] = Rationalize[(n − 2 p) g + (n − 2 p + q) l + m (h − θ) − m * Subscript
    [λ, n, m]];
```

```
S[l_, g_, h_, θ_, n_, m_, p_, q_] = -Subscript[J, n, m] If[Mod[n - m, 2] == 0, Cos[Ψ[l, g, h, θ, n, m, p, q]], Sin[Ψ[l, g, h, θ, n, m, p, q]]];
```

Similarly, we give the auxiliary functions that appear in the expansions of the Moon (3.18), Sun (3.21) and SRP (3.23).

Listing B.4: Moon, Sun, SRP Auxiliary Functions

```
ε[m_] := If[m == 0, 1, 2];

β[x_] := x/(1 + Sqrt[1 - x^2]);

X[x_, n_, m_, k_] := (1 + β[x]^2)^(-n - 1) * Sum[Sum[Binomial[n - m + 1, s] * Binomial[n + m + 1, t]*(-β[x])^(s + t) * BesselJ[k - m - s + t, k*x], {t, 0, If[n + m + 1 >= 0, n + m + 1, 20]}], {s, 0, If[n - m + 1 >= 0, n - m + 1, 20]}];

U[m_, s_, l_] := (-1)^(m - s) Sum[(-1)^(l - m - r)*Binomial[l + m, m + s + r]*Binomial[l - m, r] * Cos[ϵ/2]^(m + s + 2 r)*Sin[ϵ/2]^(-m - s + 2 (l - r)), {r, Max[0, -(m + s)], Min[l - s, l - m]}];

K1[m_] := IntegerPart[m/2];

K2[l_, m_, s_] := Mod[l - 1, 2]*(m + s - 1) + 1;

K3[l_, m_, s_] := Mod[l - 1, 2]*(m + s);

Ys[s_] := If[Mod[s, 2] == 0, 0, 1/2];

H[x_, l_, p_, j_] := X[x, l, l - 2 p, l - 2 p + j];

G[x_, l_, q_, r_] := X[x, -(l + 1), l - 2 q, l - 2 q + r];
```

B.1.2 Kaula's expansions of the Earth's Hamiltonian functions

The secular expansion of the Earth's Hamiltonian is given by

Listing B.5: Secular part of the Earth's Hamiltonian expansion

```
H^secular_Earth = -(μ_E/a) Sum[Sum[(R_E/a)^n * Sum[F[i, n, m, p] Sum[ If[n - 2*p + q == 0,
    FullSimplify[Γ[e, β[e], n, p, q]]* S[M, ω, Ω, θ, n, m, p, q], 0],
  {q, -n + 1, n - 1}], {p, 0, n}], {m, 0, n}], {n, 2, nmax}]
```

Listing B.6: Resonant part of the Earth's Hamiltonian expansion

```
H^resonant_Earth = -(μ_E/a) Sum[Sum[(R_E/a)^n * Sum[F[i, n, m, p] * Sum[ If[j (n - 2p + q) == l m && m != 0,
    FullSimplify[Γ[e, β[e], n, p, q]] * S[M, ω, Ω, θ, n, m, p, q], 0],
  {q, -n + 1, n - 1}], {p, 0, n}], {m, 0, n}], {n, 2, nmax}]
```

B.1.3 Kaula-Lane expansions of the Moon and Sun

The expansion of the Moon is computed as

Listing B.7: Hamiltonian expansion of the Moon

```
H_Moon = -(μ_M/2) Sum[a^l/a_M^(l + 1) Sum[Sum[(-1)^K1[m] ε[m] ε[s] (l - s)!/(l + m)!
    Sum[F[i, l, m, p] Sum[F[i_M, l, s, q] Sum[Sum[
      If[l - 2 p + j == 0, Normal[Series[H[e, l, p, j], {e, 0, 2}]], 0]
      If[l - 2 q + r == 0, Normal[Series[G[e_M, l, q, r], {eM, 0, 2}]], 0]
      (U[m, -s, l]*Cos[Rationalize[(l - 2 p) ω + (l - 2 p + j) M + m Ω + (l - 2q) ω_M + (l - 2 q + r) M_M
        + s Ω_M - (s π)/2 - Ys[s] π]]*(-1)^K2[l, m, s] +
```

```
6       U[m, s, l ]* Cos[Rationalize[(l – 2 p) ω + (l – 2 p + j )* M + m Ω – (l – 2q) ω_M – (l – 2 q + r) M_M
            – s Ω_M + (s*π)/2 – Ys[s]*π]]*(–1)^K3[l, m, s]),
7   {r, –l, l }], {j , –l, l }], {q, 0, l }], {p, 0, l }], {s, 0, l }], {m, 0, l }], {l , 2, 2 }];
```

while for the Sun we have the following code

Listing B.8: Hamiltonian expansion of the Sun

```
1 H_Sun =–μ_S Sum[a^n/a_S^(n + 1) Sum[ε[m] (n – m)!/(n + m)! Sum[F[i, n, m, p]*Sum[F[i_S , n, m, h] Sum[
2     If [n – 2 p + q == 0,  Normal[Series[H[e, n, p, q], {e, 0, 2}]], 0]
3       Sum[If[n – 2 h + j == 0,  Normal[Series[ G[e_S , n, h, j], {e_S , 0, 2}]], 0] Cos[Chop[(n – 2 p) ω + (n
            – 2 p + q) M – (n – 2 h) ω_s – (n – 2 h + j) M_S + m (Ω – Ω_s)]],
4   {j , –2, 2}], {q, –2, 2}], {h, 0, n }], {p, 0, n }], {m, 0, n }], {n, 2, 2}];
```

B.1.4 Hughes expansion of the SRP

The formula described in (3.23) can be implemented in Mathematica© as

Listing B.9: Hamiltonian expansion of the SRP

```
1 H_SRP = Sum[C_R*P_r A/m a_S^2 a^n / a_S^(n+1) Sum[ε[m] (n – m)!/(n + m)! Sum[F[i, n, m, p] Sum[F[i_S , n, m, h]
2     Sum[ Normal[ Series[ If[n – 2 p + q == 0, X[e, n, n – 2 p, n – 2 p + q], 0], {e, 0, 2}]]
3     Sum[ Normal[ Series[ X[e_S , –(n + 1), n – 2 h, n – 2 h + j ], {e_S , 0, 2}]]
4       Cos[Rationalize[(n – 2 p) ω + (n – 2 p + q) M – (n – 2 h)*ω_s – (n – 2 h + j) M_S + m (Ω – Ω_s)]],
5   {j , –2, 2}], {q, –2, 2}], {h, 0, n }], {p, 0, n }], {m, 0, n }], {n, 1, 1 }];
```

B.2 JAVA© - Cartesian integration

In this section we provide the JAVA© code that computes the perturbation function due to Earth, Moon, Sun, SRP and effect of the atmospheric drag in the Cartesian coordinates.
We mention that all the numerical computations are done by using a 4th order Runge-Kutta method, and every quantity involved in the computation is scaled to the proper units as described in Section 3.2.
We need to solve the system of equations defined by:

$$\begin{cases} \dot{\boldsymbol{x}} = \boldsymbol{f_1}(\boldsymbol{x}, \boldsymbol{v}) \\ \dot{\boldsymbol{v}} = \boldsymbol{f_2}(\boldsymbol{x}, \boldsymbol{v}), \end{cases} \tag{B.1}$$

where $\dot{\boldsymbol{x}} = (x, y, z)$, $\dot{\boldsymbol{v}} = (v_x, v_y, v_z)$, and $\boldsymbol{f_1}(\boldsymbol{x}, \boldsymbol{v}) = (v_x, v_y, v_z)$.
The function f_2 is a sum of different functions that describe the equations of the perturbations involved. For example, the Keplerian part is described by the following function:

Listing B.10: Keplerian equations of motion

```
1   public double[] fKep(double x, double y, double z, double vx, double vy, double vz, double t){
2       double[] out = new double[3];
3       double r, r3;
4
5       r = Math.sqrt(x*x+y*y+z*z);
6       r3 = r*r*r;
7
8       out[0] = –nmiue*x/r3;
9       out[1] = –nmiue*y/r3;
10      out[2] = –nmiue*z/r3;
11
12      return out;
13  }
```

The perturbation of the non-spherical shape of the Earth is split in two parts: the perturbation due to the J_2 terms

Listing B.11: J_2 function

```
public double[] fJ2(double x, double y, double z, double vx, double vy, double vz, double t){
    double[] out = new double[3];
    double r, r2, r5, C20, C22, S22, cs, Cs, re;

    r = Math.sqrt(x*x+y*y+z*z);
    r2 = r*r; r5 = r2*r2*r;
    re = 6371/anorm;

    double theta = 280.4606 * Math.PI/180 + t;
    C20 = -1082.6261e-6;
    C22 = 1.57462e-6;
    S22 = -0.90387e-6;
    cs = C22*Math.cos(2*theta) - S22*Math.sin(2*theta);
    Cs = C22*Math.sin(2*theta) + S22*Math.cos(2*theta);

    out[0] = (nmiue*re*re/r5)*( C20*(1.5*x - (7.5*x*z*z)/r2) + 6*cs*x + 6*Cs*y + 15*x*(cs*(y*y - x*x)
        - 2*x*y*Cs)/r2);
    out[1] = (nmiue*re*re/r5)*( C20*(1.5*y - (7.5*y*z*z)/r2) + 6*Cs*x - 6*cs*y + 15*y*(cs*(y*y - x*x)
        - 2*x*y*Cs)/r2);
    out[2] = (nmiue*re*re/r5)*( C20*(4.5*z - (7.5*z*z*z)/r2) + 15*z*(cs*(y*y - x*x)
        - 2*x*y*Cs)/r2);

    return out;
}
```

and the J_3 terms

Listing B.12: J_2 function

```
public double[] fJ3(double x, double y, double z, double vx, double vy, double vz, double t){
    double[] out = new double[3];
    double r, r2;

    r = Math.sqrt(x*x+y*y+z*z);
    r2 = r*r;

    out[0] = (0.00172489302057874*(0.00001266205*x*z*(3*(x*x + y*y) - 4*z*z) + 3*((8.7726e-6*x*x
        + 1.3404349999999998e-6*x*y - 2.19315e-6*y*y)*(x*x + y*y) + 3*(-2.6808699999999996e
        -6*x*y + 2.19315e-6*(-9*x*x + y*y))*z*z + 8.7726e-6*z*z*z*z)*Math.cos(t) + 30*z*(-2.11431
        e-7*y*z*(-6*x*x + y*y + z*z) + 3.0903999999999997e-7*x*(-5*x*x + 9*y*y + 2*z*z))*Math.
        cos(2*t) + 30*(1.97222e-7*x*y*(-15*x*x + 13*y*y + 6*z*z) + 1.00583e-7*(-4*x*x*x*x - 3*y*y
        *(y*y + z*z) + 3*x*x*(7*y*y + z*z)))*Math.cos(3*t) - 3*((1.072348e-6*x*x -
        0.000010965749999999999*x*y - 2.68087e-7*y*y)*(x*x + y*y) +
        3*(0.000021931499999999998*x*y + 2.68087e-7*(-9*x*x + y*y))*z*z + 1.072348e-6*z*z*z*z
        )*Math.sin(t) - 15*z*(-1.2361599999999999e-6*y*(-6*x*x + y*y + z*z) - 2.11431e-7*x*z
        *(-5*x*x + 9*y*y + 2*z*z))*Math.sin(2*t) + 30*(1.00583e-7*x*y*(-15*x*x + 13*y*y + 6*z*z) +
        1.97222e-7*(4*x*x*x*x + 3*y*y*(y*y + z*z) - 3*x*x*(7*y*y + z*z)))*Math.sin(3*t)))/Math.pow(r2
        ,4.5);

}
```

```
10        out[1] = (0.00172489302057874*(0.00001266205*y*z*(3*(x*x + y*y) - 4*z*z) + 3*((-2.68087e-7*
              x*x + 0.000010965749999999999*x*y + 1.072348e-6*y*y)*(x*x + y*y) +
              3*(-0.000021931499999999998*x*y + 2.68087e-7*(x*x - 9*y*y))*z*z + 1.072348e-6*z*z*z*z*z
              )*Math.cos(t) + 30*z*(3.0903999999999997e-7*y*(-9*x*x + 5*y*y - 2*z*z) - 2.11431e-7*x*z
              *(x*x - 6*y*y + z*z))*Math.cos(2*t) + 30*(1.00583e-7*x*y*(-13*x*x + 15*y*y - 6*z*z) +
              1.97222e-7*(3*x*x*x*x*x - 21*x*x*y*y + 4*y*y*y*y + 3*(x - y)*(x + y)*z*z))*Math.cos(3*t) +
              3*(-((x*x + y*y)*(1.3404349999999998e-6*x*y + 2.19315e-6*(x*x - 4*y*y)))+
              3*(2.6808699999999996e-6*x*y + 2.19315e-6*(x*x - 9*y*y))*z*z + 8.7726e-6*z*z*z*z*z)*
              Math.sin(t) + 15*z*(1.2361599999999999e-6*x*(x*x - 6*y*y + z*z) - 2.11431e-7*y*z*(9*x*x
              - 5*y*y + 2*z*z))*Math.sin(2*t) + 30*(1.97222e-7*x*y*(13*x*x - 15*y*y + 6*z*z) + 1.00583e
              -7*(3*x*x*x*x*x - 21*x*x*y*y + 4*y*y*y*y + 3*(x - y)*(x + y)*z*z))*Math.sin(3*t)))/Math.pow(r2
              ,4.5);
11
12        out[2] = (0.00172489302057874*(2.53241e-6*(-3*(x*x + y*y)*(x*x + y*y) + 24*(x*x + y*y)*z*z - 8*
              z*z*z*z) + 15*((2.19315e-6*x + 2.68087e-7*y)*z*(3*(x*x + y*y) - 4*z*z)*Math.cos(t) +
              2*(3.0903999999999997e-7*(x - y)*(x + y)*(x*x + y*y - 6*z*z) - 2.11431e-7*x*y*z*(2*(x*x +
              y*y) - 5*z*z))*Math.cos(2*t) - 14*(1.00583e-7*x*x*x*x + 5.91666e-7*x*x*y - 3.01749e-7*x*y*
              y - 1.97222e-7*y*y*y)*z*Math.cos(3*t) + (2.68087e-7*x - 2.19315e-6*y)*z*(-3*(x*x + y*y) +
               4*z*z)*Math.sin(t) + (1.2361599999999999e-6*x*y*(x*x + y*y - 6*z*z) + 2.11431e-7*(x - y)
              *(x + y)*z*(2*(x*x + y*y) - 5*z*z))*Math.sin(2*t) + 14*(1.00583e-7*y*(-3*x*x + y*y) + 1.97222
              e-7*(x*x*x - 3*x*y*y))*z*Math.sin(3*t))))/Math.pow(r2,4.5);
13
14        return out;
15    }
```

In the case of the perturbations due to the Moon and Sun attraction, the functions that define the equation of motions are similar, only the computation of the position of the 3rd body being different (see (Montenbruck, Gill, and Lutze, 2002)).

LISTING B.13: Moon and Sun equations of motion

```
1     public double[] fMoon(double x, double y, double z, double vx, double vy, double vz, double t){
2
3         double[] out = new double[3];
4         double rm3, rrm3, mx, my, mz;
5         double[] rm = moonpos(t);
6         mx = rm[0]; my = rm[1]; mz = rm[2];
7         rm3 = (mx*mx+my*my+mz*mz)*Math.sqrt(mx*mx+my*my+mz*mz);
8         rrm3 = ((mx-x)*(mx-x)+(my-y)*(my-y)+(mz-z)*(mz-z))*Math.sqrt((mx-x)*(mx-x)+(my-y)*(my-y)
              +(mz-z)*(mz-z));
9
10        out[0] = -nmium*((x-mx)/rrm3 + mx/rm3);
11        out[1] = -nmium*((y-my)/rrm3 + my/rm3);
12        out[2] = -nmium*((z-mz)/rrm3 + mz/rm3);
13
14        return out;
15    }
16
17    public double[] fSun(double x, double y, double z, double vx, double vy, double vz, double t){
18        double[] out = new double[3];
19
20        double rs3, rrs3, sx, sy, sz;
21        double[] rs = sunpos(t);
22        sx = rs[0]; sy = rs[1]; sz = rs[2];
23        rs3 = (sx*sx+sy*sy+sz*sz)*Math.sqrt(sx*sx+sy*sy+sz*sz);
24        rrs3 = ((sx-x)*(sx-x)+(sy-y)*(sy-y)+(sz-z)*(sz-z))*Math.sqrt((sx-x)*(sx-x)+(sy-y)*(sy-y)+(sz-z)
              *(sz-z));
25
26        out[0] = -nmius*((x-sx)/rrs3 + sx/rs3);
27        out[1] = -nmius*((y-sy)/rrs3 + sy/rs3);
28        out[2] = -nmius*((z-sz)/rrs3 + sz/rs3);
29
30        return out;
```

```
31      }
```

For the position of the Moon we use the function

Listing B.14: Moon position

```
1       private double[] moonpos(double t){
2       double[] out = new double[3];
3       double eps, tau, L0, l, lp, F, D, Lm, Bm, r;
4
5       eps = pi2*23.4392911/360;
6
7       tau = (365.242196/366.242196)*t/(36525*pi2);
8
9       L0 = pi2*(218.31617 + 481267.88088*tau - 4.06*tau*tau/3600)/360;
10      l = pi2*(134.96292 + 477198.86753*tau)/360;
11      lp = pi2*(357.52543 + 35999.04944*tau)/360;
12      F = pi2*(93.27283 + 483202.01873*tau)/360;
13      D = pi2*(297.85027 + 445267.11135*tau)/360;
14
15      Lm = L0 + pi2*(22640*Math.sin(l) + 769*Math.sin(2*l) - 4586*Math.sin(l-2*D) + 2370*Math.sin(2*D) -
              668*Math.sin(lp) - 412*Math.sin(2*F) - 212*Math.sin(2*l-2*D) - 206*Math.sin(l+lp-2*D) + 192*
              Math.sin(l+2*D) - 165*Math.sin(lp-2*D) + 148*Math.sin(l-lp) - 125*Math.sin(D) - 110*Math.sin(l
              +lp) - 55*Math.sin(2*F - 2*D))/(360*3600);
16
17      Bm = pi2*(18520*Math.sin(F+Lm-L0+412*Math.sin(2*F)/3600 + 541*Math.sin(lp)/3600) - 526*Math.
              sin(F-2*D) + 44*Math.sin(l+F-2*D) - 31*Math.sin(-l+F-2*D) - 25*Math.sin(-2*l+F) - 23*Math.
              sin(lp+F-2*D) + 21*Math.sin(-l+F) + 11*Math.sin(-lp+F-2*D))/(360*3600);
18
19      r = (385000 - 20905*Math.cos(l) - 3699*Math.cos(2*D - l) - 2956*Math.cos(2*D) - 570*Math.cos(2*l
              ) + 246*Math.cos(2*l-2*D) - 205*Math.cos(lp-2*D) - 171*Math.cos(l+2*D) - 152*Math.cos(l+lp
              -2*D))/anorm;
20
21      out[0] = r*Math.cos(Lm)*Math.cos(Bm);
22      out[1] = r*Math.sin(Lm)*Math.cos(Bm)*Math.cos(eps) - r*Math.sin(Bm)*Math.sin(eps);
23      out[2] = r*Math.sin(Lm)*Math.cos(Bm)*Math.sin(eps) + r*Math.sin(Bm)*Math.cos(eps);
24
25      return out;
26  }
```

while the position of the Sun is given by

Listing B.15: Sun position

```
1       private double[] sunpos(double t){
2           double[] out = new double[3];
3           double eps, tau, Ms, Ls, r;
4
5           eps = pi2*23.4392911/360;
6           tau = 365.242196*t/(36525.6363*366.242196*pi2);
7
8           Ms = pi2*(357.5256 + 35999.049*tau)/360;
9           Ls = pi2*(282.94+6892*Math.sin(Ms)/3600 + 72*Math.sin(2*Ms)/3600)/360 + Ms;
10          r = (149.619 -2.499*Math.cos(Ms) - 0.021*Math.cos(2*Ms))*1e6/anorm;
11          out[0] = r*Math.cos(Ls);
12          out[1] = r*Math.sin(Ls)*Math.cos(eps);
13          out[2] = r*Math.sin(Ls)*Math.sin(eps);
14
15          return out;
16      }
```

The position of the Sun is also used in the equations of motion of the SRP as follows:

Listing B.16: Solar radiation pressure

```
1   public double[] fSrp(double x, double y, double z, double vx, double vy, double vz, double t,
        double atm){
2       double[] out = new double[3];
3
4       double rrs3, sx, sy, sz, Cr, Pr, as, Atom, amparam;
5       double[] rs = sunpos(t);
6       sx = rs[0]; sy = rs[1]; sz = rs[2];
7       rrs3 = ((sx-x)*(sx-x)+(sy-y)*(sy-y)+(sz-z)*(sz-z))*Math.sqrt((sx-x)*(sx-x)+(sy-y)*(sy-y)+(sz-z)
            *(sz-z));
8
9       Cr = 1;
10      Pr = 2.03376986239423e-05;
11      as = Math.sqrt(sx*sx+sy*sy+sz*sz);//149597871/ageo;
12      amparam = 256.09468404128717;
13      Atom = atm;
14
15      out[0] = amparam*Atom*(x-sx)/rrs3;
16      out[1] = amparam*Atom*(y-sy)/rrs3;
17      out[2] = amparam*Atom*(z-sz)/rrs3;
18
19      return out;
20  }
```

The last perturbation used in our computations is the dissipative effect due to the atmosphere, which is implemented as:

Listing B.17: Drag effect

```
1   public double[] fDrag(double x, double y, double z, double vx, double vy, double vz, double t,
        double atm){
2       double[] out = new double[3];
3
4       double r0 = Math.sqrt(x*x+y*y+z*z);
5
6       double we = 1;
7       double rp = Math.sqrt(vx*vx+vy*vy+vz*vz + x*x+y*y - 2*we*(x*vy-y*vx));
8       double cd = 2.2;
9       double H = r0 * this.anorm - 6378.137;
10
11      double rhozero = this.rhozero(H);
12      //System.out.println("Drag: " + H + " " + rhozero);
13      out[0] = -(cd/2)*1e-15*atm*rp*(vx+y)*rhozero;
14      out[1] = -(cd/2)*1e-15*atm*rp*(vy-x)*rhozero;
15      out[2] = -(cd/2)*1e-15*atm*rp*z*rhozero;
16
17      return out;
18  }
```

The function "rhozero" does basically return the ρ value from the equation (3.11) for a given altitude. The values are taken from (Vallado and McClain, 2007).

Appendix C

SIMPRO - Simulator and Propagator of Space Objects

C.1 Description

The SIMPRO application (Apetrii et al., 2022) is a tool for simulating break-up events by using the model EVOLVE 4.0 built by NASA Johnson Space Center (JSC) using ground-based impact and explosion test data ((Johnson et al., 2001), (NASA, 2017)). Alongside with the main characteristic, SIMPRO also includes several propagators of the generated fragments and for single objects.
The number of fragments, their size distribution, the area-to-mass ratio, and the relative velocity distribution of the fragments with regard to the parent body are only a few of the characteristics of the fragments that may be determined using the break-up model. It has been validated for debris sizes larger than 1 mm.
It is required to describe the distributions as a function of a specific parameter, such as the mass or the characteristic length, because the aforementioned values are not the same for every debris. In addition, the initial conditions and parameters of the break-up, such as the total mass of the parent body or the collision velocity, can have a significant impact on the simulations.
Break-ups typically fall into two categories: those caused by explosions, and those caused by collisions. In both cases, the inputs are the parent body semi-major axis a, eccentricity e, inclination i, mean anomaly M, argument of perigee ω, longitude of the ascending node Ω, and the minimum size of the resulting fragments. In case of a collision, the additional inputs are the masses of the parent body and the projectile, the collision velocity and the type of parent body (e.g., upper stage or spacecraft). A more specific classification is given below.

C.1.1 Explosions

There are two types of explosions: low-intensity explosions and high-intensity explosions.

i) Low intensity: In case of simple disintegration, such as battery explosions, only a small portion of the body's total mass is treated as a debris cloud;

ii) High intensity: 10% of mass in the debris cloud is used in the high density distribution function, and 90% of the mass in the debris cloud is used in the low density distribution function.

C.1.2 Collisions

In collisions, a distinction can be made between non-catastrophic and catastrophic collisions; the mass ratio of parent body to projectile is important because it determines the mass of the incoming ejecta, the remaining mass, and whether the remaining structure is broken.

i) Non-catastrophic: A collision in which fragments are created, but the parent body remains mostly intact. There is not enough energy in the collision to cause the target to break up and all of the fragment mass goes into the distribution function;

ii) Catastrophic: Collision that produces ejecta and the remaining material is destroyed; some debris mass (the ejecta) goes into the ejecta distribution function, and some debris mass (the remainder of the target) goes into the low-intensity distribution function. The ejecta distribution function always includes the impactor mass.

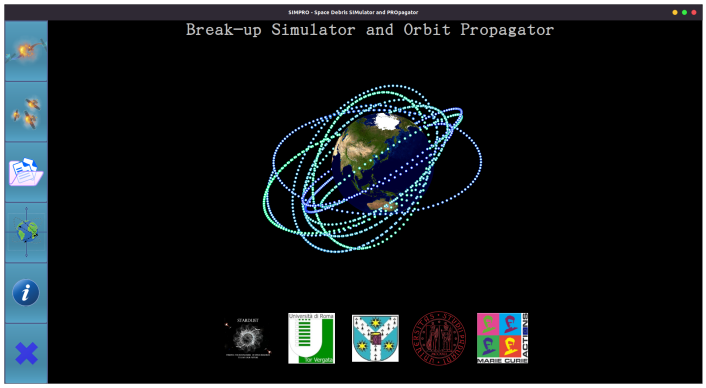

FIGURE C.1: Screenshot of the SIMPRO application - the main window and the menu bar

C.2 The JAVA© application

SIMPRO is an application created in JAVA© using the Java Swing© framework. It contains several features, from the simulation of break-up events (including the possibility to vary parameters which are given as constants in (Johnson et al., 2001)) to the propagation of the single objects and appropriate visualizations of the results. We give in this section the screenshots of the main features from the application. In Figure C.1 we see the main window

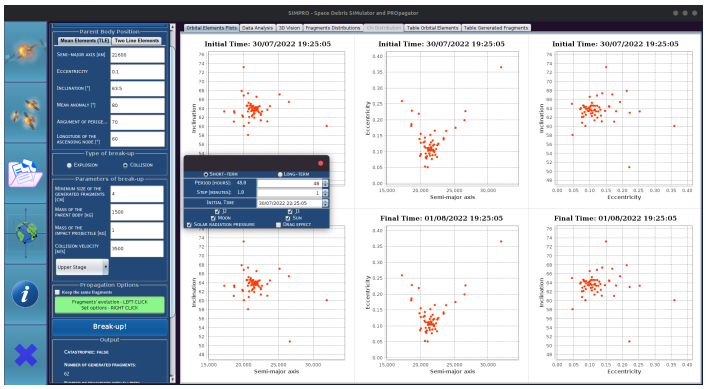

FIGURE C.2: Screenshot of the SIMPRO application - the break-up simulation window.

of the application. The left panel contains the menu bar with the following options (from top to bottom): simulate a break-up event, simulate multiple (2 or 3) break-up events, visualize the saved experiments, propagate single orbits, information about the application and the exit button. Figure C.2 shows an example of a break-up event simulation with the option of the fragments' propagation for a short time selected.

In Figure C.3 we show the possibility of the user to run an experiment with multiple break-up events (including the propagation as well). Figure C.4 is a simple example of comparison

FIGURE C.3: Screenshot of the SIMPRO application - the multiple break-up event window.

between the numerical integration of the Cartesian equation of motion and the integration of the Hamilton's equation for a given orbit. All the parameters of the numerical integration

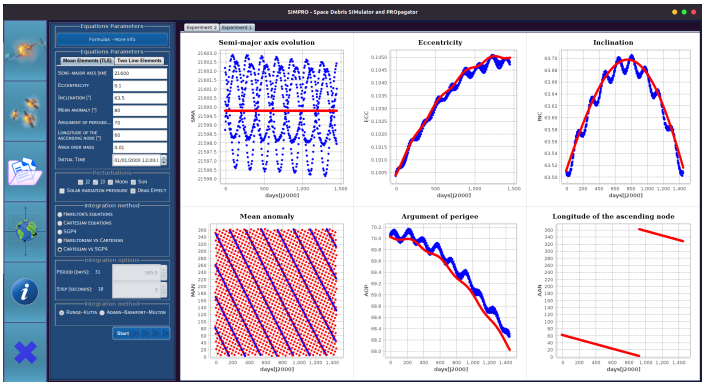

FIGURE C.4: Screenshot of the SIMPRO application - the single orbit propagation window.

can be tuned, and the application can be used in several ways to produce different results. A more detailed description of the application is given in (Apetrii et al., 2022).

Bibliography

Apetrii, Marius et al. (2022). "Simulating a Breakup Event and Propagating the Orbits of Space Debris". en. In: *Working*.

Arnold, V. I. (1978). *Mathematical methods of classical mechanics*. eng. Graduate texts in mathematics 60. New York: Springer-Verlag. ISBN: 978-0-387-90314-9.

Bien, R. and J. Schubart (1983). "Methods of Determination of Periods in the Motion of Asteroids". In: URL: https://articles.adsabs.harvard.edu/cgi-bin/nph-iarticle_query?1983acm..proc..161B&defaultprint=YES&filetype=.pdf (visited on 08/03/2022).

Breiter, S. (Sept. 2001). "Lunisolar Resonances Revisited". In: *Celestial Mechanics and Dynamical Astronomy* 81. DOI: 10.1023/A:1013363221377.

Brouwer, Dirk (Mar. 1951). "Secular variations of the orbital elements of minor planets". In: *The Astronomical Journal* 56, p. 9. ISSN: 00046256. DOI: 10.1086/106480. URL: http://adsabs.harvard.edu/cgi-bin/bib_query?1951AJ.....56....9B (visited on 08/01/2022).

— (Nov. 1959). "Solution of the problem of artificial satellite theory without drag". en. In: *The Astronomical Journal* 64, p. 378. ISSN: 00046256. DOI: 10.1086/107958. URL: http://adsabs.harvard.edu/cgi-bin/bib_query?1959AJ.....64..378B (visited on 04/13/2022).

Brouwer, Dirk and Gen-Ichiro Hori (June 1961). "Theoretical evaluation of atmospheric drag effects in the motion of an artificial satellite". In: *The Astronomical Journal* 66, p. 193. ISSN: 00046256. DOI: 10.1086/108399. URL: http://adsabs.harvard.edu/cgi-bin/bib_query?1961AJ.....66..193B (visited on 08/03/2022).

Carpino, M., A. Milani, and A. M. Nobili (1987). "Long-term numerical integrations and synthetic theories for the motion of the outer planets". In: *Astronomy and Astrophysics (ISSN 0004-6361), vol. 181, no. 1, July 1987, p. 182-194. SERC-CNR-supported research.*

Carruba, V, S Aljbaae, and A Lucchini (Sept. 2019). "Machine-learning identification of asteroid groups". en. In: *Monthly Notices of the Royal Astronomical Society* 488.1, pp. 1377–1386. ISSN: 0035-8711, 1365-2966. DOI: 10.1093/mnras/stz1795. URL: https://academic.oup.com/mnras/article/488/1/1377/5526253 (visited on 05/08/2022).

Celletti, A. (2010). *Stability and chaos in celestial mechanics*. en. Springer-Praxis books in astronomy and planetary sciences. OCLC: ocn401157563. Berlin ; New York, NY : Chichester, UK: Springer ; Published in associaiton with Praxis Publishing. ISBN: 978-3-540-85145-5.

Celletti, Alessandra and Catalin Galeş (Dec. 2014). "On the dynamics of space debris: 1:1 and 2:1 resonances". en. In: *Journal of Nonlinear Science* 24.6. arXiv: 1408.1254, pp. 1231–1262. ISSN: 0938-8974, 1432-1467. DOI: 10.1007/s00332-014-9217-6. URL: http://arxiv.org/abs/1408.1254 (visited on 04/13/2022).

Celletti, Alessandra, Catalin Galeş, and Christoph Lhotka (May 2020). "Resonances in the Earth's Space Environment". en. In: *Communications in Nonlinear Science and Numerical Simulation* 84. arXiv: 1912.04593, p. 105185. ISSN: 10075704. DOI: 10.1016/j.cnsns.2020.105185. URL: http://arxiv.org/abs/1912.04593 (visited on 04/13/2022).

Celletti, Alessandra and Cătălin Galeş (Oct. 2015). "Dynamical investigation of minor resonances for space debris". en. In: *Celestial Mechanics and Dynamical Astronomy* 123.2, pp. 203–222. ISSN: 0923-2958, 1572-9478. DOI: 10.1007/s10569-015-9636-1. URL: http://link.springer.com/10.1007/s10569-015-9636-1 (visited on 04/13/2022).

— (Oct. 2017). "Dynamics of resonances and equilibria of Low Earth Objects". en. In: *arXiv:1710.02519 [astro-ph, physics:math-ph]*. arXiv: 1710.02519. URL: http://arxiv.org/abs/1710.02519 (visited on 04/13/2022).

Celletti, Alessandra, Cătălin Galeş, and Giuseppe Pucacco (Mar. 2016). *Bifurcations of lunisolar secular resonances for space debris orbits*. en. Number: arXiv:1512.02178 arXiv:1512.02178 [astro-ph]. URL: http://arxiv.org/abs/1512.02178 (visited on 06/21/2022).

Celletti, Alessandra and Cătălin B. Galeş (Mar. 2016). "A Study of the Lunisolar Secular Resonance $2\omega + \Omega$=0". en. In: *Frontiers in Astronomy and Space Sciences* 3. ISSN: 2296-987X. DOI: 10.3389/fspas.2016.00011. URL: http://journal.frontiersin.org/Article/10.3389/fspas.2016.00011/abstract (visited on 06/22/2022).

Celletti, Alessandra, Giuseppe Pucacco, and Tudor Vartolomei (Dec. 2021). "Reconnecting groups of space debris to their parent body through proper elements". en. In: *Scientific Reports* 11.1, p. 22676. ISSN: 2045-2322. DOI: 10.1038/s41598-021-02010-x. URL: https://www.nature.com/articles/s41598-021-02010-x (visited on 07/27/2022).

— (Apr. 2022). "Proper elements for space debris". en. In: *Celestial Mechanics and Dynamical Astronomy* 134.2, p. 11. ISSN: 0923-2958, 1572-9478. DOI: 10.1007/s10569-022-10064-w. URL: https://link.springer.com/10.1007/s10569-022-10064-w (visited on 08/03/2022).

Celletti, Alessandra et al. (Apr. 2017). "Dynamical models and the onset of chaos in space debris". en. In: *International Journal of Non-Linear Mechanics* 90. arXiv: 1612.08849, pp. 147–163. ISSN: 00207462. DOI: 10.1016/j.ijnonlinmec.2016.12.015. URL: http://arxiv.org/abs/1612.08849 (visited on 04/18/2022).

Chao, Chia-Chun George (Nov. 2005). *Applied Orbit Perturbation and Maintenance*. en. Washington, DC: American Institute of Aeronautics and Astronautics, Inc. ISBN: 978-1-884989-17-9. DOI: 10.2514/4.989179. URL: http://arc.aiaa.org/doi/book/10.2514/4.989179 (visited on 04/13/2022).

Coffey, Shannon L., Andre Deprit, and Bruce R. Miller (Dec. 1986). "The critical inclination in artificial satellite theory". en. In: *Celestial Mechanics* 39.4, pp. 365–406. ISSN: 0008-8714, 1572-9478. DOI: 10.1007/BF01230483. URL: http://link.springer.com/10.1007/BF01230483 (visited on 04/13/2022).

Colombo, Camilla (July 2019). "Long-Term Evolution of Highly-Elliptical Orbits: Luni-Solar Perturbation Effects for Stability and Re-entry". en. In: *Frontiers in Astronomy and Space Sciences* 6, p. 34. ISSN: 2296-987X. DOI: 10.3389/fspas.2019.00034. URL: https://www.frontiersin.org/article/10.3389/fspas.2019.00034/full (visited on 05/06/2022).

Colombo, Camilla, Charlotte Lücking, and Colin R McInnes (Dec. 2012). "Orbital dynamics of high area-to-mass ratio spacecraft with J2 and solar radiation pressure for novel Earth observation and communication services". en. In: *Acta Astronautica* 81.1, pp. 137–150. ISSN: 00945765. DOI: 10.1016/j.actaastro.2012.07.009. URL: https://linkinghub.elsevier.com/retrieve/pii/S009457651200272X (visited on 05/08/2022).

Cook, G.E. (May 1966). "Perturbations of near-circular orbits by the earth's gravitational potential". en. In: *Planetary and Space Science* 14.5, pp. 433–444. ISSN: 00320633. DOI:

10.1016/0032-0633(66)90015-8. URL: https://linkinghub.elsevier.com/retrieve/pii/0032063366900158 (visited on 04/13/2022).

Daquin, Jérôme et al. (Aug. 2021). "Dynamical properties of the Molniya satellite constellation: long-term evolution of the semi-major axis". en. In: *Nonlinear Dynamics* 105.3, pp. 2081–2103. ISSN: 0924-090X, 1573-269X. DOI: 10.1007/s11071-021-06708-5. URL: https://link.springer.com/10.1007/s11071-021-06708-5 (visited on 08/03/2022).

Daquin, Jérôme et al. (Feb. 2022). "A deep dive into the $$2g+h$$ resonance: separatrices, manifolds and phase space structure of navigation satellites". en. In: *Celestial Mechanics and Dynamical Astronomy* 134.1, p. 6. ISSN: 0923-2958, 1572-9478. DOI: 10.1007/s10569-021-10060-6. URL: https://link.springer.com/10.1007/s10569-021-10060-6 (visited on 08/03/2022).

De Blasi, Irene, Alessandra Celletti, and Christos Efthymiopoulos (Dec. 2021). "Semi-Analytical Estimates for the Orbital Stability of Earth's Satellites". en. In: *Journal of Nonlinear Science* 31.6, p. 93. ISSN: 0938-8974, 1432-1467. DOI: 10.1007/s00332-021-09738-w. URL: https://link.springer.com/10.1007/s00332-021-09738-w (visited on 08/04/2022).

Delhaise, Fabienne (1991). "Analytical treatment of air drag and earth oblateness effects upon an artificial satellite". en. In: *CELESTIAL MECHANICS AND DYNAMICAL ASTRONOMY* 52.1, pp. 85–103. ISSN: 0923-2958, 1572-9478. DOI: 10.1007/BF00048589. URL: http://link.springer.com/10.1007/BF00048589 (visited on 08/03/2022).

Deprit, Andre (Mar. 1969). "Canonical transformations depending on a small parameter". en. In: *Celestial Mechanics* 1.1, pp. 12–30. ISSN: 0008-8714, 1572-9478. DOI: 10.1007/BF01230629. URL: http://link.springer.com/10.1007/BF01230629 (visited on 04/13/2022).

Deprit, Andre and Arnold Rom (June 1970). "The main problem of artificial satellite theory for small and moderate eccentricities". en. In: *Celestial Mechanics* 2.2, pp. 166–206. ISSN: 0008-8714, 1572-9478. DOI: 10.1007/BF01229494. URL: http://link.springer.com/10.1007/BF01229494 (visited on 04/13/2022).

Efthymiopoulos, C (2011). *Canonical perturbation theory, stability and diffusion in Hamiltonian systems: applications in dynamical astronomy*. en. Workshop Series of the Asociacion Argentina de Astronomia.

Ely, Todd A. and Kathleen C. Howell (Jan. 1997). "Dynamics of artificial satellite orbits with tesseral resonances including the effects of luni- solar perturbations". en. In: *Dynamics and Stability of Systems* 12.4, pp. 243–269. ISSN: 0268-1110, 1465-3389. DOI: 10.1080/02681119708806247. URL: http://www.tandfonline.com/doi/abs/10.1080/02681119708806247 (visited on 04/13/2022).

ESA Space Debris Office (2022). *ESA's Annual Space Environment Report*. Tech. rep. ESA. URL: https://www.sdo.esoc.esa.int/environment_report/Space_Environment_Report_latest.pdf (visited on 08/06/2022).

Fenucci, M., G. F. Gronchi, and M. Saillenfest (June 2022). "Proper elements for resonant planet-crossing asteroids". en. In: *Celestial Mechanics and Dynamical Astronomy* 134.3. arXiv:2201.11392 [astro-ph], p. 23. ISSN: 0923-2958, 1572-9478. DOI: 10.1007/s10569-022-10078-4. URL: http://arxiv.org/abs/2201.11392 (visited on 08/03/2022).

Ferraz-Mello, Sylvio (2007). *Canonical perturbation theories: degenerate systems and resonance*. en. Astrophysics and space science library v. 345. New York: Springer. ISBN: 978-0-387-38900-4 978-0-387-38905-9.

Gachet, Fabien (Sept. 2016). "Forced Equilibrium of the Geostationary Ring and Proper Elements for Space Debris". en. In: *AIAA/AAS Astrodynamics Specialist Conference*.

Long Beach, California: American Institute of Aeronautics and Astronautics. ISBN: 978-1-62410-445-9. DOI: 10.2514/6.2016-5431. URL: https://arc.aiaa.org/doi/10.2514/6.2016-5431 (visited on 08/03/2022).

Gachet, Fabien et al. (June 2017). "Geostationary secular dynamics revisited: application to high area-to-mass ratio objects". en. In: *Celestial Mechanics and Dynamical Astronomy* 128.2-3, pp. 149–181. ISSN: 0923-2958, 1572-9478. DOI: 10.1007/s10569-016-9746-4. URL: http://link.springer.com/10.1007/s10569-016-9746-4 (visited on 08/03/2022).

Giorgilli, Antonio (2022). *Notes on Hamiltonian dynamical systems*. London mathematical society student texts 102. Cambridge, United Kingdom ; New York, NY: Cambridge University Press. ISBN: 978-1-00-915114-6.

Gkolias, Ioannis et al. (Oct. 2016). "FROM ORDER TO CHAOS IN EARTH SATELLITE ORBITS". en. In: *The Astronomical Journal* 152.5, p. 119. ISSN: 1538-3881. DOI: 10.3847/0004-6256/152/5/119. URL: https://iopscience.iop.org/article/10.3847/0004-6256/152/5/119 (visited on 04/13/2022).

Gkolias, Ioannis et al. (Oct. 2019). "Chaotic transport of navigation satellites". en. In: *Chaos: An Interdisciplinary Journal of Nonlinear Science* 29.10, p. 101106. ISSN: 1054-1500, 1089-7682. DOI: 10.1063/1.5124682. URL: http://aip.scitation.org/doi/10.1063/1.5124682 (visited on 04/13/2022).

Gronchi, G. F. and A. Milani (July 2001). "Proper Elements for Earth-Crossing Asteroids". In: *Icarus* 152.1, pp. 58–69. DOI: 10.1006/icar.2001.6610.

Henrard, Jacques (Mar. 1970). "On a perturbation theory using Lie transforms". In: *Celestial Mechanics* 3. ADS Bibcode: 1970CeMec...3..107H, pp. 107–120. ISSN: 0008-8714. DOI: 10.1007/BF01230436. URL: https://ui.adsabs.harvard.edu/abs/1970CeMec...3..107H (visited on 04/13/2022).

Hirayama, Kiyotsugu (Oct. 1918). "Groups of asteroids probably of common origin". In: *The Astronomical Journal* 31, p. 185. ISSN: 00046256. DOI: 10.1086/104299. URL: http://adsabs.harvard.edu/cgi-bin/bib_query?1918AJ.....31..185H (visited on 08/01/2022).

— (1922). "Families of asteroids". In: *Japanese Journal of Astronomy and Geophysics* 1, p. 55. URL: https://adsabs.harvard.edu/pdf/1922JaJAG...1...55H (visited on 08/08/2022).

Hori, G. (Jan. 1966). "Theory of General Perturbation with Unspecified Canonical Variable". In: *Publications of the Astronomical Society of Japan* 18. ADS Bibcode: 1966PASJ...18..287H, p. 287. ISSN: 0004-6264. URL: https://ui.adsabs.harvard.edu/abs/1966PASJ...18..287H (visited on 07/07/2022).

— (1971). "Theory of General Perturbations for Non-Canonical Systems". In: *Publications of the Astronomical Society of Japan* 23. URL: https://articles.adsabs.harvard.edu/cgi-bin/nph-iarticle_query?1971PASJ...23..567H&defaultprint=YES&filetype=.pdf (visited on 06/21/2022).

Hughes, S. (1980). "Earth Satellite Orbits with Resonant Lunisolar Perturbations. I. Resonances Dependent Only on Inclination". en. In: *Proceedings of the Royal Society of London. Series A, Mathematical and Physical Sciences* 372.1749, pp. 243–264. URL: http://www.jstor.org/stable/2990367.

Johnson, N.L. et al. (Jan. 2001). "NASA's new breakup model of evolve 4.0". en. In: *Advances in Space Research* 28.9, pp. 1377–1384. ISSN: 02731177. DOI: 10.1016/S0273-1177(01)00423-9. URL: https://linkinghub.elsevier.com/retrieve/pii/S0273117701004239 (visited on 04/13/2022).

Junkins, John L. and Hanspeter Schaub (Jan. 2009). *Analytical Mechanics of Space Systems, Second Edition: Second Edition*. en. Reston ,VA: American Institute of Aeronautics and Astronautics. ISBN: 978-1-60086-721-7 978-1-60086-723-1. DOI: 10.2514/4.

867231. URL: https://arc.aiaa.org/doi/book/10.2514/4.867231 (visited on 04/13/2022).

Kamel, Ahmed Aly (June 1969). "Expansion Formulae in Canonical Transformations Depending on a Small Parameter". In: *Celestial Mechanics* 1. ADS Bibcode: 1969CeMec...1..190K, pp. 190–199. ISSN: 0008-8714. DOI: 10.1007/BF01228838. URL: https://ui.adsabs.harvard.edu/abs/1969CeMec...1..190K (visited on 05/19/2022).

— (Dec. 1971). "Lie transforms and the Hamiltonization of non-Hamiltonian systems". en. In: *Celestial Mechanics* 4.3-4, pp. 397–405. ISSN: 0008-8714, 1572-9478. DOI: 10.1007/BF01231400. URL: http://link.springer.com/10.1007/BF01231400 (visited on 04/13/2022).

Kamel, Albmed Aly (1970). *PERTURBATION THEORY BASED ON LIE TRANSFORMS ND ITS APPLICATION TO THE STABILITY QF MOTION NEAR SUN-PERTURBED EARTH-MOON TRIANGULAR LIBRATION POINTS*. NATIONAL AERONAUTICS and SPACE ADMINISTRATION. URL: https://ntrs.nasa.gov/api/citations/19700026379/downloads/19700026379.pdf (visited on 04/13/2022).

Kaula, William M. (2000). *Theory of satellite geodesy: applications of satellites to geodesy*. Dover ed. Mineola, N.Y: Dover Publications. ISBN: 978-0-486-41465-2.

Kessler, Donald J. and Burton G. Cour-Palais (1978). "Collision frequency of artificial satellites: The creation of a debris belt". en. In: *Journal of Geophysical Research* 83.A6, p. 2637. ISSN: 0148-0227. DOI: 10.1029/JA083iA06p02637. URL: http://doi.wiley.com/10.1029/JA083iA06p02637 (visited on 08/06/2022).

Klinkrad, H. (2006). *Space debris: models and risk analysis*. en. Springer-Praxis books in astronautical engineering. Berlin ; New York : Chichester, UK: Springer ; Published in association with Praxis Pub. ISBN: 978-3-540-25448-5.

Knežević, Z. and A. Milani (2001). "Synthetic Proper Elements for Outer Main Belt Asteroids". en. In: *New Developments in the Dynamics of Planetary Systems*. Ed. by Rudolf Dvorak and Jacques Henrard. Dordrecht: Springer Netherlands, pp. 17–46. ISBN: 978-90-481-5702-0 978-94-017-2414-2. DOI: 10.1007/978-94-017-2414-2_2. URL: http://link.springer.com/10.1007/978-94-017-2414-2_2 (visited on 05/31/2022).

Knežević, Zoran (Aug. 2015). "Asteroid Family Identification: History and State of the Art". en. In: *Proceedings of the International Astronomical Union* 10.S318, pp. 16–27. ISSN: 1743-9213, 1743-9221. DOI: 10.1017/S1743921315008728. URL: https://www.cambridge.org/core/product/identifier/S1743921315008728/type/journal_article (visited on 08/03/2022).

Knežević, Zoran, Anne Lemaître, and Andrea Milani (Dec. 2002). *Asteroids III*. en. Ed. by William F. Bottke et al. University of Arizona Press. ISBN: 978-0-8165-4651-0 978-0-8165-2281-1. DOI: 10.2307/j.ctv1v7zdn4. URL: http://www.jstor.org/stable/10.2307/j.ctv1v7zdn4 (visited on 08/01/2022).

Knežević, Zoran and Andrea Milani (1994). "Asteroid Proper Elements: The Big Picture". en. In: *Symposium - International Astronomical Union* 160, pp. 143–158. ISSN: 0074-1809. DOI: 10.1017/S0074180900046519. URL: https://www.cambridge.org/core/product/identifier/S0074180900046519/type/journal_article (visited on 08/01/2022).

Kozai, Yoshihide (Nov. 1959). "The motion of a close earth satellite". en. In: *The Astronomical Journal* 64, p. 367. ISSN: 00046256. DOI: 10.1086/107957. URL: http://adsabs.harvard.edu/cgi-bin/bib_query?1959AJ.....64..367K (visited on 06/08/2022).

— (Nov. 1962). "Secular perturbations of asteroids with high inclination and eccentricity". In: *The Astronomical Journal* 67, p. 591. ISSN: 00046256. DOI: 10.1086/108790. URL: http://adsabs.harvard.edu/cgi-bin/bib_query?1962AJ.....67..591K (visited on 08/01/2022).

Lane, Mark T. (1989). "On analytic modeling of lunar perturbations of artificial satellites of the earth". en. In: *Celestial Mechanics and Dynamical Astronomy* 46.4, pp. 287–305. ISSN: 0923-2958, 1572-9478. DOI: 10.1007/BF00051484. URL: http://link.springer.com/10.1007/BF00051484 (visited on 08/03/2022).

Lemaître, A., N. Delsate, and S. Valk (Aug. 2009). "A web of secondary resonances for large A/ m geostationary debris". In: *Celestial Mechanics and Dynamical Astronomy* 104.4, pp. 383–402. DOI: 10.1007/s10569-009-9217-2.

Lemaître, Anne (1993). "Proper elements: What are they?" en. In: *Celestial Mechanics and Dynamical Astronomy* 56.1-2, pp. 103–119. ISSN: 0923-2958, 1572-9478. DOI: 10.1007/BF00699724. URL: http://link.springer.com/10.1007/BF00699724 (visited on 08/01/2022).

Lemaître, Anne and Alessandro Morbidelli (Sept. 1994). "Proper elements for highly inclined asteroidal orbits". en. In: *Celestial Mechanics & Dynamical Astronomy* 60.1, pp. 29–56. ISSN: 0923-2958, 1572-9478. DOI: 10.1007/BF00693091. URL: http://link.springer.com/10.1007/BF00693091 (visited on 08/01/2022).

Lhotka, C., A. Celletti, and C. Galeş (July 2016). "Poynting–Robertson drag and solar wind in the space debris problem". en. In: *Monthly Notices of the Royal Astronomical Society* 460.1, pp. 802–815. ISSN: 0035-8711, 1365-2966. DOI: 10.1093/mnras/stw927. URL: https://academic.oup.com/mnras/article-lookup/doi/10.1093/mnras/stw927 (visited on 04/13/2022).

Lyddane, R. H. (Oct. 1963). "Small eccentricities or inclinations in the Brouwer theory of the artificial satellite". en. In: *The Astronomical Journal* 68, p. 555. ISSN: 00046256. DOI: 10.1086/109179. URL: http://adsabs.harvard.edu/cgi-bin/bib_query?1963AJ.....68..555L (visited on 04/13/2022).

Milani, Andrea and Zoran Knežević (Dec. 1990). "Secular perturbation theory and computation of asteroid proper elements". In: *Celestial Mechanics and Dynamical Astronomy* 49. ADS Bibcode: 1990CeMDA..49..347M, pp. 347–411. ISSN: 0923-2958. DOI: 10.1007/BF00049444. URL: https://ui.adsabs.harvard.edu/abs/1990CeMDA..49..347M (visited on 05/19/2022).

— (1998). "Asteroid Mean Elements: Higher Order and Iterative Theories". In: *Celestial Mechanics and Dynamical Astronomy* 71.1, pp. 55–78. ISSN: 09232958. DOI: 10.1023/A:1008315029975. URL: http://link.springer.com/10.1023/A:1008315029975 (visited on 08/03/2022).

Montenbruck, O, E Gill, and Fh Lutze (2002). "Satellite Orbits: Models, Methods, and Applications". en. In: *Applied Mechanics Reviews* 55.2, B27. ISSN: 00036900. DOI: 10.1115/1.1451162. URL: http://AppliedMechanicsReviews.asmedigitalcollection.asme.org/article.aspx?articleid=1396996 (visited on 04/13/2022).

Morbidelli, Alessandro (Sept. 1993). "Asteroid Secular Resonant Proper Elements". en. In: *Icarus* 105.1, pp. 48–66. ISSN: 00191035. DOI: 10.1006/icar.1993.1110. URL: https://linkinghub.elsevier.com/retrieve/pii/S0019103583711103 (visited on 08/03/2022).

Murray, Carl D. and Stanley F. Dermott (Feb. 2000). *Solar System Dynamics*. en. 1st ed. Cambridge University Press. ISBN: 978-0-521-57295-8 978-0-521-57597-3 978-1-139-17481-7. DOI: 10.1017/CBO9781139174817. URL: https://www.cambridge.org/core/product/identifier/9781139174817/type/book (visited on 05/10/2022).

NASA (2017). *NASA Standard Breakup Model 1998 Revision*.

Perko, Lawrence (2001). *Differential equations and dynamical systems*. en. 3rd ed. Texts in applied mathematics 7. New York: Springer. ISBN: 978-0-387-95116-4.

Rosengren, Aaron Jay, Claudio Bombardelli, and Davide Amato (June 2019). "Geocentric Proper Orbital Elements". In: *AAS/Division of Dynamical Astronomy Meeting*. Vol. 51. AAS/Division of Dynamical Astronomy Meeting, P3, P3.

Rosengren, Aaron Jay et al. (2019). "Resident space object proper orbital elements". In: *Astronautical Sciences AAS/AIAA Spaceflight Mechanics*. Vol. 168.

Rossi, Alessandro (Apr. 2008). "Resonant dynamics of Medium Earth Orbits: Space debris issues". In: *Celestial Mechanics and Dynamical Astronomy* 100, pp. 267–286. DOI: 10.1007/s10569-008-9121-1.

Schubart, J (1982). "Three characteristic parameters of orbits of Hilda-type asteroids". In: *Astronomy and Astrophysics*. URL: https://articles.adsabs.harvard.edu/cgi-bin/nph-iarticle_query?1982A%26A...114..200S&defaultprint=YES&filetype=.pdf (visited on 08/03/2022).

Vallado, David A. and Wayne D. McClain (2007). *Fundamentals of astrodynamics and applications*. en. 3. ed., 1. printing. Space technology library 21. Hawthorne, Calif.: Microcosm Press [u.a.] ISBN: 978-1-881883-14-2 978-0-387-71831-6.

Vallado, David Anthony and Wayne D. McClain (2001). *Fundamentals of astrodynamics and applications*. eng. 2. ed. Space technology library 12. Dordrecht: Kluwer Academic Publishers. ISBN: 978-1-881883-12-8 978-0-7923-6903-5.

Wiggins, Stephen (2003). *Introduction to applied nonlinear dynamical systems and chaos*. en. 2nd ed. Texts in applied mathematics 2. New York: Springer. ISBN: 978-0-387-00177-7.

Williams, James Gerard (1969). "SECULAR PERTURBATIONS IN THE SOLAR SYSTEM." en. PhD thesis. United States – California: University of California, Los Angeles.

Williams, J.G. (1971). "Proper Elements, Families, and Belt Boundaries". en. In: *International Astronomical Union Colloquium* 12, pp. 177–181. ISSN: 0252-9211. DOI: 10.1017/S0252921100089028. URL: https://www.cambridge.org/core/product/identifier/S0252921100089028/type/journal_article (visited on 08/03/2022).

Williams, J.G. and J.E. Hierath (Nov. 1987). "Palomar-Leiden minor planets: Proper elements, frequency distributions, belt boundaries, and family memberships". en. In: *Icarus* 72.2, pp. 276–303. ISSN: 00191035. DOI: 10.1016/0019-1035(87)90176-X. URL: https://linkinghub.elsevier.com/retrieve/pii/001910358790176X (visited on 08/01/2022).

Wu, Di and Aaron J Rosengren (2021). "RSO Proper Elements for Space Situational and Domain Awareness". en. In: *Advanced Maui Optical and Space Surveillance Technologies Conference (AMOS*, p. 13.